Title

CubeSat Attitude Control Using Hard Disk Drives as Reaction Wheels

Author

Negi, Abhay

Publication Date

2023

Peer reviewed|Thesis/dissertation

CubeSat Attitude Control Using Hard Disk Drives as Reaction Wheels

By

Abhay Negi

Thesis

Submitted in partial satisfaction of the requirements for the degree of

Master of Science

in

Mechanical and Aerospace Engineering

in the

Office of Graduate Studies

of the

University of California

Davis

Approved:

Stephen K. Robinson, Chair

Sanjay S. Joshi

Zhaodan Kong

Committee in Charge

2023

Contents

List of Figures

List of Tables

Abstract

CubeSat Attitude Control Using Hard Disk Drives as Reaction Wheels

Reaction wheels play an essential role in the attitude control of small satellites; however, the trade-off between cost and reliability of commercial and in-house manufactured reaction wheels is a common pain point for small satellite developers. Hard disk drives (HDDs) repurposed as reaction wheels (HDD-RWs) are a low-cost, commercial-off-the-shelf (COTS) solution to the cost versus reliability trade-off for small satellite reaction wheels - they are one to three orders of magnitude less expensive than commercial reaction wheels and demonstrate competitive performance. HDD-RWs have the potential to dramatically lower barriers to entry, allowing resource-constrained organizations to develop CubeSat missions with reliable attitude control.

This thesis presents the research efforts to develop, test, and demonstrate the HDD-RW technology. Lab testing of the HDD-RW was performed to identify a working hardware configuration for the HDD-RWs and develop an actuator model. Preliminary environmental testing was conducted to ensure the HDD-RW can survive vibration loads and a vacuum environment. Single-axis ground testing of the attitude controller using the HDD-RWs was performed to verify its performance. Demonstration of three-axis attitude control using the HDD-RWs was performed through microgravity parabolic flight testing. Successful demonstrations of stabilization and pointing of a HDD-RW CubeSat testbed in microgravity environment raised the Technology Readiness Level (TRL) of the HDD-RW technology from TRL 4 to TRL 6. Data from parabolic flight testing is used to perform system identification of the HDD-RWs and CubeSat system. Simulation results based on the system model further demonstrates pointing control with the HDD-RWs for various target attitudes and stabilization from various initial rotation rates. A guide for using HDD-RWs and developing a controller is presented. Recommendations and lessons learned are provided, and next steps for the HDD-RW technology are discussed.

Acknowledgments

The Zero-G HDD project has been both the most challenging and rewarding three years of my career thus far. I would like to express my deepest gratitude to everyone who has supported me and the HDD-RW technology through this journey.

Firstly, to my parents - thank you for everything. Your many personal sacrifices have allowed me to be where I am today and to be pursuing my dreams. To my mother - thank you for teaching me perseverance and passion; and to my father - thank you for teaching me kindness and humility. You both continuously inspire me to strive to do my best.

To Professor Robinson, thank you for being an incredible mentor. It goes without saying that this project would not have been possible without your wisdom and guidance. I would especially like to thank you for placing a lot of trust in myself and Kylie and providing us with freedom and independence in our leadership of this project (however unreasonable the Gantt chart might have looked). I would also like to thank you for the personal support that we could always count on which helped us navigate through several challenges.

To Kylie Cooper, thank you for being the best co-lead anyone could ask for. I say with no exaggeration that collaborating with you has truly been an honor. I always marvel at your abilities to come up with creative ideas and clever solutions and to anticipate and prevent complex problems. Working with you has always been fun. Thank you for always being the voice of reason, an excellent engineer, and an all-around amazing human being.

To all the undergraduate researchers who have supported this project, thank you for all your hard work and dedication. To Miranda Godinez and Ashna Reddy, thank you for kicking-off the computer vision system. To Ashna Reddy and Chris Andrade, thank you for your persistence through all of the challenges of our first flight campaign. To Chris Andrade, Natasha Evans, and Dzuy Nguyen, thank you for your efforts on hardware designs and for your amazing work that propelled us through the second flight campaign. To Zoe Wilf and Kelden Ben-Ora, thank you for being so open-minded and adaptive - your abilities to learn so quickly helped us complete the third flight campaign.

To Adam Zufall, thank you for your efforts towards the third flight campaign and the collaboration with NASA JSC. And thank you for always willing to be a sounding board.

To Chris Andrade and Rachel Pride, thank you for continuing development of the HDD-RW technology. There is a lot more to be done and I am confident that you both will do excellent work.

To all members, past and present, of the Human/Robotics/Vehicle Integration & Performance (HRVIP) Lab, thank you for being such inspiring, charismatic, and motivating researchers. You all make HRVIP a very special place.

To all members, past and present, of the Space and Satellite Systems (SSS) club at UC Davis, thank you for taking on the challenge of developing UC Davis' first CubeSat and for the beginnings of the HDD-RW.

Finally, to NASA, this project would not have been possible without you. In particular, thank you to the NASA CubeSat Launch Initiative (CSLI) program, which allowed dozens of students in SSS, including Kylie and myself, to become involved in spaceflight and launch our careers as aerospace engineers. The CSLI program also directly led to initial development of the HDD-RW technology. Lastly, I would like to express my gratitude to the NASA Flight Opportunities program, which has made microgravity parabolic flight testing of the HDD-RW technology possible. Thank you for placing your trust in the HDD-RW technology and our team's technical abilities.

Chapter 1

Introduction

1.1 Overview

The work presented in this thesis is the product of the Zero-G HDD project at the University of California, Davis (UC Davis) Center for Spaceflight Research (CSFR). The objective of the Zero-G HDD project was to demonstrate the use of hard disk drives (HDDs) as CubeSat reaction wheels through microgravity parabolic flight testing. This project was selected by the NASA Flight Opportunities Program's "TechFlights" solicitation, which made parabolic flight testing possible. The Zero-G HDD project was led by two masters students - Kylie Cooper and the author. The work and results from the Zero-G HDD project is presented in two master theses - this thesis and Cooper's thesis [1]. The work presented within this thesis is the reflection of the combined efforts of both the author and Cooper.

Chapter 1 discusses the motivation behind using hard disk drive reaction wheels (HDD-RWs), the HDD-RW technology state of the art, and the parabolic flight experiment design. Chapter 2 describes the hard disk drive technology, implementation of the hard disk drive reaction wheel, preliminary environmental testing, and compatibility of HDD-RWs with the space environment. Chapter 3 presents modeling of the HDD-RW, development of the HDD-RW controller, results from parabolic flight, system identification, and results of simulation. Chapter 4 describes the process of converting a HDD into a HDD-RW and presents a guide on controlling the HDD-RW. Lastly, Chapter 5 concludes the thesis and discusses recommendations, lessons learned, and future work.

1.2 Motivation

1.2.1 CubeSats

Satellites provide many essential services such as communications, weather monitoring, Earth observations, and space science research. Building and launching a traditional full-scale satellite can cost upwards of $200 million [2]. One of the main drivers behind the high cost of a satellite is the required reliability to survive and operate in the hostile environment of space without the need for repairs. The recent rise of small satellites, called CubeSats, have revolutionized the space industry by demonstrating that small satellites are capable of providing essential satellite services at a far lower cost [2] [3] [4].

A CubeSat is a class of small satellites that follow specific form factor standards [5]. CubeSats come in various sizes, quantified by their volume in "U's", or 10 cm cubes. Due to their small and standard sizes, dozens of CubeSats can be simultaneously launched on a single rocket, dramatically reducing the launch cost per satellite. Furthermore, the advent of the cell-phone industry has significantly reduced the cost of integrated components (ICs) and micro-electromechanical systems-based (MEMS) components. Consequently, CubeSats have become relatively inexpensive as their risk-tolerant missions can leverage these low-cost commercial-off-the-shelf (COTS) electronic components.

CubeSats currently perform many types of missions such as Earth observation, Earth science, astronomy, and technology test and demonstration [2]. The relatively low cost of developing and launching a CubeSat has enabled the participation of university students. As low-cost and risk-tolerant missions, CubeSats play an important role in spacecraft technology demonstration and training of engineering students in the aerospace field [6] [2].

1.2.2 Attitude Control

The attitude of a spacecraft, or its three-dimensional orientation with respect to another frame of reference, is an important state for almost all spacecraft missions. For example, in CubeSats, attitude control is important to be able to stabilize to take a photograph without motion-blur or to point an antenna towards a ground station to relay data.

Attitude systems are often divided into two subsystems - attitude determination and attitude control. Whereas the objective of the former is calculating the attitude of the spacecraft

with respect to a defined reference frame, the objective of the latter is to maneuver the spacecraft to a target state of attitude. The two primary elements of spacecraft attitude control are stabilization and pointing [7]. Spacecraft stabilization consists of controlling the rotation rate of the spacecraft, which typically has a target value of zero in the inertial reference frame. Spacecraft pointing consists of reorienting the spacecraft to a desired attitude with respect to a specified frame of reference.

Most attitude control systems utilize reaction wheels as actuators [8]. The operating principle of the reaction wheel is conservation of angular momentum, shown in Equation 1.1. In a reaction wheel, the rotation rate of a wheel is precisely controlled by a motor. By spinning its wheel, the reaction wheel transfers angular momentum from the CubeSat bus to the wheel, allowing it to alter the inertial attitude of the spacecraft. Furthermore, changing the rotational velocity of the wheel applies a torque, which can be used to reorient the spacecraft. A minimum of three reaction wheels are required for a spacecraft to have full three-axis attitude control. In some cases, four or more reaction wheels are used in a non-orthogonal configuration to provide redundancy, in case a reaction wheel fails; however, this is not common in CubeSats due to their constrained volumes.

$$L_{TOT} = L_{CS} + L_{RW} = I_{CS}\omega_{CS} + I_{RW}\omega_{RW} \tag{1.1}$$

1.2.3 Commercial CubeSat Reaction Wheels

Like most spacecraft, CubeSats primarily use reaction wheels for attitude control. Several companies exist that sell CubeSat reaction wheels. A list of commercial CubeSat reaction wheel specifications and prices found in 2023 is shown in Table 1.1. Note that the listed prices are not fixed and are subject to change by their respective vendor. Prices were found to range from 2700 to 35000 USD, with the RW25 by Serenum Space (2700 USD, 2023) being the most inexpensive option. Thus, a three-axis control system using commercial reaction wheels would cost, at a minimum, 8100 USD, excluding additional costs from taxes, customs fees, and shipping fees. The total cost is further magnified if test units are desired, as is typically the case for CubeSat developers. Consequently, the cost of commercial reaction wheels are often prohibitively expensive for university CubeSat programs, leading them to partially or fully forfeit attitude control, which severely limits mission capabilities. This

barrier is illustrated by the fact that of 483 nanosatellites launched between 2003 and 2016, less than 60% had full three-axis attitude control [9].

Table 1.1: Commercial CubeSat Reaction Wheels (2023)

Company	**Model**	**Mass (g)**	**Dimen -sions (mm x mm x mm)**	**Max Momentum (mNms)**	**Max Torque (mNm)**	**Lead Time**	**Price (USD)**
AAC Clyde Space	RW222 (3 mNms)	-	25 x25 x15	3	2	-	16200
AAC Clyde Space	RW222 (6 mNms)	-	25 x25 x15	6	2	-	-
Astrofein	RW1 Type A	25	21 x21 x12	0.58	0.023	-	11850
Astrofein	RW1 Type A	16	21 x21 x12	0.1	0.004	-	11850
Astrofein	RW25	250	50 x50 x25.5	30	2	-	12500
Berlin Space Tech	RW-05	1550	105.0 x106.6 x109.5	500	16	6 months	29750
Comat	RW20	180	48 x48 x28.2	20	2	6 month	16200

CubeSpace	Cube-Wheel S	60	28 x28 x26.2	1.77	0.23	12 weeks	5170
CubeSpace	Cube-Wheel S+	90	33.4 x33.4 x29.7	3.6	2.3	12 weeks	6550
CubeSpace	Cube-Wheel M	150	46 x46 x31.5	10.8	1	12 weeks	7540
CubeSpace	Cube-Wheel L	225	57 x57 x31.5	30.6	2.3	-	-
CubeSpace	CW0017	60	28 x28 x26	2.36	0.23	-	5170
CubeSpace	CW0057	115	35 x35 x24	9.5	4	-	7220
CubeSpace	CW0162	144	46 x46 x24	27	12	-	8950
CubeSpace	CW0500	400	67 x67 x25	83.3	10	-	11450
CubeSpace	CW1200	-	76 x76 x30	200	15	-	-

CubeSpace	CW2500	-	88 x88 x40	417	20	-	-
CubeSpace	CW5000	-	100 x100 x40	417	30	-	-
Rocket Lab	RW-0.003	50	33.5 x33.5 x17	5	1	-	15000
Rocket Lab	RW-0.01	120	50 x50 x30	18	1	-	20000
Rocket Lab	RW-0.03	185	50 x50 x40	40	2	-	25000
Rocket Lab	RW-0.06	226	77 x65 x38	180	20	-	35000
Serenum Space	RW25	40	25 x25 x25	0.6	0.2	6 weeks	2700

1.2.4 In-House Developed Reaction Wheels

For university CubeSat missions that require attitude control, the price points of commercial reaction wheels are prohibitively expensive and often drive these missions to design and develop in-house reaction wheels. Examples of university students designing CubeSat reaction wheels can be found in [10], [11], [12], [13], [14], [15], and [16]. Each of these sources cite lowering cost as the motivation behind developing in-house reaction wheels. As of the writing of this thesis, each of these designs have yet to be tested in space environment.

The most well-documented in-house development of a CubeSat reaction wheel is given by Bonafede [10] and Lee [12]. This section will use Bonafede [10] and Lee [12] as a case study for in-house developed reaction wheels for university CubeSats. Both Bonafede [10] and Lee [12] are written by students from the California Polytechnic State University, San Luis Obispo (Cal Poly SLO) - the birthplace of the first CubeSat and an institute with world-class CubeSat knowledge, facilities, and connections. Bonafede [10] is a Masters thesis in which the author designs and simulates a low-cost CubeSat reaction wheel and Lee [12] is a senior design project where the authors manufacture and test the reaction wheel design described in Bonafede [10].

Designing and manufacturing a reaction wheel is difficult for university students due to their resource constraints in time, money, knowledge, and experience. Lee et al. [12] successfully manufacture and perform benchmark testing of a single reaction wheel. Their estimated total cost of manufacturing their three reaction wheels is 2,237 USD - a significantly lower price when compared to commercial reaction wheel options. Lee et al.'s [12] report provides details of the issues that they encountered, which highlights the difficulties that university students face when developing a reaction wheel. Three of the main challenges - manufacturing, mounting, and testing - are discussed along with how Lee et al. [12] approached and resolved each of these challenges.

Manufacturing a reaction wheel is challenging due to the mechanical precision requirements of the wheel. The wheel of a reaction wheel must be precisely manufactured as misalignment of the center of mass and inertia axis of the wheel with the axis of rotation will cause undesired vibrations in the CubeSat. Most academic institutions do not have the precision manufacturing equipment required to meet the precision tolerances of a reaction wheel, as was the case for Lee et al. [12]. Using a Haas TL-1 CNC lathe, Haas VF3 mill, and Haas Mini mill, Lee et al. [12] manufactured an initial out-of-tolerance wheel and outsourced balancing of the wheel to a local vendor who shaved mass from the initial wheel manufactured in the university.

Another challenge in developing a reaction wheel is mounting the wheel to the shaft of the motor. The security of the wheel mounting has demanding requirements as it must withstand harsh launch and thermal loads. Initially, Lee et al. [12] designed the wheel to have

an interference fit with the motor shaft; however, this was changed to a large clearance fit due to concerns regarding bending the shaft. The clearance fit design required the team to use a shaft-locking adhesive. Adhesives can be difficult to work with as they can have inconsistent results due to challenges in consistent application of the adhesive, as described by Lee et al. [12] Additionally, adhesives require a curing process which can become fairly involved, sometimes requiring a vacuum chamber. After having difficulties with RT48 adhesive, Lee et al. [12] had success using 3M Scotch-Weld two-part Epoxy Adhesive for securing the wheel to the motor shaft. Due to the relatively high cost of the motors (approximately 300 USD each), it is expensive to test wheel fitting and adhering on flight units or engineering units; thus, Lee et al. [12] used test disks and test shafts to validate their processes.

Once the wheel is manufactured, balanced, and adhered, the reaction wheel must go through environmental testing to ensure that it would survive launch loads and be able to operate in the vacuum and microgravity environment of space, while undergoing thermal loads. The primary environmental tests performed for reaction wheels are vibration testing, shock testing, vacuum testing, and thermal vacuum (TVAC) testing. Each of these tests requires special in-house facilities and expertise which are not always available for students and are expensive to outsource. Cal Poly SLO has facilities for vibration, vacuum, and TVAC testing; however, Lee et al. [12] were not able to complete these tests due to time constraints caused by setbacks in manufacturing and assembly, issues arising in adhesive curing, and manufacturing of an attachment plate for vibration testing.

From this case study, it can be seen that in-house reaction wheel development is especially difficult for university students because it requires specialty equipment and knowledge and is time-demanding. Balancing the wheel requires precise CNC machines and/or outsourcing; wheel mounting requires development and validation of an elaborate process; and environmental testing requires special facilities and time to verify and validate processes. Although in-house design and development of CubeSat reaction wheels is effective as a cost-saving strategy, it is significantly expensive in time for university CubeSat programs, which are characterized by limited expertise and high turnover rates.

Furthermore, in addition to programmatic risks to their development timelines, university CubeSat missions that choose to develop in-house reaction wheels also incur significant

technical risks to their missions. Reaction wheels are notoriously prone to failure, even in large class missions such as the Hubble Space Telescope. According to [17], "Guidance, Navigation, and Control causes 28% of Civil satellite EOL failure and 24% of Military spacecraft failure, with reaction wheels and gyros being a root cause for a large portion of the failures." Three studies conducted by Saleh and Caste [18], Tafazoli [19], and Sperber [20] each conclude that the attitude control system is major driver of spacecraft failures and unreliability, with reaction wheels being a significant failure source.

1.3 Hard Disk Drive Reaction Wheels

Hard disk drives repurposed as reaction wheels show promising potential as a cost-effective and reliable solution for CubeSat attitude control. The uniform and well-balanced disk, high speed motor, and low-cost of the HDD make it a strong candidate for CubeSat reaction wheels. Figure 1.1 shows the angular momentum storage vs. price of commercial CubeSat reaction wheels available in 2023. Commercial CubeSat reaction wheels for 1U to 6U sized CubeSats cost between 2700 and 35000 USD. HDD-RWs on the other hand cost 50 - 200 USD, reducing reaction wheel price by 1 to 3 orders of magnitude while having comparable performance. HDD-RWs have the exciting potential of significantly lowering the cost of entry for university students to learn to design, test, and fly CubeSats with attitude control systems that can be afforded on university budgets.

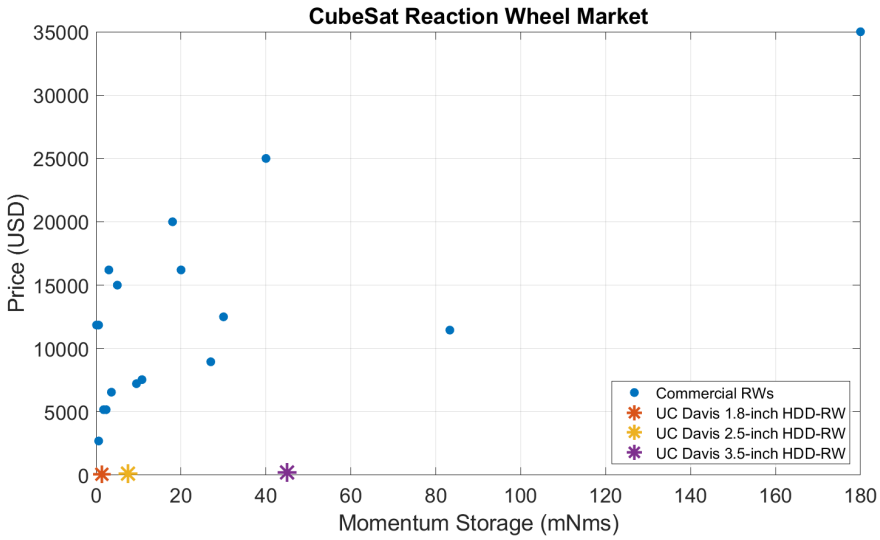

Figure 1.1: CubeSat Reaction Wheels Market

Furthermore, commercial reaction wheels have a typical lead time of 6 weeks to 6 months – a significant amount of time for CubeSat missions, considering that a spacecraft's attitude control system is highly coupled with other spacecraft systems and often requires the most time for integration and testing. HDD-RWs can be ready within 2 weeks, enabling CubeSat budgets and timelines to be significantly reduced. Cost reductions can lower barriers to entry, allowing resource-constrained organizations to develop CubeSat missions, while shorter development times can allow CubeSat developers to focus their efforts on payload development rather than reaction wheel development or procurement.

1.3.1 Literature Review

The idea of repurposing HDDs as CubeSat reaction wheels was first proposed in literature in 2018 by Sahar et al. [21] from the Israel Institute of Technology. Later in 2018, a second paper by the same group from the Israel Institute of Technology was published that described Drivesat - a student CubeSat mission to demonstrate HDDs as reaction wheels, which has not yet flown in space. Later in 2019, a conference paper published by Driedger et al. [22] from the University of Manitoba described TSAT5 - a student CubeSat mission to utilize HDDs as reaction wheels, which has also not yet flown in space. As of the writing of this thesis, these three papers are the only existing literature that discuss repurposing a HDD as a CubeSat reaction wheel and to this date, hard disk drive-based reaction wheels have yet to be flown in space.

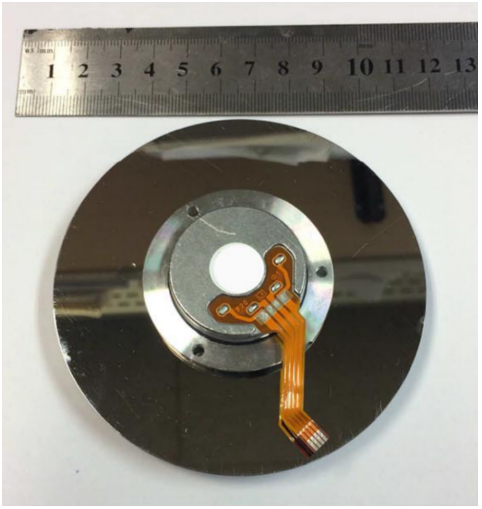

Figure 1.2: Institute of Israel HDD-RW [21]

1.3.2 UC Davis Development of HDD-RW

At the University of California, Davis, the student-led 2U CubeSat mission, REALOP, encountered the trade-off between purchasing expensive commercial reaction wheels and accepting mission and schedule risks to develop in-house designed reaction wheels. Upon literature review, the student team encountered the previously mentioned paper by Sahar et al. [21] on HDD reaction wheels. As the Attitude Determination and Control System (ADCS) leads for the REALOP mission at the time, Kylie Cooper and the author chose to adopt the idea for the REALOP mission in 2019. The REALOP mission aims to demonstrate a single 1.8-inch HDD, aligned with the CubeSat's longest axis, as a CubeSat reaction wheel.

Cooper and the author continued development of HDD-RWs as graduate students in the Center for Spaceflight Research (CSFR) at the University of California, Davis. They co-wrote the proposal to the NASA Flight Opportunities Program [23] to test the HDD-RW technology in microgravity parabolic flight [24] and subsequently co-led the Zero-G HDD project where they demonstrated the HDD-RWs.

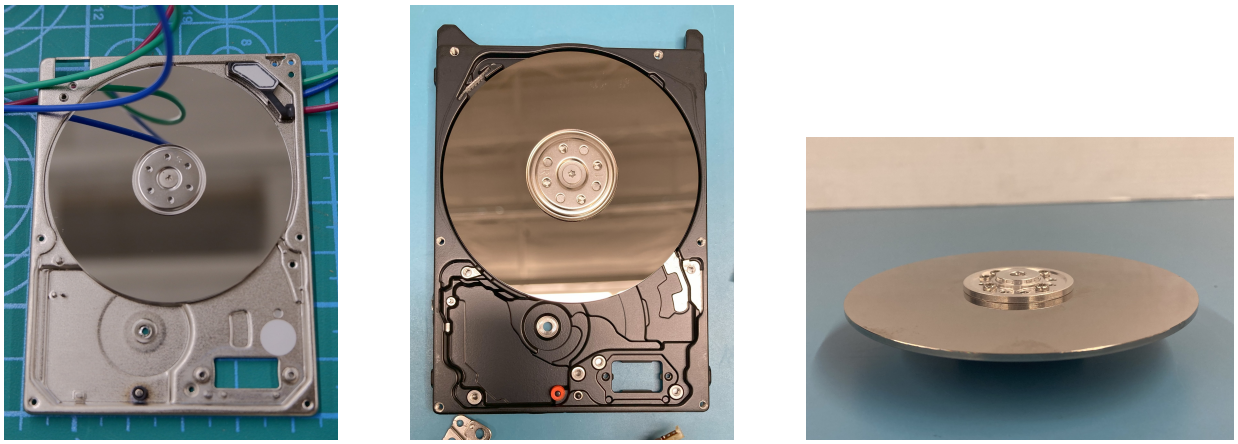

(a) 1.8-inch HDD-RW **(b)** 2.5-inch HDD-RW **(c)** 3.5-inch HDD-RW

Figure 1.3: UC Davis HDD-RWs

Through the Zero-G HDD project, the HDD-RW technology has been developed and tested in a lab setting and has been demonstrated to perform 3-DOF attitude stabilization and pointing of a CubeSat testbed in microgravity parabolic flight. Design of the parabolic flight experiment system is briefly discussed in Section 1.4; a detailed description of the parabolic flight experiment is described in Cooper's thesis [1]. Results from flight testing are presented in Section 3.4.

1.4 Microgravity Parabolic Flight Testing

Due to the dynamic nature of the reaction wheel's function, demonstrating the HDD-RWs performing their nominal operations of satellite stabilization and pointing requires three degrees of rotational freedom. Although one rotational degree of freedom is achievable through ground testing and each of the three rotation axes of a satellite could be tested individually, it is insufficient for demonstration of three-axis attitude control due to the coupled nature of rotational dynamics.

Short of operation in space, only a handful of methods exist by which three degrees of rotational freedom can be achieved, each with its own limitations. The most common type of three axis rotational is the spherical air bearing; however, most COTS spherical air bearings offer less than 45 degrees of roll and pitch capability [25] and in-house spherical air bearings, by design, can not exceed 90 degrees in roll and pitch. Microgravity parabolic flight is the only method that provides full three degrees of rotational freedom with virtually zero friction. The primary goal of this project is to perform three-axis stabilization and pointing of a CubeSat testbed in microgravity parabolic flight using HDD-RWs to demonstrate their function and performance as low-cost, reliable CubeSat reaction wheels. Demonstration of the HDD-RWs in microgravity environment serves as a stepping stone between ground testing and demonstration in space environment.

The HDD-RWs were tested in six microgravity parabolic flights during three flight campaigns in December 2021, June 2022, and November 2022. Each flight campaign consisted of two flights each on consecutive days. Each flight consisted of 30 parabolas that occurred in sets of 5. The first set of 5 parabolas were used for acclimation and consisted of 2 martian-g and 3 lunar-g parabolas; the remaining 25 parabolas were all zero-g. The parabola duration and quality varied by air conditions and pilots. Typically, the parabolas had a duration of 10 to 20 seconds and the microgravity quality was on the order of 10^{-2} to 10^{-3} g's. The microgravity parabolic flights and technology development for the HDD-RWs was funded by NASA Flight Opportunities program and the flights were provided by Zero-G Corp [26]. For each flight, the flight experiment was operated by the author, Kylie Cooper, and supporting researchers from the UC Davis CSFR. Further details on the parabolic flight experiment are discussed in Cooper's thesis [1].

The objectives of the HDD-RW microgravity parabolic flight experiment were as follows:

1. Collect data of the transient response of the HDD-RW to develop an actuator model.
2. Demonstrate the ability of the HDD-RW and controller system to stabilize rotation along an arbitrary 3D axis.
3. Demonstrate the ability of the HDD-RW and controller system to rotate to a pre-specified 3D orientation.

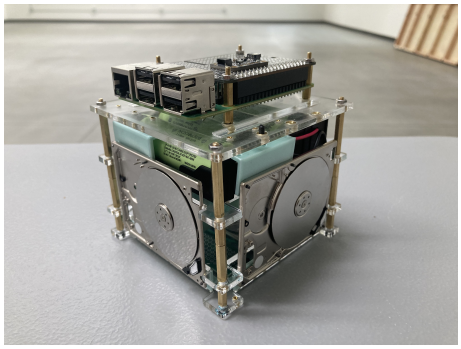

(a) 1.8-inch HDD-RW CubeSat without casing

(b) 2.5-inch HDD-RW CubeSat

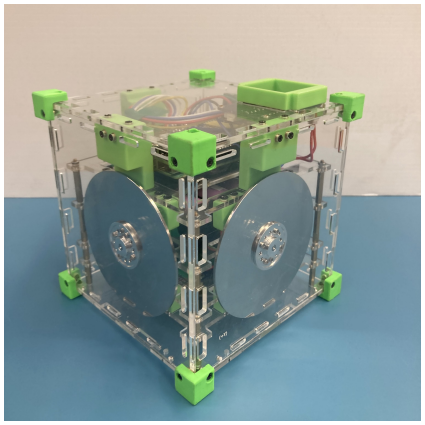

(c) 3.5-inch HDD-RW CubeSat with clear casing

Figure 1.4: HDD-RW CubeSats

To achieve these objectives, a CubeSat testbed platform, with a set of three HDD-RWs, was utilized in the microgravity parabolic flight experiments. The CubeSat testbed freely floated within the aircraft cabin during the microgravity period and was programmed to perform attitude control maneuvers using the HDD-RWs. Three different CubeSat testbed

designs were utilized for each of the three HDD-RW sizes. One 1.8-inch HDD-RW CubeSat, one 2.5-inch HDD-RW CubeSat, and two 3.5-inch HDD-RW CubeSats were manufactured in-house for the parabolic flight experiments.

Each CubeSat testbed is equipped with three orthogonally oriented HDD-RWs, ESCs for each HDD-RW, a Raspberry Pi 3B+ microcomputer, an IMU, a power sensor, a buck-boost voltage regulator, an interface display, 2 buttons, and a set of 18650 battery cells. The IMU measured the CubeSat testbed's rotation rate and appropriately commanded the HDD-RWs such that the CubeSat testbed performed the desired attitude maneuver. With the exception of one of the 3.5-inch HDD-RW CubeSats, each CubeSat face had a set of four unique ArUco markers that were used as a second system for pose estimation. Figure 1.5 shows a photograph of the 2.5-inch HDD-RW CubeSat floating inside the Chamber during parabolic flight. Figure 1.6 shows the electrical schematic for the 2.5-inch HDD-RW CubeSat. The 3.5-inch HDD-RW CubeSat has a similar electrical schematic, with the only difference being the HDDs used and their respective current draws.

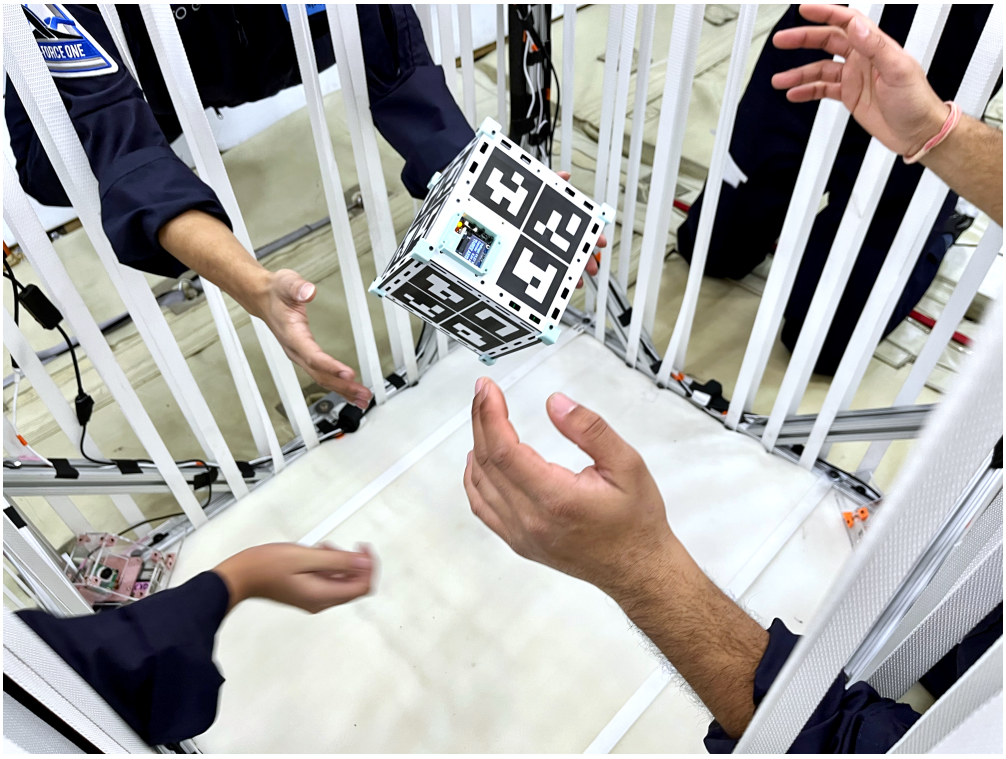

Figure 1.5: 2.5-inch HDD-RW CubeSat floating in Chamber

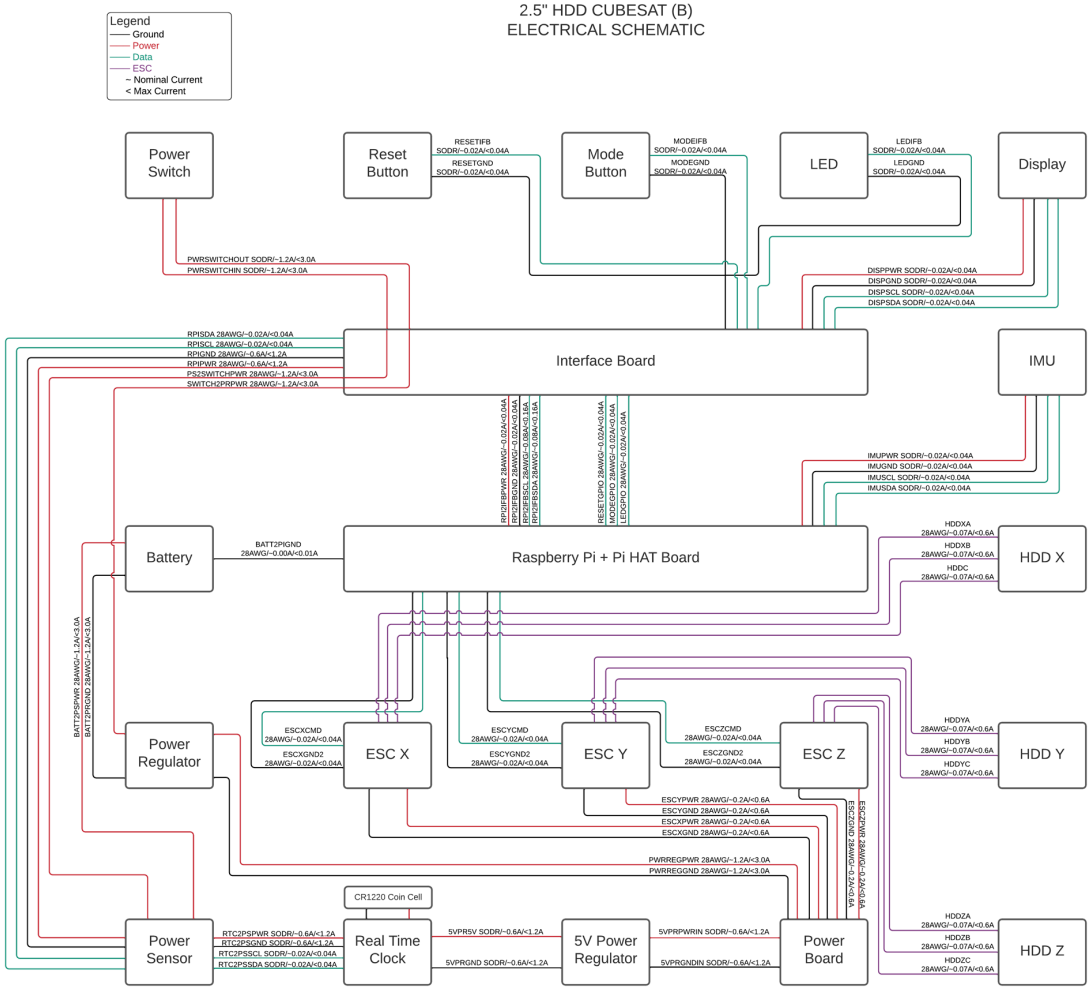

Figure 1.6: 2.5-inch HDD-RW CubeSat electrical schematic

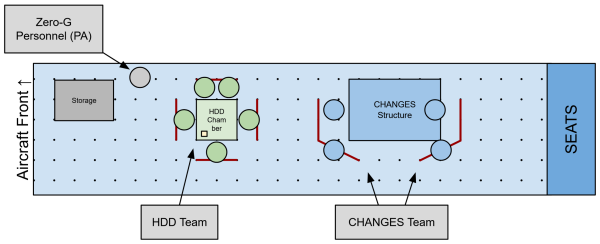

(a) Flight Campaign 1 Floorplan Configuration

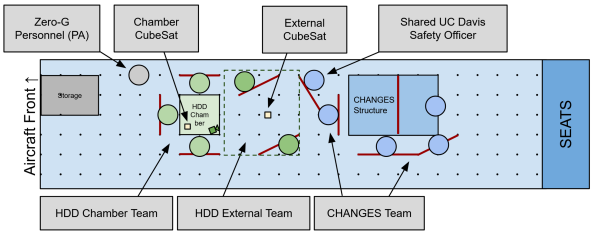

(b) Flight Campaign 2 Floorplan Configuration

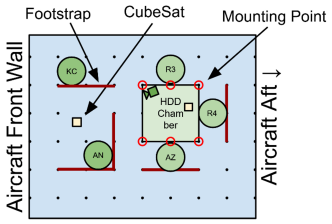

(c) Flight Campaign 3 Floorplan Configuration

Figure 1.7: Aircraft Floorplan Configurations

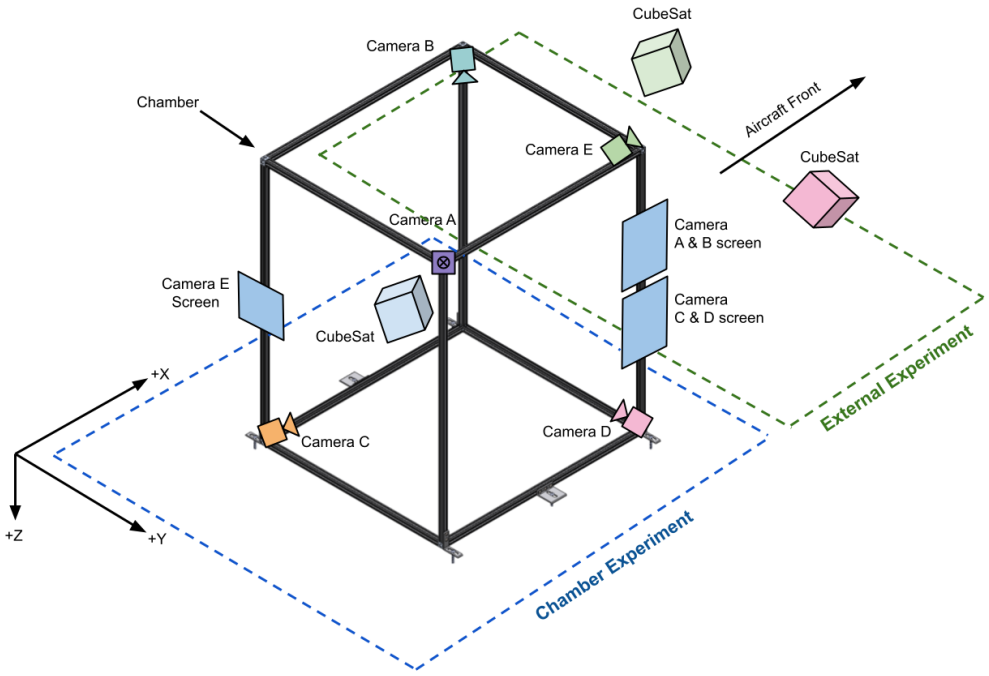

Figure 1.8: Flight Campaign 3 Configuration - Orthogonal View

Figure 1.9: Flight 5 External and Chamber Experiments

Two experiment setups were utilized during the parabolic flights: the Chamber Experiment and the External Experiment. During Flights 1 and 2, only the Chamber Experiment was conducted; during Flights 3, 4, 5, and 6, both the Chamber Experiment and External Experiment were conducted. The Chamber Experiment took place within an aluminum frame structure, referred to as the "chamber". The chamber enclosed the CubeSat of the Chamber Experiment to ensure a safe working space. The chamber was constructed using T-slotted 80-20 beams and had a width of 41.5 inches, length of 45 inches, and height of 51 inches. The chamber was mounted to the aircraft floor to allow for a fixed, rigid working space. The main purpose of the chamber was to: 1) restrict the CubeSat from floating away and potentially causing injury or damage, and 2) provide mounting for the computer vision (CV) system. Each face of the chamber was lined with fabric straps that were spaced such that the gap was narrow enough to prevent the Chamber Experiment CubeSat from escaping the chamber and wide enough such that a researcher could reach into the chamber and manipulate the CubeSat, as shown in Figure 1.10.

Figure 1.10: Researcher reaching for CubeSat through chamber straps

The External Experiment took place adjacent to the Chamber Experiment in a sectioned off area instead of an enclosure. Performing an experiment outside the chamber removed two constraints - the vertical height of the chamber that limited the vertical distance the CubeSat can traverse before contacting the floor or chamber's top straps and the longitudinal & lateral lengths of the chamber that limited the distance the CubeSat could traverse before contacting the chamber side straps. Elimination of these two constraints provided longer CubeSat floating time. Conducting an experiment within the chamber was still necessary in the case that the External Experiment became too dangerous due to unforeseen circumstances such as more aggressive parabolas or multiple experiment operators not feeling well enough to perform the External Experiment.

The computer vision (CV) system consisted of five camera assemblies mounted to the corners of the chamber, as shown in Figure 1.8. Four cameras pointed towards the center of the chamber and recorded the Chamber Experiment, while the fifth camera recorded the External Experiment area. Each camera assembly consisted of an adjustable focus 12 MP camera, a Raspberry Pi 3B+ computer, and an IMU. The videos and IMU data were post-processed to perform pose estimation of the CubeSat. The CV system and its data are discussed in further detail in Cooper's thesis [1].

Over the course of the three flight campaigns, two types of attitude control tests were performed in flight - stabilization and pointing - demonstrating crucial CubeSat attitude control maneuvers. During the stabilization tests, the CubeSat testbed was manually given a random initial rotational velocity along an arbitrary axis, which the CubeSat testbed stabilized using all three of its HDD-RWs. During the pointing tests, the HDD-RWs re-oriented the CubeSat testbed along a predetermined axis by a predetermined angle, requiring all three HDD-RWs. Results from parabolic flight are presented in Section 3.4.

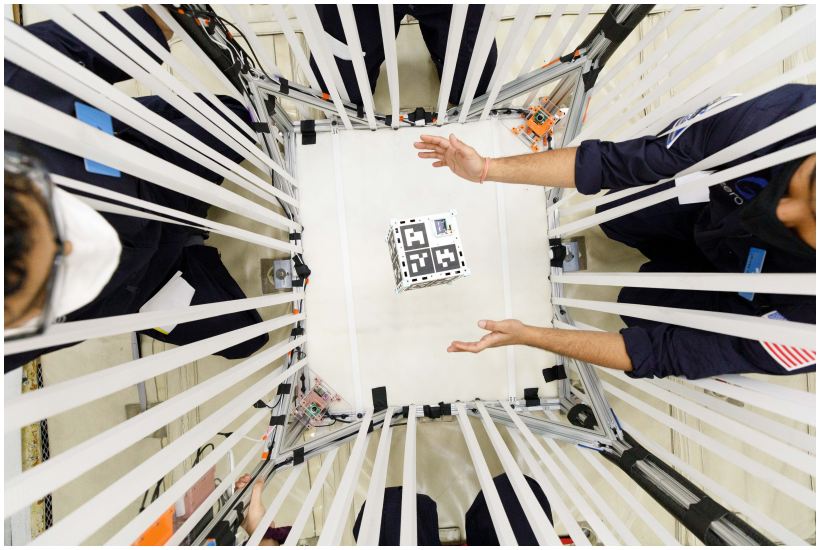

Figure 1.11: Top view of CubeSat floating in chamber

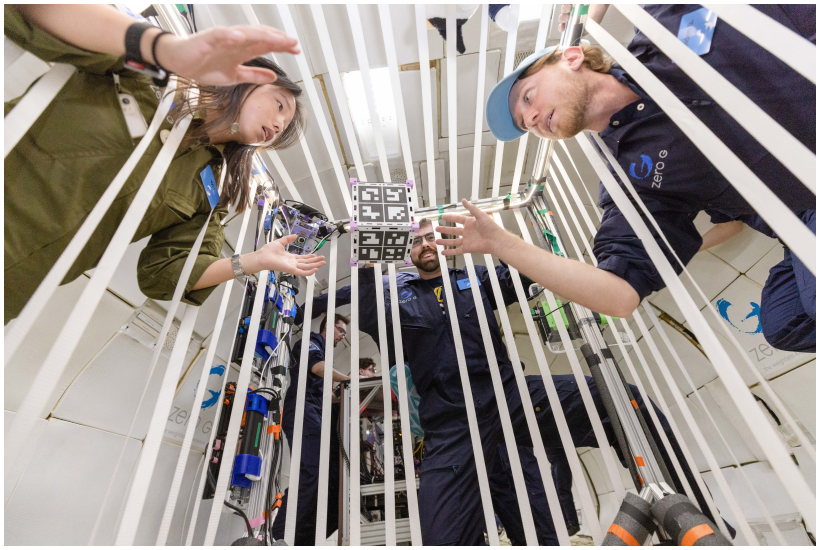

Figure 1.12: Bottom view of CubeSat floating in chamber

Chapter 2

Hard Disk Drive Reaction Wheel Hardware, Implementation, & Compatibility in Space Environment

2.1 Introduction

As described in Section 1.2, the trade-off between the high costs of commercial reaction wheels and risk of in-house manufactured reaction wheels is a pain point for many CubeSat developers. The high cost of reaction wheels often leads small companies and universities to manufacture their own reaction wheel systems. Due to the limited amount of resources available to these CubeSat developers, the in-house manufacturing of reaction wheels has proven to be a major root-cause for premature failures of small satellites [17].

This chapter will provide a background on HDD technology, describe the HDD-RW implementation used for this project, present preliminary environmental testing results, and discuss potential effects of the space environment on HDD-RWs. Section 2.2 introduces the HDD technology and its major components. Section 2.3 describes the HDD-RW implementation for this project. Section 2.4 discusses the compatibility of HDD-RWs in the space environment and presents results from preliminary environmental testing.

2.2 Hard Disk Drives as Memory Storage Devices

Before describing Hard Disk Drive Reaction Wheels, it is beneficial to understand the HDD technology. This section will briefly describe the components that comprise a modern

HDD; the following section will describe the implementation of the HDD-RW used. Most of the information in this section is gathered from [27], which the reader is encouraged to reference to find further information on HDD design, mechatronics, and controls.

2.2.1 Background on Hard Disk Drives

Hard disk drives (HDDs) are data storage devices that are mass-produced and available as commercial-off-the-shelf (COTS) products. They play a critical role in data storage for servers, data centers, and everyday desktop/laptop computer users. HDDs are relatively inexpensive, costing approximately 50 to 300 USD. This low-cost has been driven by two factors - their decades-long technology development and their mass-production which is currently on the order of hundreds of millions per year, as of 2023 [28]. With the advent of solid-state drive (SSD) memory devices, HDD production rates are declining; however, the hundreds of millions production volume of hard drives [28] overshadows the CubeSat launch rate which is on the order of thousands per year as of 2023 [29]. Furthermore, refurbished HDDs may still be used as HDD-RWs, as demonstrated in this research.

The decades of technology development has evolved the HDD into a robust precision instrument. HDDs have been described using the following analogy [27]:

"*Imagine an airplane flying at 5M miles per hour but only 1/16 inch above the ground on a highway with 100,000 lanes where the width of each lane is only fraction of an inch. The challenge of the problem is further intensified by the fact that the airplane is expected to switch lanes frequently and then follow the new lane with the same precision. A scaled down version of this scenario is what one finds in the head positioning servomechanism of an HDD.*"

To meet customer demands in data speeds and reliability, the industry has made advancements in several disciplines such as motor and actuator design, mechanics, tribology, material science, and manufacturing technology. HDDs are typically designed to operate between 5 and 60 degrees Celsius and can withstand mechanical shock on the order of 10 to 100 G's. HDDs are typically designed for a lifetime of 3 to 5 years.

HDD designs have been standardized such that they may fit in different desktop and laptop models. The standard HDD sizes are known as form factors and refer primarily to the external dimensions. Several HDD form factors have been developed; today, the most

common HDD form factors used today are 3.5-inch and 2.5-inch HDDs.

2.2.2 Main Components of Hard Disk Drives

The main components of the HDD are the disk, spindle motor, and the actuator assembly. The disk stores the data, the spindle motor spins the disk, and the actuator assembly positions the read/write arm above the disk to read and write data. Each of these components are described in further detail below.

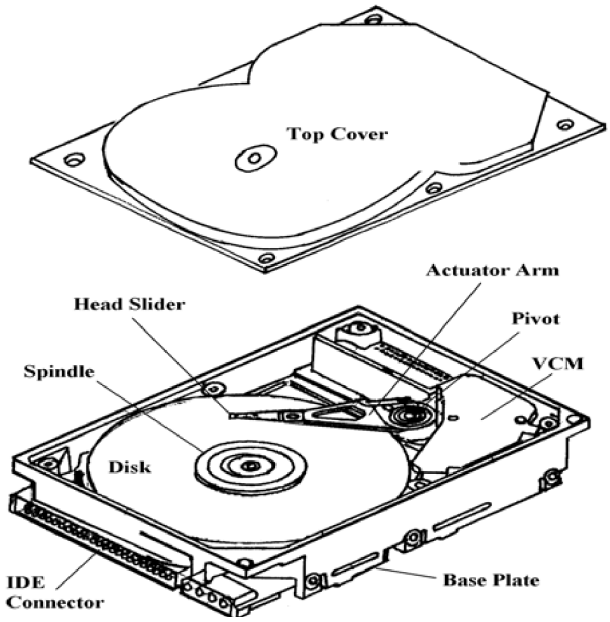

Figure 2.1: HDD Components [27]

Disk

HDDs digitally store data by magnetically encoding bits on the magnetic layer of a disk, sometimes called a platter. Many HDD models are designed to store more data by using multiple disks stacked together on a common spindle. The magnetic layer of the disk consists of annular sectors that store data bits that are read by read and write heads. The head actuator precisely controls the position of a slider holding the read and write heads over the disk. The read and write heads operate in close proximity to the disk to read and write the magnetized bits on the disk. Well characterized aerodynamic surfaces [30] on the read and write heads as well as a uniformly smooth disk surface enables the read and write heads to float approximately 5 nanometers above the disk surface on an air bearing. In order

for the disk to be extremely smooth for the read and write heads and durable for consumer use, the disk is precisely manufactured from an aluminum, glass, or ceramic substrate and coated on both side with a thin layer of magnetic material by a vacuum deposition process.

Spindle Motor

A three-phase outrunner brushless DC (BLDC) motor spins the disks at precisely regulated speeds to enable fast data reading and writing. A fixed disk speed ensures consistent read and write rates which is critical to ensure that the data is being read from and written to the correct location on the disk. Common spinning rates used in today's HDDs are 7200, 10000, and 15000 RPM. The HDD motor spins the disk in a fixed direction during use - most commonly counterclockwise (when viewed from above the disk). Most HDD motors utilize wye-connected three-phase windings, as opposed to delta-connected, due to their lower cost. Most HDD motors use 4 or 6 pole-pairs.

The rotating shaft in the HDD is supported by a bearing. Older HDD designs tended to use ball bearings; however, modern HDD designs mostly use spindle motors with an integrated fluid dynamic bearing (FDB). FDBs enable greater speed control which permits higher track density and thus higher data storage. In an FDB, illustrated in Figure 2.2, the rotating shaft is supported by dynamic pressure from rapidly moving lubricant. Grooves around the circumference of the shaft as well as on its base facilitate the dynamic stiffness of the FDB.

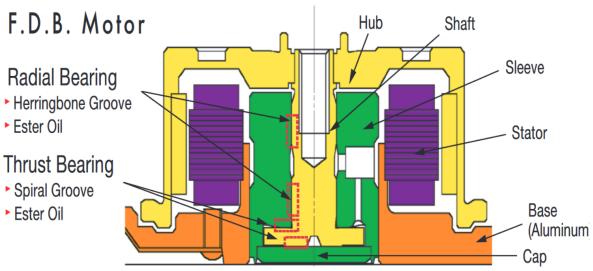

Figure 2.2: Fluid Dynamic Bearing (FDB) Diagram [31]

Actuator Assembly

The main components of the actuator assembly are the head actuator which dynamically positions the read/write arm and the read and write heads that transfer data from and to the disk. The head actuator uses a voice coil motor to precisely and quickly move the

read/write arm to the appropriate memory sector of the disk. HDDs with multiple disks have one actuator assembly per disk; some models have one arm for each side of the disk. The end of each arm has a slider which provides fine position control of the read and write heads above the disk. This allows the HDD to read from or write to different memory sectors of the disk. The slider has an aerodynamic design that allows it to float above a cushion of air between itself and the disk.

2.3 Description of Implementation of HDD-RW

2.3.1 Summary

This project tested HDD-RWs based on 1.8-inch, 2.5-inch, and 3.5-inch hard disk drive models. Table 2.1 shows models that were selected. Each of the HDD-RW's motors were controlled by a COTS electronic speed controller (ESC). The ESC was powered by a set of lithium cells in parallel. Details of the HDD-RW implementation are given in Sections 2.3.2, 2.3.3, 2.3.4, and 2.3.5. A guide detailing the process to convert a HDD into a HDD-RW is given in Chapter 4.

Table 2.1: HDD models modified into HDD-RWs

HDD Form Factor	Manufacturer	Model	Purchased Cost (2020, USD)
1.8-inch	Samsung	HS030GB	14.00
2.5-inch	HGST	Travelstar Z7K500-500	23.00
3.5-inch	Samsung	Spinpoint HD161HJ	56.00

2.3.2 Selection of Hard Disk Drive Models

Several HDD form factors and models exist which can be repurposed as reaction wheels. This project examined the 1.8-inch, 2.5-inch, and 3.5-inch hard drive form factors as they are best suited to fit within the dimensional constraints of CubeSats. HDDs of the same form factor are identical or similar in external dimensions, mounting points, disk mass and dimensions, and disk rotational speeds; however, they differ in number of platters and power. This project examined the HDD models that have the highest availability to allow future HDD-RW users to use the same models. Table 2.1 shows models that were selected for this

project along with their purchase costs.

2.3.2.1 1.8-inch HDD-RW Selection

The smallest HDD form factors that have been mass-produced are the 1.8-inch, 1.3-inch, 1-inch, and 0.85-inch HDDs, all of which have become obsolete due to the advances in flash memory storage. Of the smallest HDD form factors, the 1.8-inch HDD is the most available today due to the high number of sales of Apple's iPod Classic. From Apple's release of the 1st generation iPod Classic in 2011 until its discontinuation with the 6th and final generation in 2014, each iPod Classic used a 1.8-inch HDD. Based on sales of iPods from 2001 to 2014, it can be estimated that the number of iPod Classics sold is on the order of 10's of millions. Although they are no longer manufactured, thousands of iPod Classics and hundreds of individual 1.8-inch hard drives can be found for sale online, while the smaller HDD form factors are rare to find. The 1.8-inch HDD form factor is just 78.5mm along its longest edge, making it a suitable option for CubeSats as small as 1U to 3U. Due to its high availability and compact size, the 1.8-inch HDD was selected to be tested as a HDD-RW.

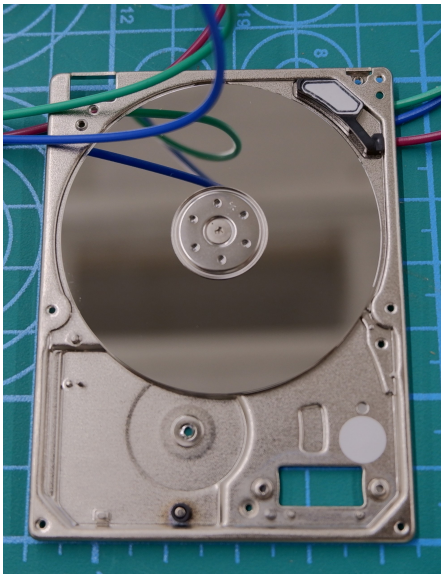

Figure 2.3: 1.8-inch HDD-RW

2.3.2.2 2.5-inch and 3.5-inch HDD Selection

The 2.5-inch and 3.5-inch HDD form factors are by far the most widely used and are still manufactured (as of 2022). Over 200 different companies have manufactured HDDs, of

which only three manufacturers still exist due to bankruptcies, mergers, and acquisitions - Seagate, Toshiba, and Western Digital. Due to their wide availability, the HGST Travelstar Z7K500-500 model HDD was selected for the 2.5-inch HDD-RW and the Samsung Spinpoint HD161HJ model HDD was selected for the 3.5-inch HDD-RW. All HDD-RWs tested were originally refurbished HDDs purchased from eBay or Amazon.

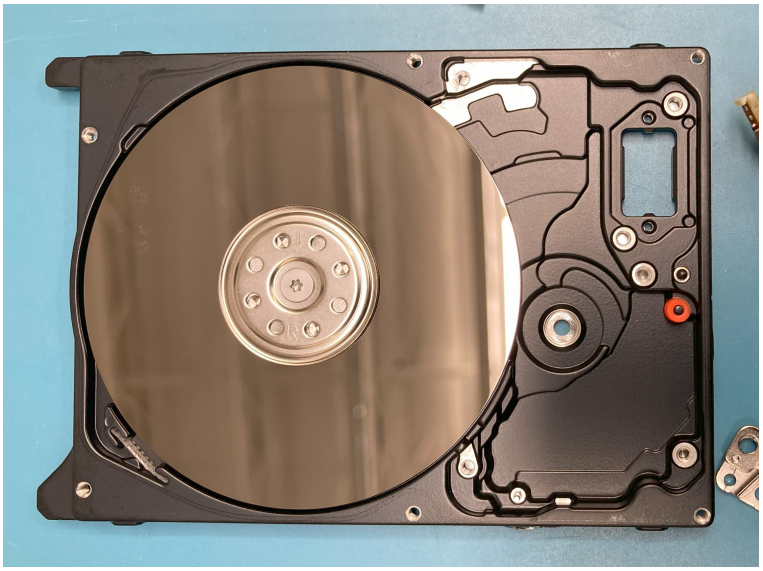

Figure 2.4: 2.5-inch HDD-RW

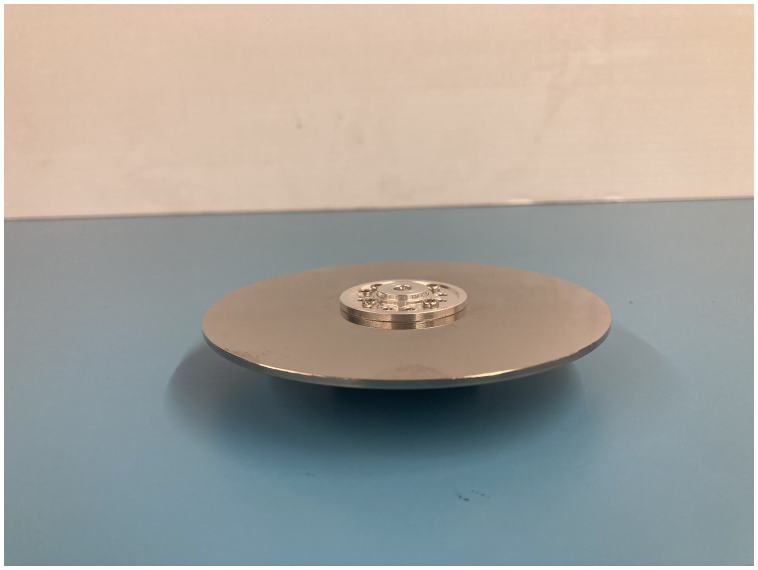

Figure 2.5: 3.5-inch HDD-RW

2.3.3 Modifications of HDDs

For each of the three HDD form factors tested, the read and write arm was removed to avoid contact between the arm and the disk, which would have caused undesired friction. Although the read and write arm is designed to float above the disk and never make contact with the disk, vibration and shock loading during rocket launch of the HDD-RW may have caused head crash. Head crash is a well-known mechanical failure, shown in Figure 2.6, of HDDs where an abrupt motion, such as impact with the ground after a fall, causes the read-write arm to make contact with the disk and possibly causing permanent damage.

Figure 2.6: Hard Disk Drive Head Crash [32]

The 1.8-inch and 2.5-inch HDD-RWs were used within their casing with their cover removed. The casing of the 3.5-inch HDD motor and disk was removed for the 3.5-inch HDD-RW, which significantly reduces its mass and volume. Jumper wires were soldered to the electrical pads on the 1.8-inch, 2.5-inch, and 3.5-inch to electrically connect the HDD-RW motors and the ESC. Electrical connection options suitable for space environment are discussed in Section 4.1.3.

2.3.4 Electronic Speed Controller

Brushless DC (BLDC) motors require a motor controller, often referred to as an electronic speed controller (ESC). The ESC is a device that drives a BLDC motor to a commanded speed by converting power from a DC supply into dynamic, coordinated voltage signals sent

to each of the BLDC motor's phases. The ESC is a critical component that has a large influence on control, performance, and behavior of the BLDC motor.

The ESC of a HDD is integrated within the PCB of the HDD. Because the HDD's factory installed ESC is designed to spin the HDD at a constant speed and in a single direction, it must be replaced for the HDD-RW. In this project, each of the HDD-RWs utilized COTS ESCs to control the HDD motors. The 1.8-inch HDD-RWs were each controlled by a Readytosky bidirectional 20A ESC [33]. The 2.5-inch and 3.5-inch HDD-RWs were controlled by a iFlight SucceX-E F4 V2 4-in-1 ESC [34]. The iFlight ESC was used to independently control the three HDD-RWs within the CubeSat testbed. The HDD-RWs may also be driven using a custom ESC - this ESC solution is further discussed in Section 4.1.2.2.

2.3.5 Power Supply

The UC Davis HDD-RW ESCs were powered by standard 18650 lithium cells, which are commonly used in CubeSats. The 1.8-inch HDD-RW ESCs used four Panasonic NCR18650B cells in series while the 2.5-inch and 3.5-inch HDD-RWs used five Samsung 30Q cells in series. The 2.5-inch and 3.5-inch HDD-RWs required higher power - thus they used the 30Q cells which have a max current rating of 15A, instead of the NCR18650B cells which have a max current rating of 4.87 A. The peak current draw measured from the 1.8-inch, 2.5-inch, and 3.5-inch HDD-RWs is 0.6 A, 0.6 A, and 1.0 A, respectively. The 1.8-inch HDD-RW used only four cells due to the volume constraints of the 1.8-inch HDD-RW CubeSat.

The voltage from the series of cells were regulated to 12V for the 1.8-inch and 15V for the 2.5-inch and 3.5-inch HDD-RWs. A COTS buck-boost converter, the DROK LM2596 [35], was used to regulate the voltage. The max current of the DROK LM2596 is 3.0 A. The input capacitors of the ESCs dampen voltage fluctuations from the power supply.

Table 2.2: HDD-RW Power Supply

HDD Form Factor	Voltage (V)	Peak Current (A)	Peak Power (W)
1.8-inch	12.0	0.6	7.2
2.5-inch	15.0	0.6	9.0
3.5-inch	15.0	1.0	15.0

2.3.6 Generality of Results

Due to the possible unavailability of the specific HDD models demonstrated as HDD-RWs, it is important to consider the generality of results of specific HDD models tested being extrapolated to other HDD models. The most critical hardware component in the HDD-RW that may lead to variations in reliability across different models is the HDD spindle motor. Since HDD manufacturers do not provide information on their HDD spindle motor suppliers, it is not possible to guarantee that different HDD models use the same spindle motor model. However, it is very likely that different spindle motors will behave similarly due to their identical or near-identical design constraints and requirements.

Only a handful of companies manufacture the majority of HDD spindle motors. As of 2021, 85% of the HDD spindle motor market share is supplied by the Japanese company Nidec [36]. The 3.5-inch HDD-RW tested in this study uses a Nidec spindle motor. The manufacturers of the 1.8-inch and 2.5-inch HDD-RWs studied are unknown.

One of the most common failure points of BLDC motors is the bearing. For several years prior to 2010, ball bearings were the most common type of bearing used in HDD spindle motors. However, as HDD designs have continued to evolve to meet demands, they have transitioned to the use of fluid dynamic bearings (FDBs) due to their better performance in higher speeds, lower noise, and improved reliability [31]. Since 2010 HDD spindle motors almost exclusively use FDBs. All of the HDD-RWs demonstrated in this study use FDBs.

2.4 Compatibility of Hard Disk Drive Reaction Wheels in Space Environment

Ensuring that components operate in space as expected and do not exhibit failures and/or limited performance due to launch loads or the space environment necessitates environmental testing. The most critical space environmental factors include: microgravity, radiation, vacuum, vibration & shock, and extreme thermal conditions. Demonstration of the HDD-RWs in microgravity parabolic flight has shown that the HDD-RWs are capable of performing CubeSat attitude maneuvers; the next step for the HDD-RWs is to perform environmental testing and demonstration in space. Although environmental testing and demonstration in space are outside of the scope of this project, the potential impacts of environmental factors

on the HDD-RWs are discussed.

Reaction wheel failures due to environmental factors can be broadly classified in two categories - early failures due to exceeding of a physical limitation and long-term failure due to degradation. Since reaction wheels consist of moving elements, they degrade over time and are oftentimes the limiting factor of a satellite's lifetime [8]. Moreover, their dynamic nature may cause a runaway effect of issues that initially had only been minor. For example, a small radial displacement of a reaction wheel motor spindle due to rocket launch loads may cause adverse motor vibrations due to imbalance, which may cause bearing wear, leading on to further increase in motor vibrations. Therefore, for reaction wheel designs, it is important to both assess whether the reaction wheel will survive the launch and space environment as well as evaluate how long they will be able to perform their function in the space environment.

In this section, potential early failures of the HDD-RWs due to the critical space environmental factors are first discussed and then followed by discussion of degradation of the HDD-RW in space environment. Environmental effects on the HDD-RW lubricant will be emphasized as motor degradation often occurs due to lubrication loss, which may be caused by lubricant evaporation, degradation, and migration.

2.4.1 Microgravity

The microgravity environment of space poses a risk to motors as fluid surface tension forces become more significant and may cause lubricant to migrate such that an insufficient amount of lubricant within a region of the bearing causes metal-on-metal contact, resulting in abrasion. In this project, the HDD-RWs have successfully functioned in microgravity parabolic flight. Additionally, the International Space Station (ISS) as well as several ISS experiments have successfully used HDDs as memory storage devices on orbit for extended periods of time. The HDD-RW parabolic flight demonstrations along with the long-term use of HDDs on the ISS indicates that the microgravity environment of space will likely not fail due to microgravity environment.

It should be noted that HDDs on the ISS have failed and have been routinely swapped. Although the causes of the HDD failures on the ISS have not been published, the failures were likely due to either radiation-induced magnetic memory failures or mechanical wear-out failures. While magnetic memory failures are not a concern for HDD-RWs as their purpose

is not memory storage, mechanical wear-out failures are relevant to the HDD-RWs - this is discussed in Section 2.4.6. It should also be noted that newer HDD models have a free fall sensor that automatically stops rotation of the HDD disk if the HDD is detected to be in free-fall. The free-fall feature is not an issue for HDD-RWs in microgravity as the original HDD's circuit board is removed.

2.4.2 Radiation

Space radiation poses a risk to both mechanical and electrical components of a satellite. Charging within the motor bearing caused by charged particle radiation may lead to accelerated degradation. Particle radiation may also cause single event effects in the HDD-RW ESC which could lead to consequences ranging in severity from a momentary error to permanent failure.

The effects of radiation on HDDs have been studied in [37] and [38]. Both studies observe HDD data failures caused by radiation; however, the failures do not occur in the HDD motor. In [37], the HDD failure points are identified to be the interface circuit and the read subsystem and in [38], the failure occurs in reading data and is resolved by power cycling the HDD. Both of these studies indicate that space radiation likely has negligible effects on the HDD-RW motor.

Similar to every electrical component of a satellite, the HDD-RW ESC is susceptible to failure due to radiation. Single event effects may cause soft or hard errors in the ESC that may result in a variety of possible failures. The failure may have no significant consequence, such as a single event upset that causes the ESC to command an incorrect but valid speed, or the failure may have severe consequence, such as a single event gate rupture in one of the ESC's MOSFETS causing permanent failure of the ESC. The likelihood of ESC failure due to radiation is dependent on the ESC model used and is difficult to predict. University CubeSat missions are relatively short in duration and generally have high risk tolerance, thus effects of radiation on most CubeSat components, including reaction wheel ESCs, are often considered to be acceptable risks. If higher radiation tolerance is desired, the ESC may be placed within a shielded enclosure.

2.4.3 Vacuum

The vacuum environment poses a risk to the HDD-RW motor lubricant as the lubricant may offgas - resulting in accelerated degradation or possibly short-term failure of the HDD-RW. At the UC Davis Center for Space Flight Research, the 2.5-inch HDD-RW were tested in a low-vacuum environment with a pressure of 6.5 kPa. During the test, the HDD-RW was commanded to a predetermined sequence where it sped up in the counter-clockwise direction, slowed down to a stop, sped up in the clockwise direction, and finally slowed down to a stop. The HDD-RW was observed to spin with no observed anomalies or damage. The current draw of the HDD-RW had no significant difference before and after vacuum testing. During vacuum testing, the current draw of the HDD-RW was observed to be approximately 30 - 40% lower than in atmosphere in both the counter-clockwise and clockwise directions - this is an expected result as there is no air resistance in vacuum, leading to less power required to run the motor at the same speed. Although the vacuum testing was not conducted at standard higher vacuum levels due to limited lab resources, the results provide more confidence in the HDD-RW technology performance in the space environment. Longer duration vacuum testing of the HDD-RWs at high-vacuum levels is necessary to confirm if offgasing of the bearing lubricant may occur in space.

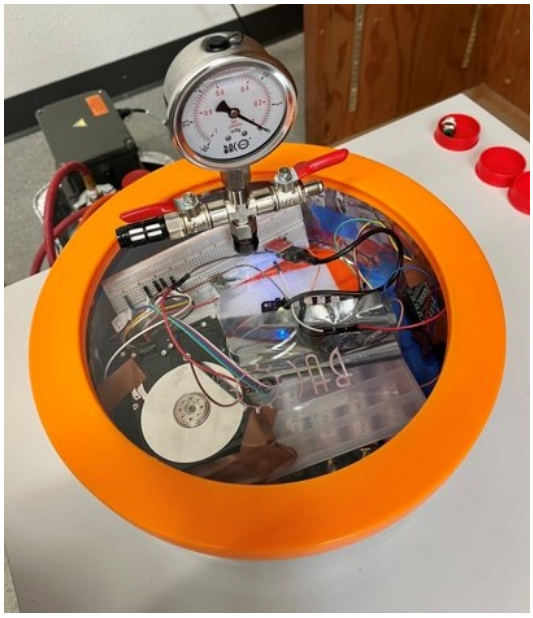

Figure 2.7: 2.5-inch HDD-RW Vacuum Testing

2.4.4 Vibration & Shock

Vibration and shock loads during rocket launch pose a risk of mechanical damage to the HDD-RW motor. HDDs are designed to withstand high vibration and shock loads. The 1.8-inch, 2.5-inch, and 3.5-inch HDD models used for HDD-RWs in this project are designed to withstand 1500 G's, 1000 G's, and 350 G's, respectively for 1 - 2 milliseconds. While acceleration loads during launch last on the order of minutes, the high shock specifications are a promising indicator that HDDs may survive the launch environment. HDDs have also functioned successfully on the ISS after being launched on board the Space Shuttle and Soyuz Rocket.

Preliminary vibration testing of the 2.5-inch HDD-RW was performed at the UC Davis Center for Geotechnical Modeling. During the vibration test, a 2.5-inch HDD-RW was vibrated along each of its three orthogonal axes with the frequency profile adhering to the NASA GEVS standards [39]. Before and after the vibration tests, the HDD-RW was commanded to a predetermined sequence where it sped up in the counter-clockwise direction, slowed down to a stop, sped up in the clockwise direction, and finally slowed down to a stop. The HDD-RW current draw shows no significant difference between testing before and after vibration, as shown in Figure 2.9.

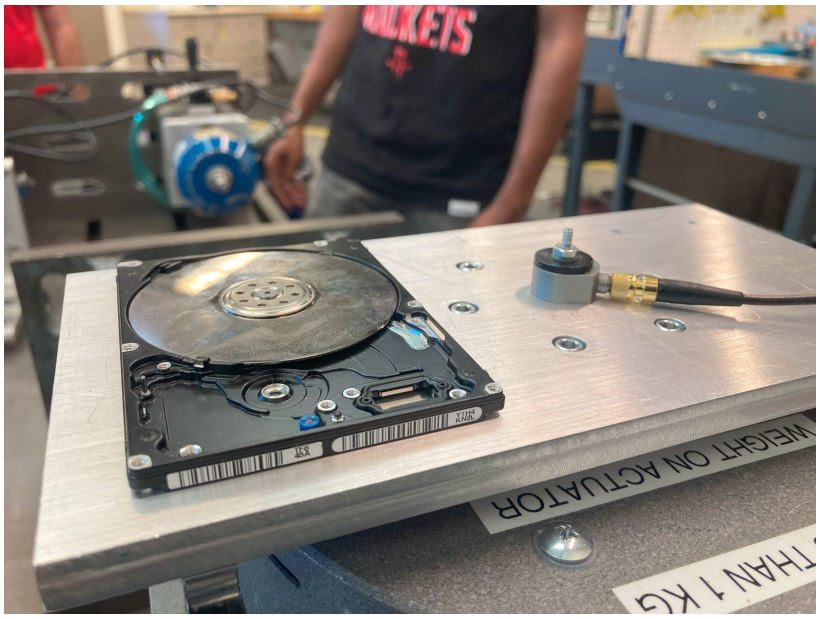

Figure 2.8: 2.5-inch HDD-RW Vibration Testing

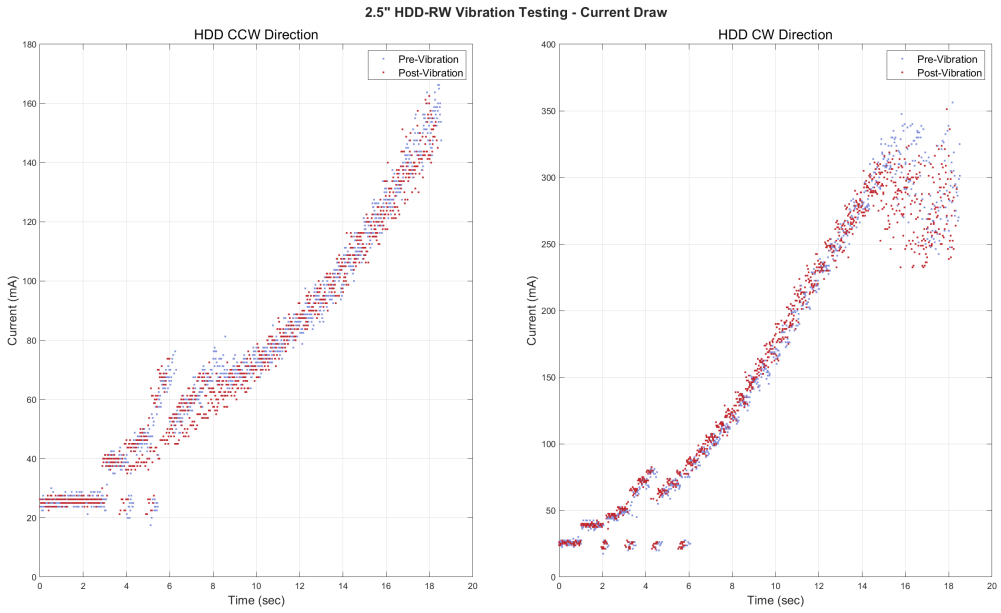

Figure 2.9: 2.5-inch HDD-RW Vibration Testing Results

The results from the preliminary vibration testing of the 2.5-inch HDD-RW suggest that the HDD-RW would likely survive the launch environment. Shock testing as well as further vibration testing is recommended for the HDD-RWs. In addition to the current draw, it would be valuable to compare the HDD-RW speed before and after vibration & shock loading. It is also recommended to verify that the electrical connection used between the HDD and ESC survives vibration and shock loads.

2.4.5 Thermal

The extreme temperature ranges in space environment poses a risk to the HDD-RW motor lubricant as the lubricant may undergo evaporation or gelation - resulting in accelerated degradation or possibly immediate failure of the HDD-RW. Additionally, thermal gradients may cause mechanical failure in the bearing due to thermal expansion or contraction. HDDs are typically designed to operate in 5 to 60 degrees Celsius. Thermal-vacuum (TVAC) testing of the HDD-RWs is critical to verify behavior of the lubricant under coupled effects of vacuum and thermal extremes.

2.4.6 Degradation

Due to their degradation rate, reaction wheels are often the limiting factor of a spacecraft's lifetime [8]; therefore, it is important to understand the expected lifetime of the HDD-RWs and techniques to minimize degradation for the HDD-RWs. HDDs typically have a design life of 2 to 5 years - this should be considered an upper limit to the lifetime of the HDD-RW as variable rotational speeds and the space environment will likely hasten the rate of degradation. If the HDD-RW has previously been used as an HDD for a long period of time, then its expected lifetime as a HDD-RW should be expected to be shorter. To minimize degradation of flight units, ground testing of the HDD-RWs should be performed with test units. However, rather than using new or almost-new HDDs for flight, it is recommended for the flight units to go through a wear-in process in both directions to ensure that they do not exhibit early failure due to potential manufacturing defects. Additionally, it is recommended for the attitude controller to utilize a torque limiting feature to minimize bearing wear of the HDD-RW.

To quantify the lifetime and reliability over time of the HDD-RWs, their degradation should be studied. Bearing lubrication is the principal life-limiting factor for reaction wheels [8]. Accordingly, the HDD-RW component that is most likely vulnerable to launch loads and the space environment is the bearing lubricant. Lubricant loss may occur by several different mechanisms and heavily depends on the pressure and temperature of the lubricant. Therefore, long-duration testing of the HDD-RWs in TVAC or space environment is important to quantify their performance over time. Such testing has not been performed during this research, but recommended for future development studies and implementation.

Chapter 3

Attitude Control with Hard Disk Drive Reaction Wheels

3.1 Introduction

The goal of this project was to raise the TRL of the HDD-RWs from TRL 4 to TRL 6 [40]. This was achieved by demonstrating attitude control in microgravity environment induced by parabolic flights. This chapter discusses modeling of the HDD-RW, development of the controller, results from parabolic flight, system-identification from flight results, and simulation. In Section 3.2, the process of developing the 2.5-inch and 3.5-inch HDD-RW actuator models is discussed. In Section 3.3, the stabilization and pointing controllers are described along with a keep-out-zone algorithm for the HDD-RWs and results from ground testing are presented. In Section 3.4, flight results of the 2.5-inch and 3.5-inch HDD-RWs are presented and discussed. And lastly, in Section 3.5, the process of system identification from flight data is presented and results from simulation of the system model are presented.

3.2 HDD-RW Actuator Modeling

To perform attitude control, an actuator model of the HDD-RWs was developed from ground testing. The HDD-RW actuator was composed of an ESC that converts ESC commands to current and the HDD motor that converts current to torque, as shown in Figure 3.1. Individually modeling the ESC and HDD motor would require a complex model of the ESC commutation and electromotive torque in the HDD motor. Instead, the HDD-RW

actuator model used, was a lumped model of the ESC and HDD motor, as shown in Figure 3.2. This lumped HDD-RW actuator model was shown to accurately model the ESC and HDD-RW system and eliminated the need for sophisticated models or intensive testing of the individual HDD-RW and ESC units. The HDD-RW actuator model is composed of an ESC mapping that converts ESC commands to RPM commands, a first order transfer function that converts RPM commands to motor RPM, gains that convert motor speed from RPM to rad/s and motor speed to HDD-RW angular momentum, and finally a derivative transfer function that converts HDD-RW angular momentum to HDD-RW torque.

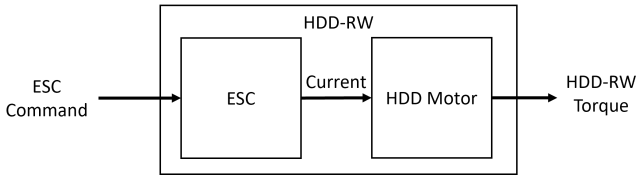

Figure 3.1: HDD-RW System Block Diagram

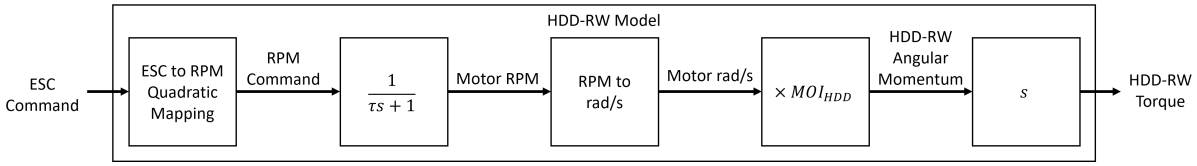

Figure 3.2: HDD-RW Model Block Diagram

Modeling of the HDD-RWs was performed by conducting a step response test, during which a series of increasing step ESC inputs were commanded and the resulting HDD-RW speed was measured. The step response test was conducted for the 2.5-inch and 3.5-inch HDD-RWs in both directions. The resulting transfer function from the step response test is specific to the ESC and HDD-RW hardware used. The step response test or an similar system identification test, such as variable frequency input [41], should be performed for each ESC and HDD-RW system, as the transfer functions will differ by HDD hardware, ESC hardware, and voltage and current supplied. Note that while this research developed a hand-crafted system model and system identification methodology, several existing system identification software tools such as System Identification Toolbox by MATLAB [42] and Comprehensive Identification from FrEquency Responses (CIFER) [43] exist which provide

additional benefits such as uncertainty quantification.

The goal of the step response test was to quantify the relationship between the ESC input and the output HDD-RW speed. A schematic of the step response test is shown in Figure 3.3. A Raspberry Pi 3B+ was used to provide a PWM signal to the iFlight SucceX-E V1 ESC which drove the HDD-RW. The ESC was powered by a buck converter which outputted either 12.0 V for the 2.5-inch HDD-RW or 15.0 V for the 3.5-inch HDD-RW. A series of step inputs were commanded to the ESC such that the HDD-RW increased in speed and reached steady state before the next step input was commanded. The HDD-RW speed was measured by a Hobbywing RPM sensor, a low-cost RPM sensor typically used for UAV BLDC motors. The RPM measurements were collected by an Arduino Uno. The step response test was performed for the HDD-RW in both the clockwise and counterclockwise direction.

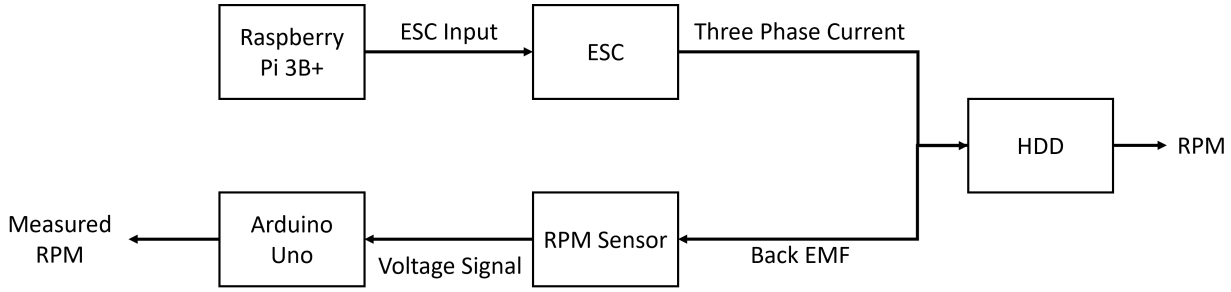

Figure 3.3: Step Response Test Schematic

3.2.1 ESC Input

The ESC takes a pulse width modulation (PWM) signal as an input from the Raspberry Pi 3B+. The input PWM signal has a frequency of 50 Hz and a duty cycle ranging from 5.0% to 10.0%, which corresponds to pulse widths of $1000\mu s$ to $20000\mu s$. Since the value of the PWM signal pulse width was inputted into the program commanding the ESC on the Raspberry Pi, the pulse width value will be referenced rather than the duty cycle. A pulse width input of $1000\mu s$ corresponds to the max motor speed in the reverse spin direction, a value of $2000\mu s$ corresponds to the max motor speed in the forward spin direction, and a value of $1500\mu s$ corresponds to zero spin. The direction is determined by the permutation of the three ESC leads and three HDD-RW phase leads.

3.2.2 2.5-inch HDD-RW Actuator Modeling

The step response test began with an ESC input of $1500\mu s$, which corresponds to zero motor speed. For the 2.5-inch HDD-RW clockwise (CW) direction test, the ESC input was incremented by $20\mu s$ from $1500\mu s$ to a final value of $2000\mu s$; each step was held for 10 seconds. The 2.5-inch HDD-RW counter-clockwise (CCW) direction test ESC input was incremented by $50\mu s$ from $1500\mu s$ to a final value of $1000\mu s$; each step was held for 10 seconds. A relatively small step size was chosen as a CubeSat attitude stabilization or pointing controller would typically slowly increment the reaction wheel speed. The step response test ESC input for the 2.5-inch HDD-RW is shown in Figure 3.4.

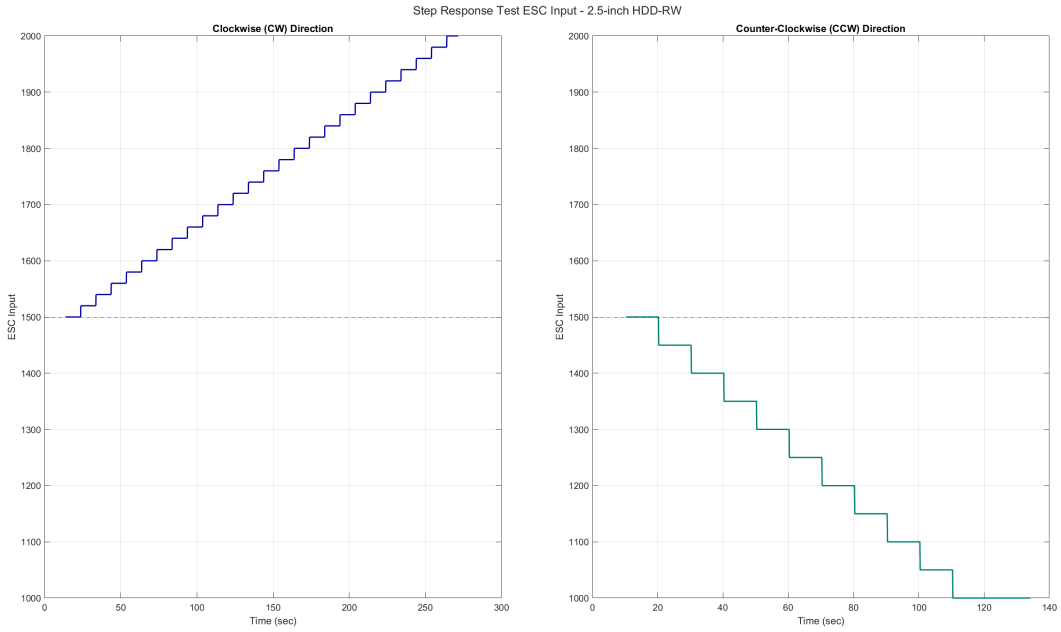

Figure 3.4: Step Response Test ESC Input - 2.5-inch HDD-RW

The RPM sensor used measured the HDD-RW speed by counting the number of voltage pulses caused by back-EMF of the motor within a fixed window of time. The RPM sensor had a resolution of 50 RPM. The equation for the RPM sensor measurement is given in Equation 3.1:

$$RPM = \frac{n/p}{T} \times 60 \frac{seconds}{minute} \tag{3.1}$$

where RPM is the revolutions-per-minute of the HDD-RW, T is the sampling period in seconds, n is the number of motor back-EMF signals detected within the sampling period, and p is the number of poles of the motor. The 2.5-inch HDD-RW model used has 12 poles.

Due to the low back-EMF of the 2.5-inch HDD-RW, the RPM sensor was prone to measurement dropout, resulting in an underestimated motor speed and frequent outliers. Since the HDD-RW was commanded to a monotonically increasing speed, the RPM sensor data was filtered by excluding data points that were less than the previous measurement, as shown in Figure 3.5.

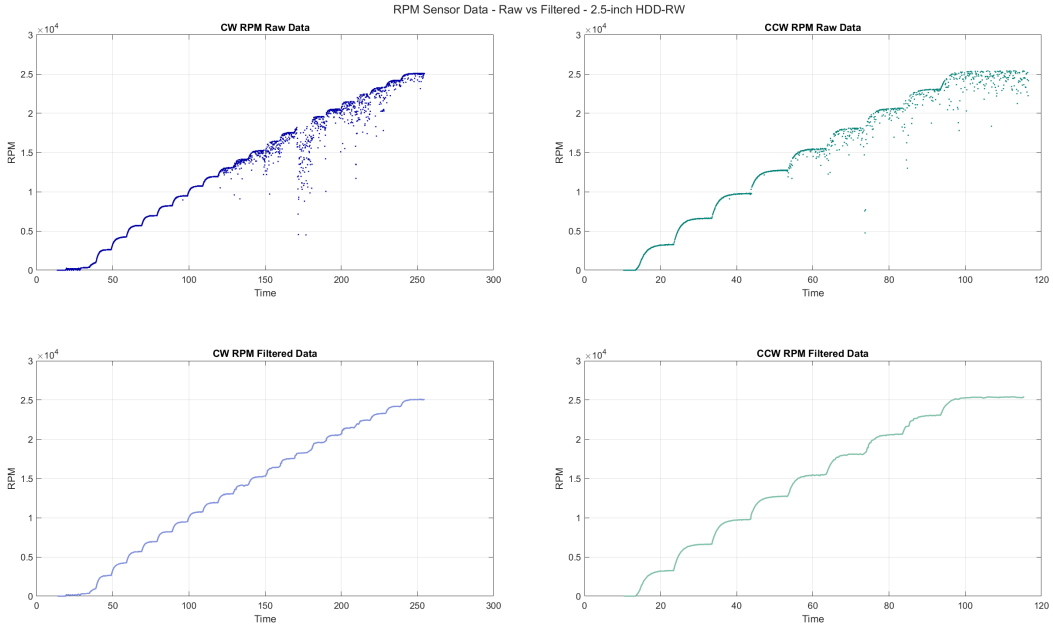

Figure 3.5: RPM Sensor Filtering

The measured and modeled HDD-RW speed vs. ESC input for both the CW and CCW direction are shown in Figures 3.6 and 3.7. The HDD-RW was observed to reach a steady state speed for each command step. The relationship between the ESC input and the HDD-RW command was determined using the steady state speeds. A quadratic fit, shown in Figure 3.8, was found to best describe the relation between the HDD-RW steady state speeds and ESC input. In Figure 3.8, the x-axis is dESC which is defined as the absolute difference between the ESC input and the neutral ESC input ($1500\mu s$), as shown in Equation

3.2. Plotting the steady state speeds with dESC input for both the CW and CCW transfer functions indicates higher speed in the CCW direction, as expected due to less friction.

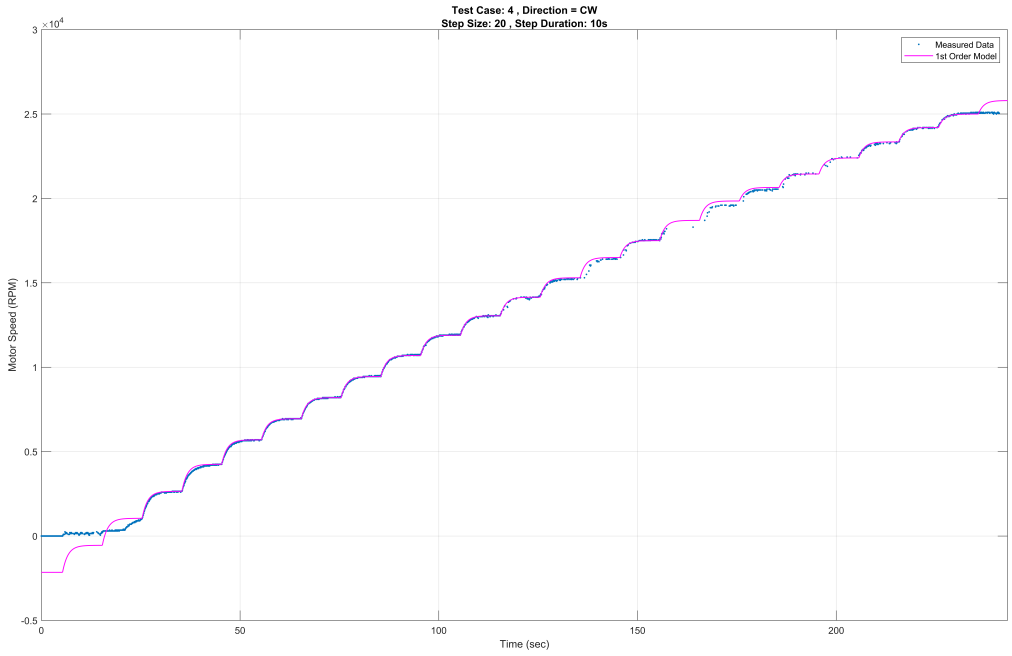

Figure 3.6: 2.5-inch HDD-RW CW Step Response RPM vs Input

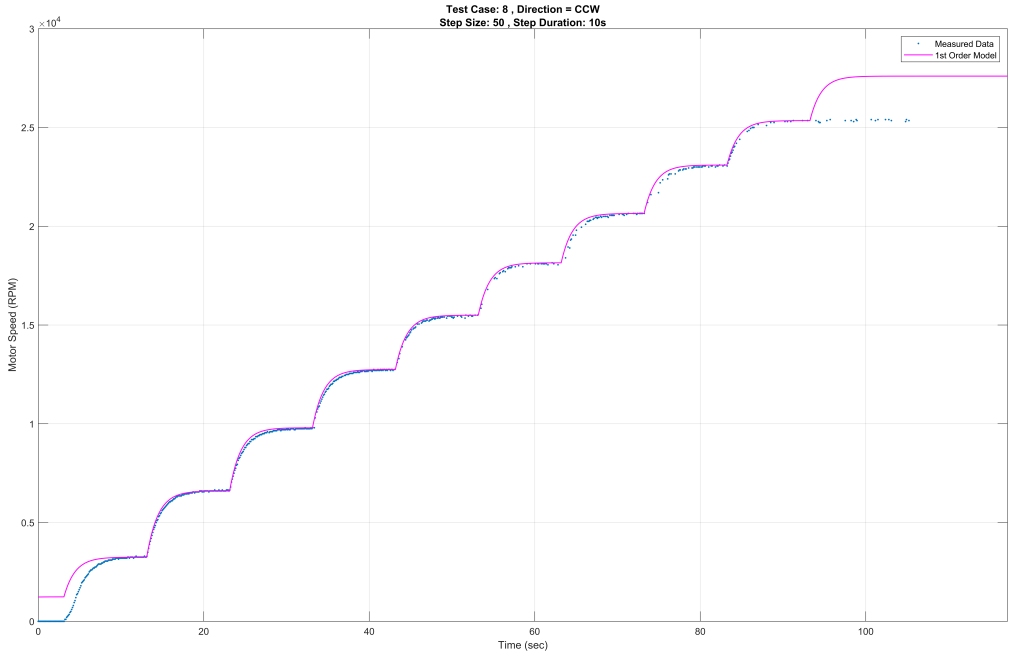

Figure 3.7: 2.5-inch HDD-RW CCW Step Response RPM vs Input

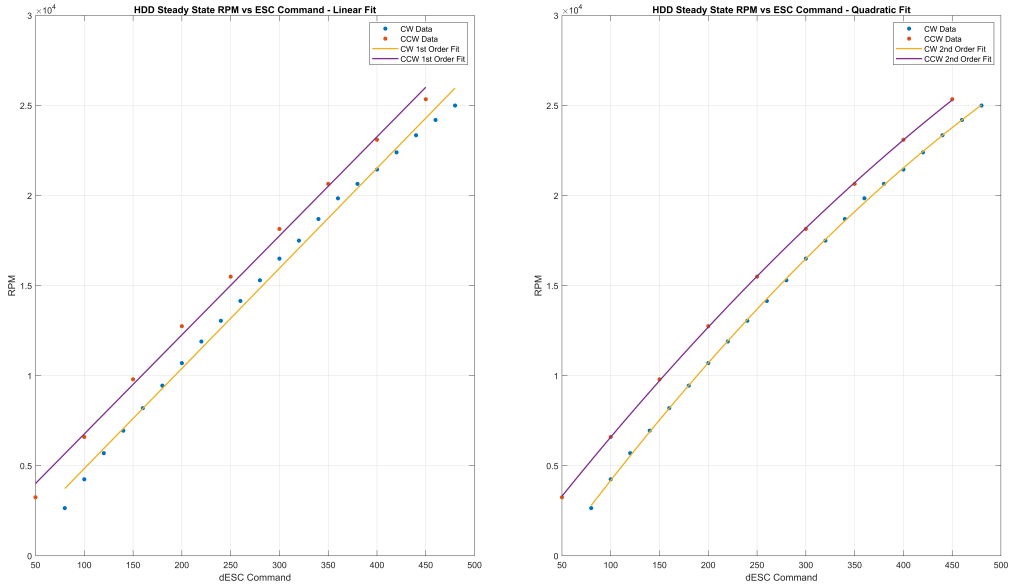

Figure 3.8: 2.5-inch HDD-RW Steady State RPM to ESC Command Fit

The coefficients for the polynomials describing the relationship between the steady state HDD-RW speed and ESC input is given for the clockwise (CW) and counter-clockwise (CCW) directions in Equations 3.3 and 3.4. The polynomials describe the ESC transfer function, which relates the ESC input to the RPM command. Note that the equation uses the dESC variable defined in Equation 3.2 in units of μs and the RPM calculated is an absolute value that does not indicate direction.

$$dESC = |ESC - ESC_{neutral}| \tag{3.2}$$

$$\text{2.5-inch HDD-RW CW: } RPM = -0.037065(dESC)^2 + 76.350(dESC) - 3076.2 \tag{3.3}$$

$$\text{2.5-inch HDD-RW CCW: } RPM = -0.030390(dESC)^2 + 70.195(dESC) - 126.19 \tag{3.4}$$

The transfer function of the HDD, which relates RPM command to motor RPM, was found by fitting a transfer function to the HDD-RW RPM data. A first order transfer function was found to fit the data. The time constant for the 2.5-inch HDD-RWs was found to be 1.3 seconds for both the CW and CCW directions. The step response modeled RPM vs. measured RPM is shown in Figures 3.6 and 3.7.

3.2.3 3.5-inch HDD-RW Actuator Modeling

The 3.5-inch HDD-RW actuator model was developed using the same process as the 2.5-inch HDD-RW. The step response test measured vs. modeled RPM values are shown in Figures 3.9 and 3.10. The ESC to RPM quadratic mapping equations are shown in Equations 3.5 and 3.6. The time constant for the 3.5-inch HDD-RWs were found to be 1.4 seconds and 1.9 seconds in the CW and CCW directions, respectively.

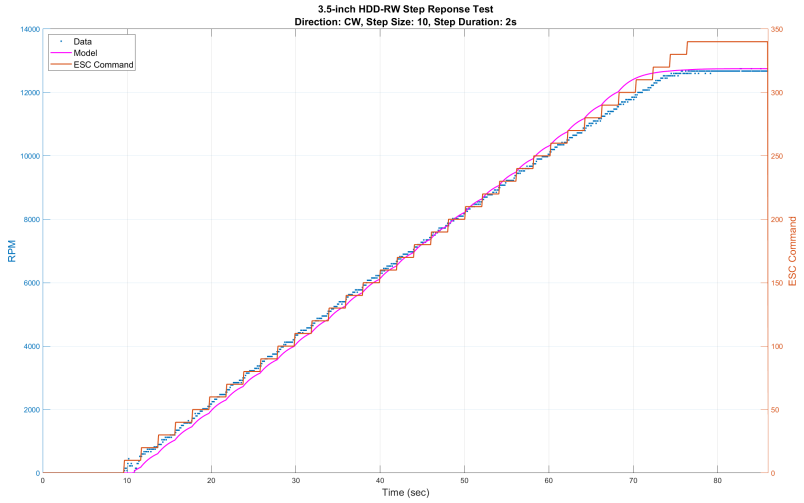

Figure 3.9: 3.5-inch HDD-RW CW Step Response RPM vs Input

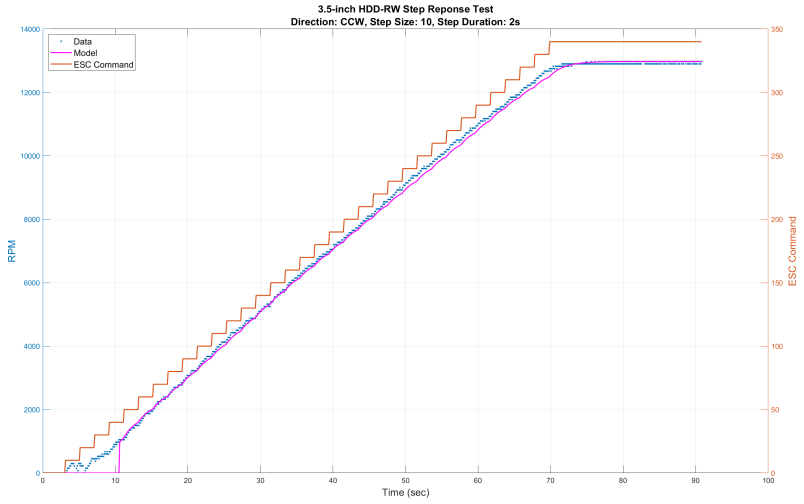

Figure 3.10: 3.5-inch HDD-RW CCW Step Response RPM vs Input

$$\text{3.5-inch HDD-RW CW: } RPM = -0.0065(dESC)^2 + 40.8(dESC) - 70.0 \tag{3.5}$$

$$\text{3.5-inch HDD-RW CCW: } RPM = -0.0065(dESC)^2 + 49.0(dESC) - -79.0 \tag{3.6}$$

3.3 Controller Implementation

To perform the attitude control demonstrations, a classical feedback control system was implemented. A high level block diagram of the control system is shown in Figure 3.11. The plant, state determination, and controller blocks are each described in the following subsections.

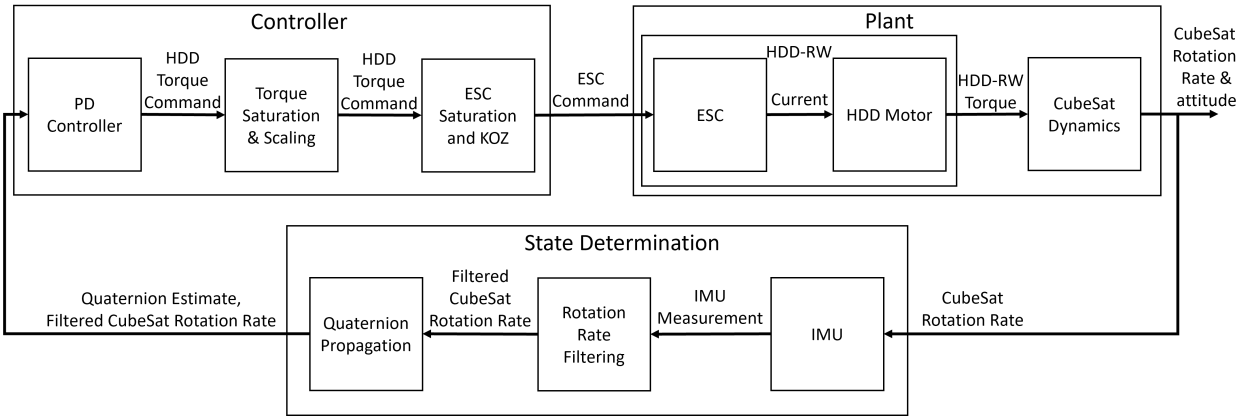

Figure 3.11: HDD-RW System Control Diagram

3.3.1 Plant

The plant consists of the ESC, HDD, and CubeSat. The ESC receives ESC commands from the controller and outputs current to the coils of the HDD motor. The HDD motor converts the electrical current to mechanical torque which rotates the HDD disk. By the action-reaction principle, torquing of the HDD disk results in a counter-torque of the CubeSat. In microgravity environment, the CubeSat has complete rotational freedom, thus its motion is governed by pure rotational dynamics in the inertial reference frame.

3.3.1.1 HDD-RW Model

The HDD-RW is comprised of the ESC and the HDD. The input of the HDD-RW is the ESC command and the output is the torque of the HDD. The HDD-RW actuator model is described in detail in Section 3.2.

3.3.1.2 CubeSat Dynamics

The rotational motion of a rigid body in free-space can be generally described by Euler's rotational equation, shown in Equation 3.7:

$$\dot{\omega}_B^{BI} = (J_B^C)^{-1} \left[L_B^C - \omega_B^{BI} \times \left(J_B^C \omega_B^{BI} \right) \right] \tag{3.7}$$

where the BI superscript denotes the body frame with respect to the inertial frame, C denotes the body frame centered at the center of mass, $\dot{\omega}_B^{BI}$ is the rate of change of the body rotational rates with respect to the inertial frame, J_B^c is the inertia matrix of the body with respect to the center of mass, L_B^c is the torque applied to the body in the body frame (centered at its center of mass), and ω_B^{BI} is the rotational rates of body in body frame with respect to the inertial frame.

For a CubeSat with reaction wheels in microgravity environment, Euler's rotational equation can be written as shown in Equation 3.8:

$$\dot{\omega}_B^{BI} = (J_B^C)^{-1} \left[L_B^C - L_B^w - \omega_B^{BI} \times \left(J_B^C \omega_B^{BI} + H_B^w \right) \right] \tag{3.8}$$

where L_B^w is the reaction wheel torque applied to the body in the body frame (centered at its center of mass), H_B^w is the angular momentum of the reaction wheels along their spin axes in the body frame (centered at its center of mass), and all other terms are the same as described earlier in Equation 3.7.

It is important to know the moment of inertia of the CubeSat as well as the HDD-RW. The moment of inertia of each CubeSat was estimated using a CAD model developed in SolidWorks. The CubeSat CAD model included each component of the CubeSat with the exception of the wire harnessing, which was considered to have negligible mass in comparison to the other components. The CAD-derived CubeSat moment of inertia values are shown in Table 3.1. The off-diagonal terms of the inertia matrix were considered negligible and set to zero in the flight software as they were estimated to be 2 orders of magnitude less than the diagonal terms. The moment of inertia of the revolving components of the HDD-RW - the disk and the spindle - was also found numerically by creating a CAD model. The disk was weighed and the mass was uniformly applied to the disk of the HDD-RW CAD model. The

density of the spindle was assumed to be uniform and to have the density of aluminum. Due to the spindle mass distribution being close to the center of mass of the disk and spindle, the spindle was found to have negligible moment of inertia. The moment of inertia values for each of the HDD-RWs is shown below in Table 3.1.

Table 3.1: CAD-based MOI values of HDD-RWs and HDD-RW CubeSats

Parameter	**Value**
1.8-inch HDD-RW MOI	$8.031\, gcm^2$
2.5-inch HDD-RW MOI	$49.0562\, gcm^2$
3.5-inch HDD-RW MOI	$902.78\, gcm^2$
1.8-inch HDD-RW CubeSat Inertia Matrix	$\begin{bmatrix} 992.9 & 0 & 0 \\ 0 & 993.1 & 0 \\ 0 & 0 & 999.6 \end{bmatrix} gcm^2$
2.5-inch HDD-RW CubeSat Inertia Matrix	$\begin{bmatrix} 45613.39 & 39.12 & -76.59 \\ 39.12 & 47155.66 & -24.75 \\ -76.59 & -24.75 & 49825.17 \end{bmatrix} gcm^2$
3.5-inch HDD-RW CubeSat Inertia Matrix	$\begin{bmatrix} 59325.93 & -982.28 & -119.33 \\ -982.28 & 62010.87 & 782.17 \\ -119.33 & 782.17 & 67481.00 \end{bmatrix} gcm^2$

3.3.2 State Determination

The state determination block computes the CubeSat's rotation rates and attitude which is subsequently used in the controller to determine what torque to output to stabilize or point the CubeSat. The rotation rate is measured by the CubeSat's gyroscope. After the gyroscope bias is removed and the raw measurement is filtered, the measurement is used to propagate the CubeSat's attitude. The filtered rotation rate along with the CubeSat's quaternion error is then passed on to the controller.

3.3.2.1 Gyroscope and Filtering

The gyroscope bias and noise were estimated using a static calibration test during which the gyroscope data was recorded while it was stationary. Static calibration tests of each of the CubeSat's gyroscopes was performed for periods of 90 minutes. The gyroscope bias was

found by taking the average of the gyroscope measurements over the period of the static calibration test. The flight software subtracted the bias from the raw gyroscope value to obtain the unbiased gyroscope value. The unbiased gyroscope values were filtered using a discrete first-order low-pass filter where the smoothing factor was $\alpha = 0.8$ ($\tau = 0.075s$).

3.3.2.2 Quaternion Propagation

The CubeSat's current quaternion was computed by propagating the previous quaternion with the CubeSat's current body rotation rate. The initial CubeSat quaternion was defined to be the unit quaternion, as shown in Equation 3.9. Note that the scalar last quaternion convention is used here. The propagation equation is shown in Equations 3.10, 3.11, and 3.12:

$$q^{i=1} \equiv \begin{bmatrix} 0 & 0 & 0 & 1 \end{bmatrix}^T \tag{3.9}$$

$$q^i = q^{i-1} + \Delta t \dot{q}^i \tag{3.10}$$

$$\dot{q}^i = \frac{1}{2}\Xi(q^{i-1})\omega \tag{3.11}$$

$$\Xi(q) = \begin{bmatrix} +q_4 & -q_3 & +q_2 \\ +q_3 & +q_4 & -q_1 \\ -q_2 & +q_1 & +q_4 \\ -q_1 & -q_2 & -q_3 \end{bmatrix} \tag{3.12}$$

The quaternion error is calculated using equation 3.13:

$$\begin{bmatrix} q_1^e \\ q_2^e \\ q_3^e \\ q_4^e \end{bmatrix} = \begin{bmatrix} +Q_4 & +Q_3 & -Q_2 & -Q_1 \\ -Q_3 & +Q_4 & +Q_1 & -Q_2 \\ +Q_2 & -Q_1 & +Q_4 & -Q_3 \\ +Q_1 & +Q_2 & +Q_3 & +Q_4 \end{bmatrix} \begin{bmatrix} q_1 \\ q_2 \\ q_3 \\ q_4 \end{bmatrix} \tag{3.13}$$

where q^e is the error quaternion, Q is the desired quaternion attitude, and q is the currently estimated quaternion attitude. The quaternions shown follow the scalar-last convention. Q and q must be with respect to the same inertial reference frame. For the parabolic

flight experiment, the reference frame for a given trial is taken to be the CubeSat's attitude at the beginning of the trial, and i is the iteration index.

3.3.3 Controller

3.3.3.1 PD Controller

For both the stabilization and pointing demonstrations in microgravity parabolic flight, the CubeSat testbeds utilized a PD controller. The simplicity of the PD controller allows the HDD-RW controller to be more easily replicated in future implementations and avoids complex behavior that may convolute performance of the HDD-RWs. A quaternion controller was used for the pointing controller to avoid angular singularities or discontinuities in the controller.

The stabilization controller follows the control law shown in Equation 3.14:

$$\text{Stabilization Controller: } T = -\left[K_P\omega + K_D\dot{\omega}\right] \tag{3.14}$$

where T is the desired stabilization torque, K_P is the proportional stabilization gain, K_D is the derivative stabilization gain, ω is the CubeSat body rotation rate, and $\dot{\omega}$ is the time derivative of the CubeSat body rotation rate.

$\dot{\omega}$ was estimated using a backwards difference derivative, shown in Equation 3.15:

$$\dot{\omega} = \frac{\omega^i - \omega^{i-1}}{\Delta t} \tag{3.15}$$

where ω^i is the current body rotation rate measurement, ω^{i-1} is the previous body rotation rate measurement, and Δt is the time step.

The pointing controller followed the quaternion control law found in [44] and shown in Equation 3.16:

$$\text{Pointing Controller: } T_u = -\left[\text{sign}(q_4^e)K_P q_u^e + K_D\omega_u\right], u = x, y, z \tag{3.16}$$

where u denotes the axis (x, y, or z), T is the desired pointing torque about axis u, q^e is the quaternion error, K_P is the proportional pointing gain, K_D is the derivative pointing gain, and ω is the CubeSat body rotation rate. The quaternion shown follows the scalar-last convention.

3.3.3.2 Torque Scaling

A rapid change in rate of ESC command to the HDD-RWs may have led to the ESC commutation becoming out of phase with the motor position, resulting in the motor stopping or causing permanent damage. To avoid such a scenario, the ESC command rate of change was limited by implementing a torque limit. The maximum allowable torque was defined for the HDD-RW by mapping the maximum allowable ESC command change over a controller loop duration to change in angular momentum over a controller loop duration. Due to the coupled nature of rotational motion, it is important to preserve the direction of the desired torque; this was done by scaling the torque vector. If the absolute value of any of the torque vector elements exceeded the maximum allowable torque, torque scaling was performed, as defined in Equation 3.17:

$$T_{scaled} = T_{pre-scaled} \frac{T_{max}}{max(|T_{pre-scaled}|)} \tag{3.17}$$

where T_{scaled} is the scaled torque, $max(|T_{pre-scaled}|)$ is the element of maximum absolute value in the pre-scaled torque vector, $T_{pre-scaled}$ is the torque value prior to torque scaling, and T_{max} is the maximum allowable torque.

3.3.3.3 ESC Saturation and Keep-Out-Zone

The torque command was converted to an ESC command with a linear mapping that was found from the HDD-RW step response test, shown in Equation 3.18:

$$ESC^i = ESC^{i-1} + kT^i \tag{3.18}$$

where ESC^i is the current ESC command, ESC^{i-1} is the previous ESC command, k is the linear mapping from torque to change in ESC command found from the step response test, and T is the desired torque.

The outputted ESC command was allowed to range from $1000\mu s$ to $2000\mu s$. If any element of the computed ESC command was less than the minimum allowable ESC value, that element was set to the minimum allowable ESC value before being sent to the ESC. Similarly, if the ESC command was greater than the maximum allowable ESC value, that element was set to the maximum allowable ESC value before being sent to the ESC. It is

worth noting that this ESC saturation feature would change the command torque direction from the torque direction computed by the PD controller; however, if the computed ESC command exceeded its allowable range, stabilization would not have been possible as the HDD-RW would have been saturated.

BLDC motors, which are used in hard disk drives, are generally not well-suited for spinning at low speeds - this makes motor start-up, low-speed operation, and direction-switching challenging. When the BLDC motor is stationary, if the rate of change of the ESC commands is not sufficiently fast, the ESC will not provide sufficient current to overcome the motor's static friction. On the other hand, at low speeds, if the rate of change of the ESC commands is not sufficiently slow and smooth, the ESC commutation will become out of phase with motor position and the motor will stop spinning. Direction-switching combines these two challenges since the motor will need to transition through a low-speed in one direction, coming to a complete stop, and start-up in the other direction.

The motor start-up problem was addressed for the HDD-RW controller by defining a standard start-up sequence for each direction that was always used when commanding the HDD-RW from zero speed to a non-zero speed. The low-speed and direction-switching problems were addressed by implementing a "keep-out-zone" - a range of ESC command values centered around zero that were not permitted, preventing the HDD-RW from spinning at low-speeds or stopping. If the torque command mapped to an ESC value that was within the keep-out-zone (KOZ), the ESC was instead commanded to either the upper or lower bound of the keep-out-zone, depending on whether the controller was attempting to command a lower speed in the same direction or a speed in the opposite direction. A "desired ESC command" state was tracked to differentiate between the controller attempting to command a lower speed in the same direction or a speed in the opposite direction. The ESC command algorithm is shown in Algorithm 1 and an example is shown in Figure 3.12 and explained below:

Algorithm 1 ESC Command Algorithm

```
i ← 0
while Controller = on do
    ESC_des[i] ←ESC_cmd[i-1] + kT[i]
   if ESC_des[i] > KOZ_upper_bound or ESC_des[i] < KOZ_lower_bound then
    ESC_cmd[i] ← ESC_des[i]
   else if ESC_des[i] > ESC_neutral and ESC_des[i] < KOZ_upper_bound then
    ESC_des[i] ← ESC_des[i-1] + kT[i]
      if ESC_des[i] < KOZ_lower_bound then
    ESC_cmd[i] ← KOZ_lower_bound
      else
    ESC_cmd[i] ← KOZ_upper_bound
      end if
   else if ESC_des[i] < ESC_neutral and ESC_des[i] > KOZ_lower_bound then
    ESC_des[i] ← ESC_des[i-1] + kT[i]
      if ESC_des[i] > KOZ_upper_bound then
    ESC_cmd[i] ← KOZ_upper_bound
      else
    ESC_cmd[i] ← KOZ_lower_bound
      end if
   end if
   i ← i + 1
end while
```

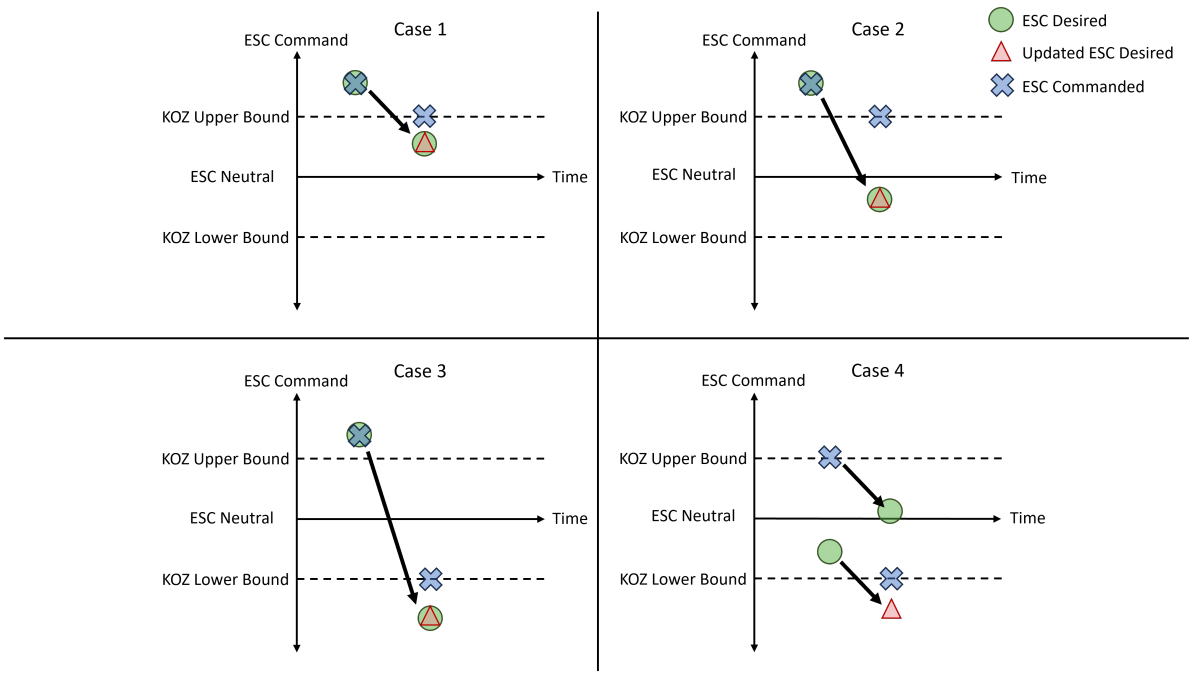

Figure 3.12: Keep-out-zone examples

In Case 1, the previous ESC commanded is above the KOZ upper bound and the next desired ESC command is in the KOZ. An updated desired ESC command is calculated based on the previously desired ESC command, which happens to be the same as the previous ESC command. Since the updated desired ESC command is still in the KOZ, the outputted ESC command is set to the KOZ upper bound. In Case 2, the previous ESC command and previous desired ESC command are the same as Case 1, but the current desired ESC command is below the neutral point. An updated desired ESC command is again computed, which is still in the KOZ, thus the outputted ESC command is again the KOZ upper bound. In Case 3, the previous ESC command and previous desired ESC command are again the same as Case 1 and 2, but the current desired ESC command and updated desired ESC command are on the other side of the KOZ. Thus, the outputted ESC command is set to the KOZ lower bound - this allows the motor to transition from one direction to another. In Case 4, the previous ESC command is the KOZ upper bound but the previous desired ESC command is in the opposite direction. The current ESC desired is within the KOZ, leading to calculation of the updated ESC desired which is below the KOZ lower bound. Since the updated desired ESC command is on the other side of the KOZ, the outputted ESC

command is the KOZ lower bound which allows the motor to transition from one direction to another.

Note that the use of saturation along with the PD controller may lead to issues such as wind-up. Such issues can be resolved with controller techniques such as anti-windup terms or by use of more advanced controllers such as model predictive control (MPC).

3.3.4 Fishing Line Testing

Testing and tuning of the controller was performed on the ground with fishing line testing where the CubeSat was suspended by a fishing line, allowing for a single degree of rotational freedom about the gravitational axis. Fishing line testing is a common low-cost method used to test CubeSat attitude control. Fishing line testing can be used to test three-axis attitude control by suspending the CubeSat from a corner, requiring engagement of all reaction wheels - this technique was predominantly used during ground testing of the HDD-RWs. In this research, the fishing line torsional dynamics, spring dynamics, and pendulum dynamics were not modeled; however, it is recommended to model these dynamics and create a simulation to be able to evaluate the HDD-RW performance through ground testing with a higher level of accuracy.

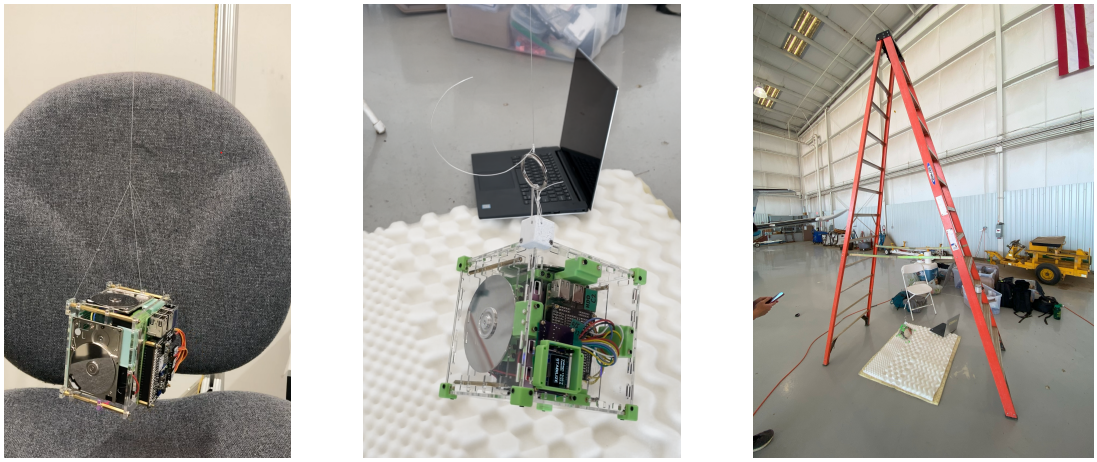

(a) 1.8-inch HDD-RW fishing line testing

(b) 3.5-inch HDD-RW fishing line testing

(c) Fishing line testing before flight campaign 2 using ladder

Figure 3.13: Fishing line testing

For fishing line testing, a longer and thinner fishing line is desirable to reduce the torsional stiffness and damping of the line, which has a stabilizing effect. Accordingly, a 30 lb fishing

line was used to suspend the HDD-RW CubeSat from a corner from a height of 1 - 2 meters. A key ring was tied to the suspended fishing line and a loop of fishing line was attached to the corner of the CubeSat. The key ring allowed for quick fastening and unfastening of the CubeSat on the fishing line. Foam was placed directly below the CubeSat as a precaution in case the fishing line or knot failed.

Similar to flight testing, during fishing line testing of the stabilization controller, the CubeSat was given an initial rotation. During testing of the pointing controller, the CubeSat was either left stationary or given an initial rotation. Rotation of the CubeSat was performed manually with two hands on each side of the CubeSat to minimize the net lateral and vertical forces thereby mitigating undesirable pendulum and spring motion.

Selected results from fishing line testing of the pointing controller of the 3.5-inch HDD-RWs are shown in Figures 3.14, 3.15, and 3.16. In each of these tests, the controller was observed to oscillate about its target attitude or approach its target with some oscillation - this is by design as the controller was intended to reach its pointing target within approximately 5-10 seconds, even if it did not stabilize. The CubeSat angular momentum was observed to significantly decrease, showing that the HDD-RWs stabilize the CubeSat. An oscillation of approximately 3.5 Hz frequency was observed in the body rotation rate. Using the pendulum natural frequency equation, shown in Equation 3.19 where f is the pendulum frequency, g is gravity, and L represents the pendulum length, showed that the 3.5 Hz frequency corresponded to a pendulum length of approximately 2.0 cm which was the approximate diameter of the key ring used.

$$f = \frac{1}{2\pi}\sqrt{\frac{g}{L}} \tag{3.19}$$

Selected results from fishing line testing of the pointing controller of the 2.5-inch HDD-RWs are shown in Figures 3.17, 3.18, and 3.19. In each of these tests, the controller reached its target attitude with minimal oscillation and also stabilized the CubeSat. The final body rotation rates for each of the trials were below 1 deg/s and the final angular errors were 0.15°, 1.24°, and 0.27° for Trials 1, 2, and 3, respectively.

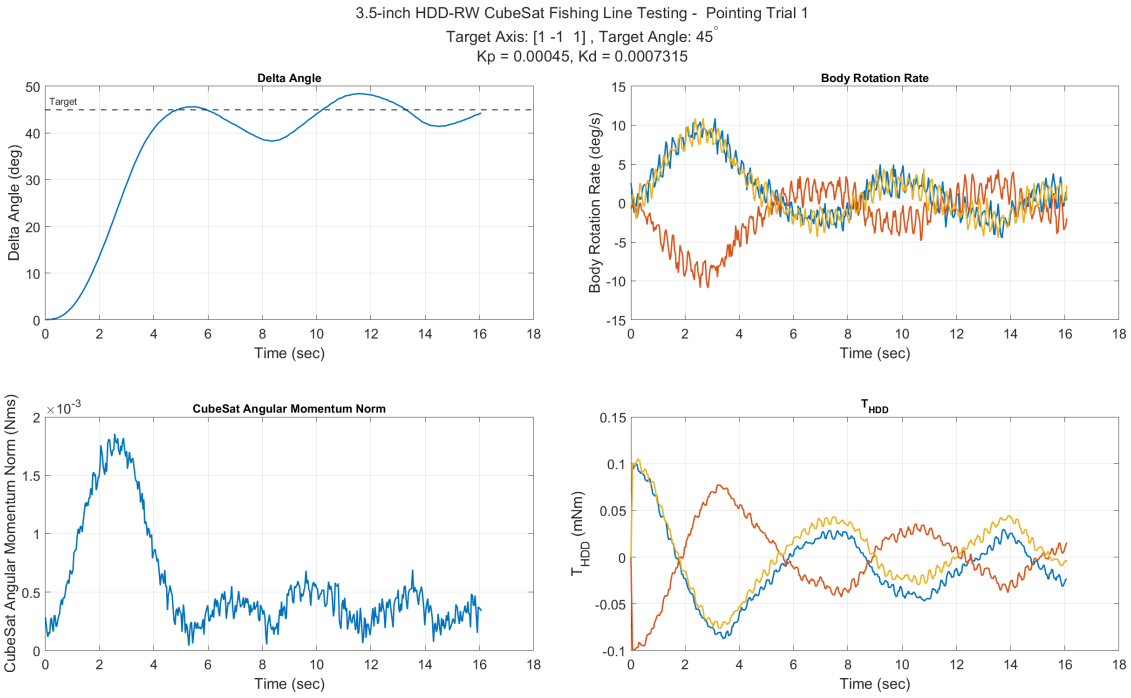

Figure 3.14: 3.5-inch HDD-RW CubeSat Fishing Line Testing Pointing Trial 1

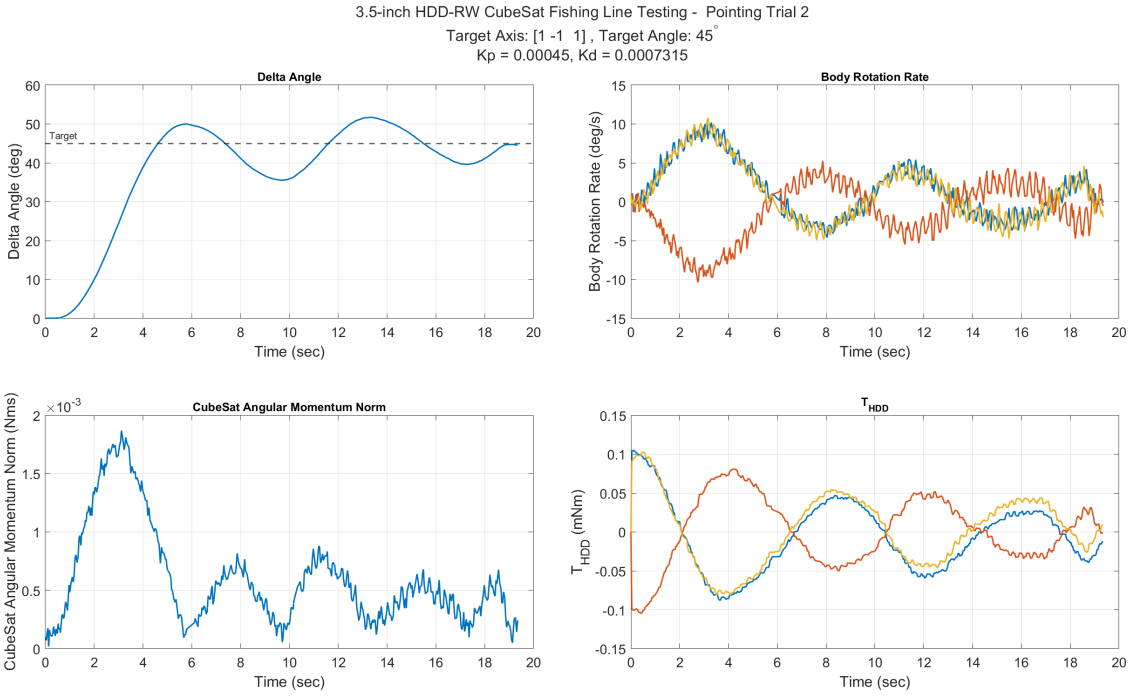

Figure 3.15: 3.5-inch HDD-RW CubeSat Fishing Line Testing Pointing Trial 2

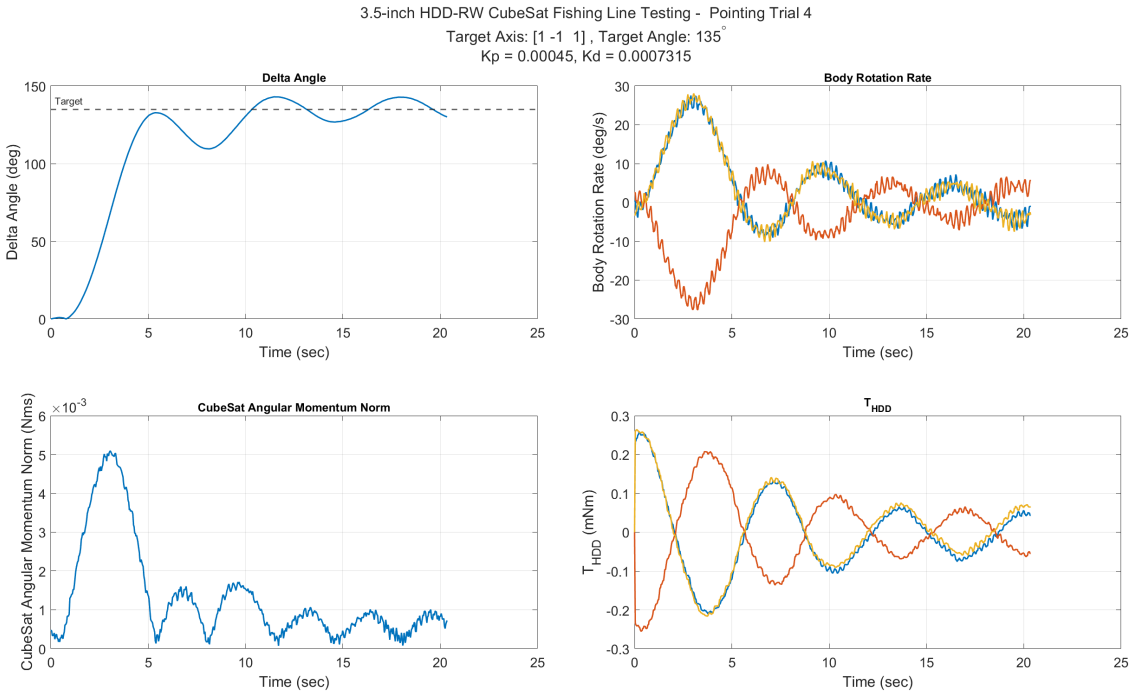

Figure 3.16: 3.5-inch HDD-RW CubeSat Fishing Line Testing Pointing Trial 4

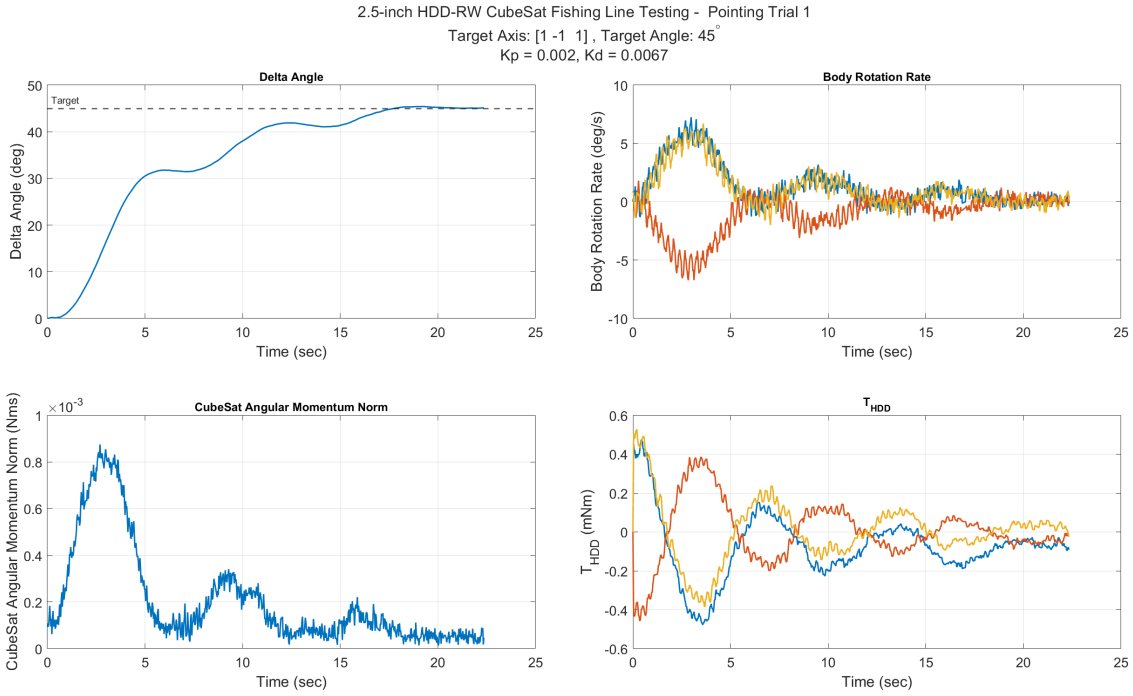

Figure 3.17: 2.5-inch HDD-RW CubeSat Fishing Line Testing Pointing Trial 1

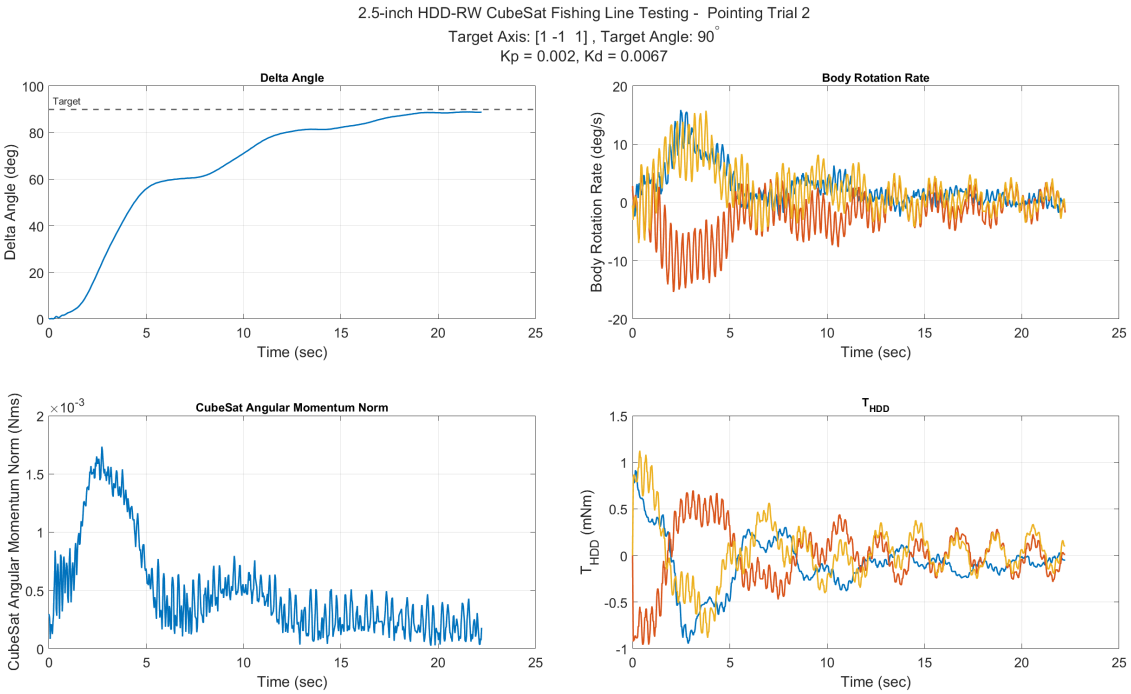

Figure 3.18: 2.5-inch HDD-RW CubeSat Fishing Line Testing Pointing Trial 2

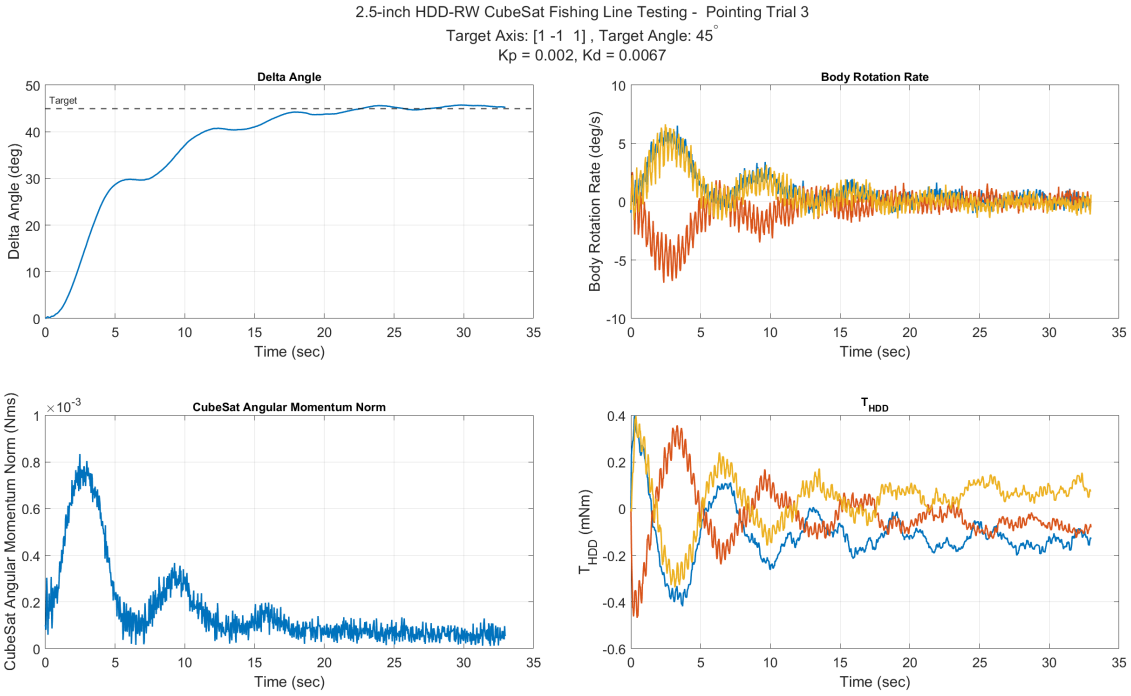

Figure 3.19: 2.5-inch HDD-RW CubeSat Fishing Line Testing Pointing Trial 3

3.4 HDD-RW Flight Testing Results

Microgravity parabolic flight testing of the HDD-RWs took place over the course of six parabolic flights. During Flights 1 and 2, the functionality of the flight experiment hardware and operations were tested. The 1.8-inch HDD-RW and 2.5-inch HDD-RW CubeSats executed a pre-programmed sequence of ESC commands. In the first two flights, the data saving rate was not fast enough to draw conclusions on the HDD-RW performance. During Flights 3 and 4, stabilization after an initial attitude disturbance was demonstrated using the 3.5-inch HDD-RWs. And during Flights 5 and 6, pointing to a predefined attitude was demonstrated using the 2.5-inch HDD-RWs. Results from Flights 3 through 6 are discussed in the following subsections.

3.4.1 Stabilization with 3.5-inch HDD-RWs

During Flights 3 and 4, two different 3.5-inch HDD-RWs performed several demonstrations of CubeSat stabilization. The two CubeSats were tested simultaneously during each flight - the "Chamber CubeSat" was tested inside the chamber, while the "External CubeSat" was tested outside the chamber. The addition of the External CubeSat demonstration provided the intended outcome of longer float duration times as well as twice the amount of flight data. During the flight, prior to the beginning of the microgravity period, the operator would press a button on the CubeSat that would initiate a 3 second countdown; by the end of the countdown the microgravity period would begin and the operator would release the CubeSat with an arbitrary rotation, after which the CubeSat would activate its stabilization controller and begin recording data.

Figures 3.20 and 3.21 show the angular momentum vs time of the External CubeSat and the Chamber CubeSat trials during Flight 3. The initial spike in angular momentum corresponds to the initial rotation imparted by the operator; release occurred at the peak angular momentum value, after which the HDD-RWs mitigated the CubeSat's angular momentum. Most trials were terminated by capture or contact with the floor or chamber before the controller settles; however, the three-axis stabilization controller clearly demonstrated consistent three-axis mitigation of initial rotation.

Figure 3.22 shows Trial 8 of the Chamber Experiment from Flight 3. The CubeSat

began with an angular momentum of approximately 32.8 mNms which the 3.5-inch HDD-RWs reduced to 9.2 mNms by the end of the trial 4.6 seconds later. The CubeSat body rotation rate at release and end of trial were [-128.2, -275.3, -251.7] deg/s and [4.8, -69.1, -62.0] deg/s, respectively.

Figure 3.23 shows Trial 10 from the External Experiment from Flight 3. The CubeSat began with an angular momentum of approximately 49.2 mNms which the 3.5-inch HDD-RWs reduced to 16.4 mNms by the end of the trial 6.5 seconds later. The CubeSat body rotation rate at release and end of trial were [-330.2, 495.0, 90.3] deg/s and [-205.1, 20.1, -27.9] deg/s, respectively.

Both Chamber Experiment Trial 8 and External Experiment Trial 10 from Flight 3 exhibited oscillation in the CubeSat angular momentum. This oscillatory behavior was observed in most trials of Flight 3 and was determined to be due to two factors - latency in the controller loop and the stabilization controller gains tuned to be too high. Although the flight software could not be changed between Flights 3 and 4, the stabilization controller gains were updated to address the controller instability. The proportional gain was reduced from 0.35 to 0.05 and the derivative gain was reduced from 0.35 to 0.1.

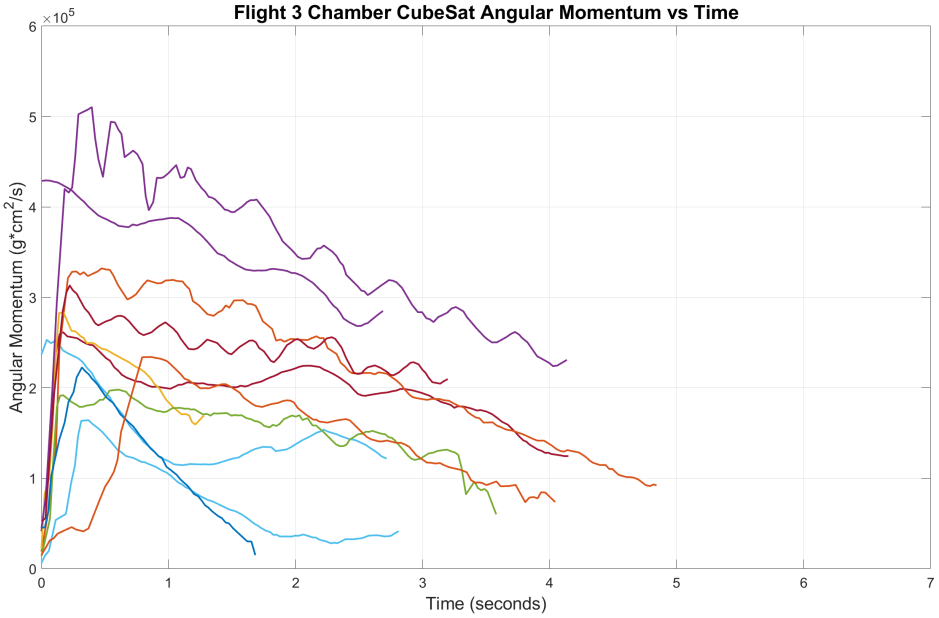

Figure 3.20: Flight 3 Chamber Experiment Stabilization Trials

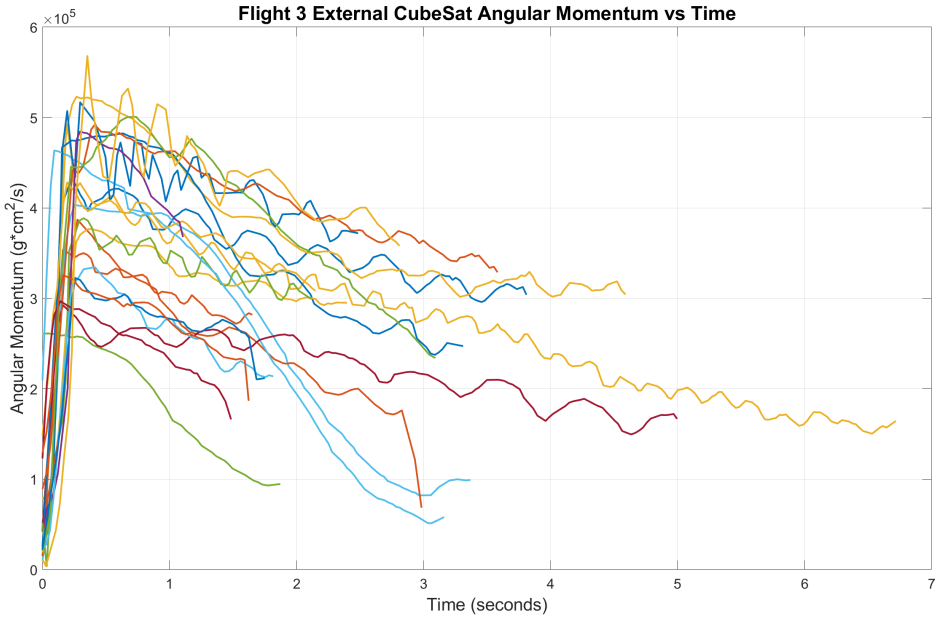

Figure 3.21: Flight 3 External Experiment Stabilization Trials

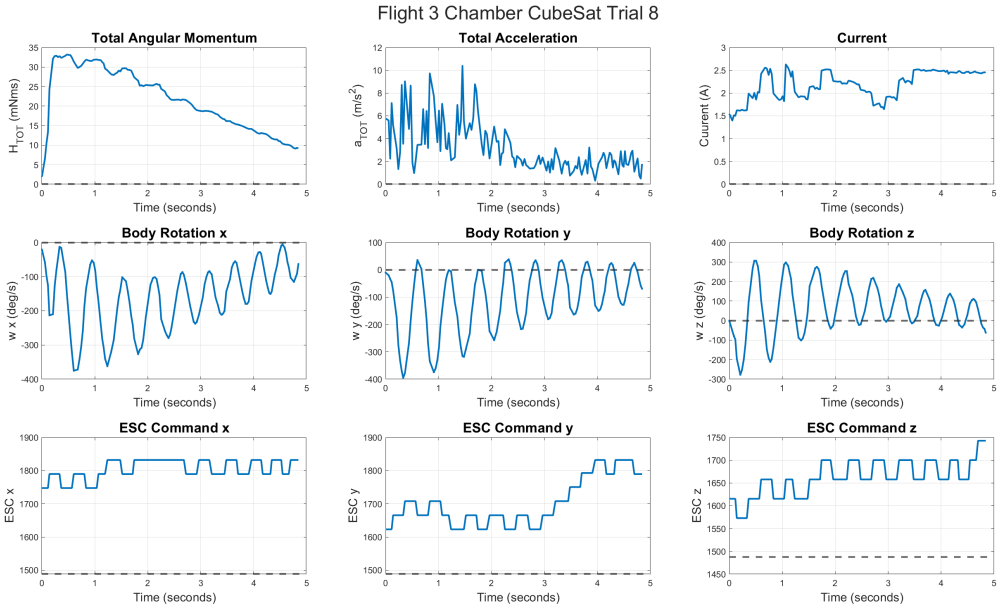

Figure 3.22: Flight 3 External Experiment Stabilization Trial 8

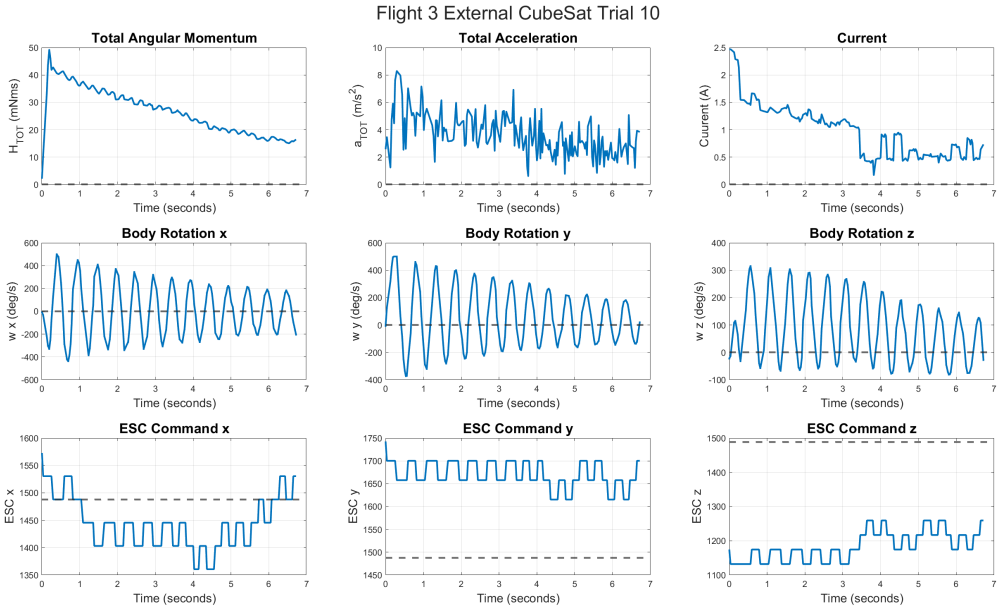

Figure 3.23: Flight 3 External Experiment Stabilization Trial 10

Figures 3.24 and 3.25 show the angular momentum vs time of the External CubeSat and the Chamber CubeSat trials during Flight 4. Although some oscillation was still present in the CubeSat angular momentum, retuning of the stabilization controller gains led to a clear improvement in the controller stability.

Figure 3.26 shows Trial 15 of the Chamber Experiment from Flight 4. The CubeSat began with an angular momentum of approximately 21.2 mNms which the 3.5-inch HDD-RWs reduced to 1.0 mNms by the end of the trial 1.8 seconds later. The CubeSat body rotation rate at release and end of trial were [184.2, -186.8, -7.4] deg/s and [2.1, -12.2, 1.8] deg/s, respectively. Figure 3.27 shows Trial 10 from the External Experiment from Flight 4. The CubeSat began with an angular momentum of approximately 31.8 mNms which the 3.5-inch HDD-RWs reduced to 1.3 mNms by the end of the trial 2.4 seconds later. The CubeSat body rotation rate at release and end of trial were [-74.5, 353.4, -129.0] deg/s and [-10.4, -5.7, -10.3] deg/s, respectively.

The change in angular momentum for each of these trials was 95.2% and 95.9%, respectively. It is clear that if the CubeSat remained in microgravity, the HDD-RWs would further reduce the CubeSat angular momentum.

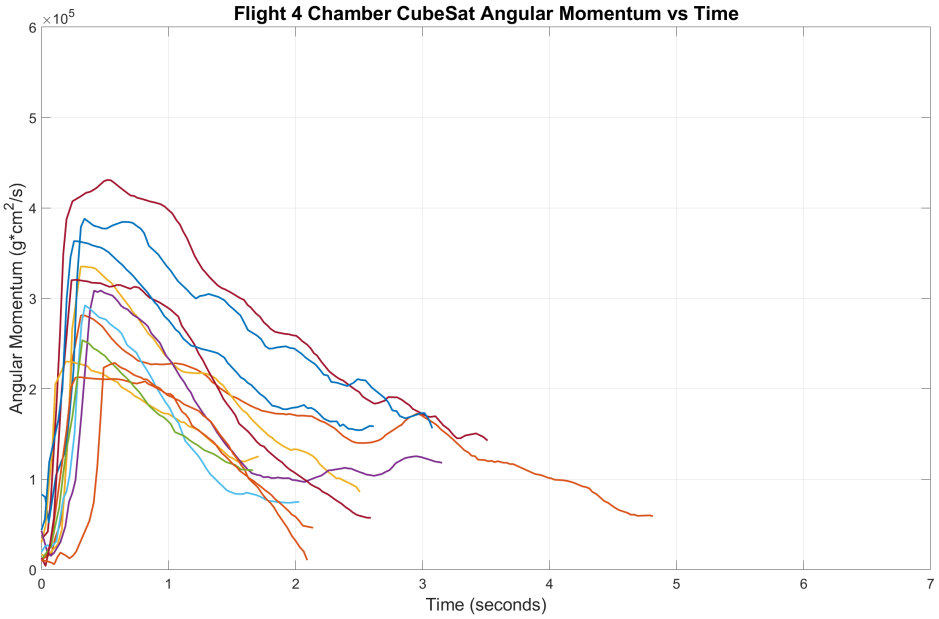

Figure 3.24: Flight 4 Chamber Experiment Stabilization Trials

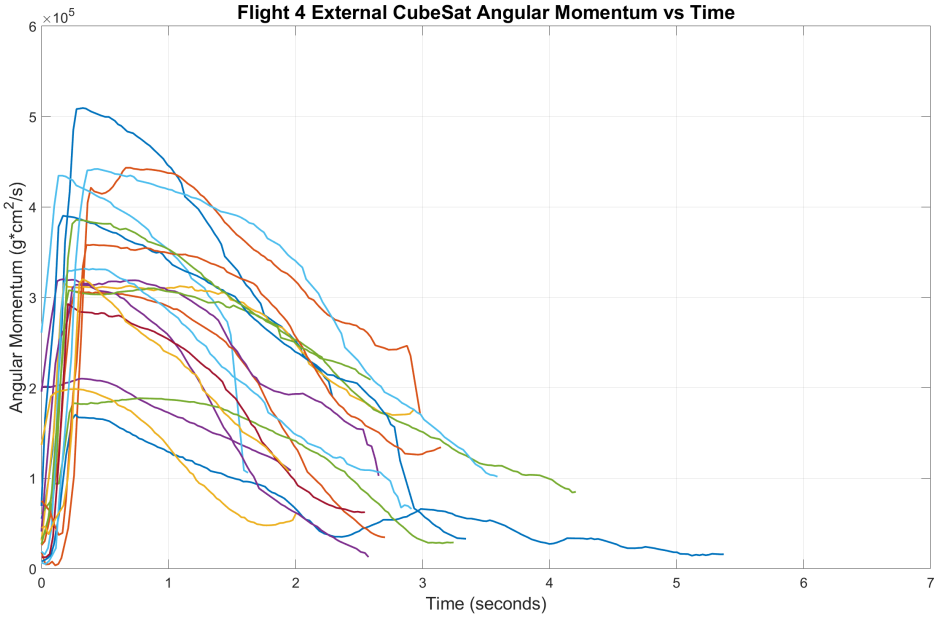

Figure 3.25: Flight 4 External Experiment Stabilization Trials

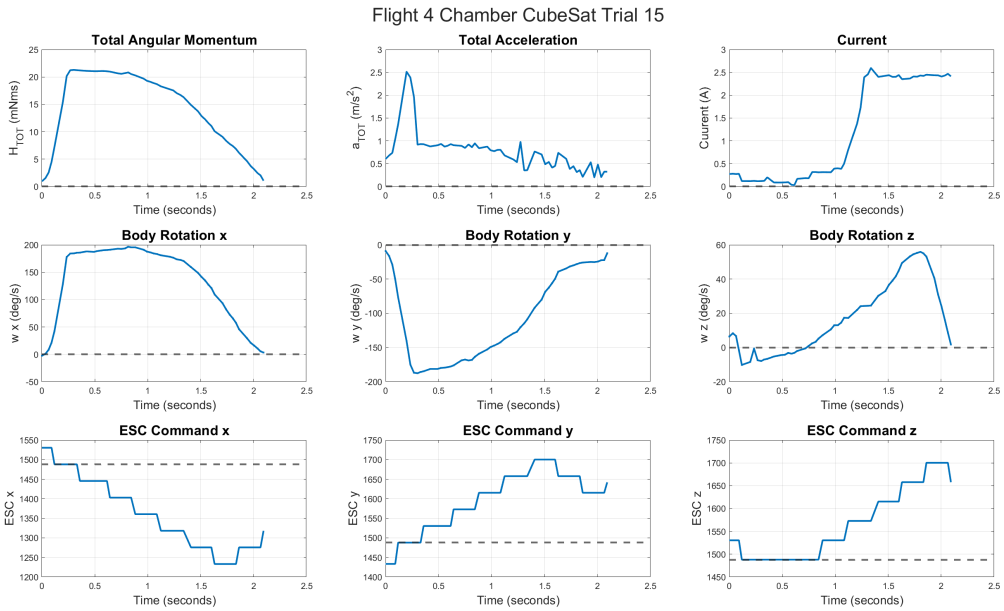

Figure 3.26: Flight 4 Chamber Experiment Stabilization Trial 15

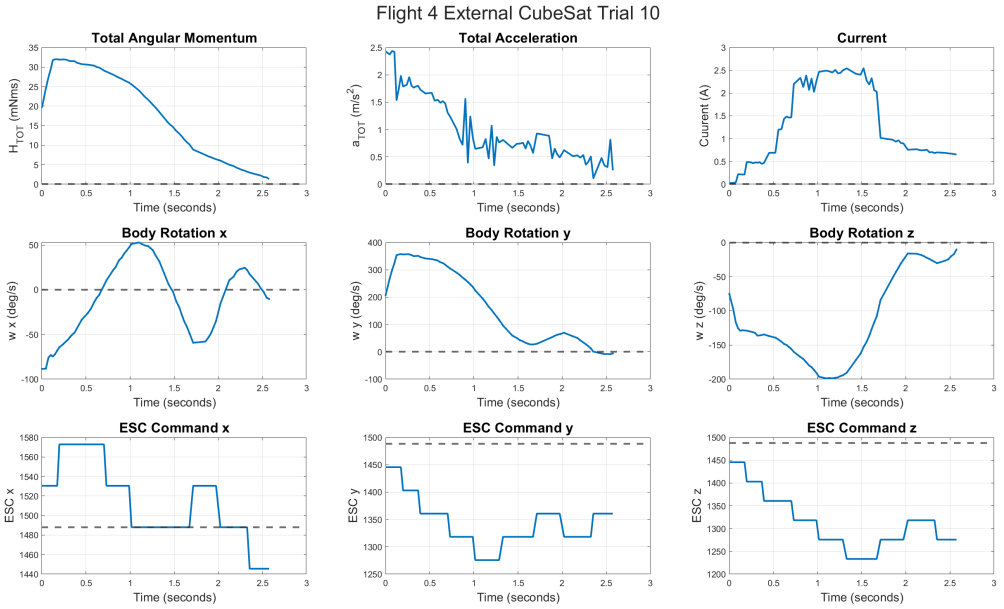

Figure 3.27: Flight 4 External Experiment Stabilization Trial 10

Through Flights 3 and 4, the 3.5-inch HDD-RWs demonstrated angular momentum storage of 45.0 mNms per HDD-RW in parabolic flight, a value comparable to larger commercial

CubeSat reaction wheels. Tuning of the stabilization controller for operation in space, where a CubeSat would have minutes to stabilize, would allow the CubeSat to stabilize to much lower rotation rates. Furthermore, increasing the controller loop frequency would likely significantly improve controller performance.

3.4.2 Pointing with 2.5-inch HDD-RWs

In Flights 5 and 6, the 2.5-inch and 3.5-inch HDD-RW CubeSats performed pointing tests. During the flight, prior to the beginning of the microgravity period, the operator pressed a button on the CubeSat that initiated a 3 second countdown; by the end of the countdown the microgravity period began and the operator released the CubeSat with minimal rotation, after which the CubeSat activated its pointing controller and began reorienting itself with respect to its initial orientation. The controller loop was improved from Flights 3 and 4 by increasing the controller loop frequency from 5 Hz to 10 Hz.

In both Flights 5 and 6, the 2.5-inch and 3.5-inch HDD-RW CubeSats decreased the angular error but were not able to stabilize the CubeSat by the end of the brief (3 - 5 second) microgravity period. Figures 3.28 and 3.29 show two sample pointing trials of the 3.5-inch HDD-RW. In Trial 5, the pointing controller reduced the angular error from 30° to approximately 7°. In Trial 17, the pointing controller reduced the error from 30° to approximately 5°, overshooting the target angle. In this case, the CubeSat almost reached its target but needed to reduce the rotation rates to remain pointing towards its target. Similar results were observed with the 2.5-inch HDD-RW pointing controller, as shown in Figure 3.30. The CubeSat's attitude trended towards its target but was not able to reach its target or stabilize within the time it had.

In each of these sample trials, the pointing controller was able to bring the CubeSat closer to the target. The oscillatory behavior in the CubeSat's angular position was expected and was due to the CubeSat's rotation and short stabilization window (3 - 5 seconds). Over an extended microgravity period, the amplitude of the oscillation and overshoot would decrease to zero. The pointing controller required a longer time to point in these trials because the controller needed time to first mitigate the relatively high initial angular velocity before the angular error could be brought to zero. Higher pointing controller gains would allow the CubeSat to more quickly stabilize the CubeSat, but would lead to higher overshoot in angle.

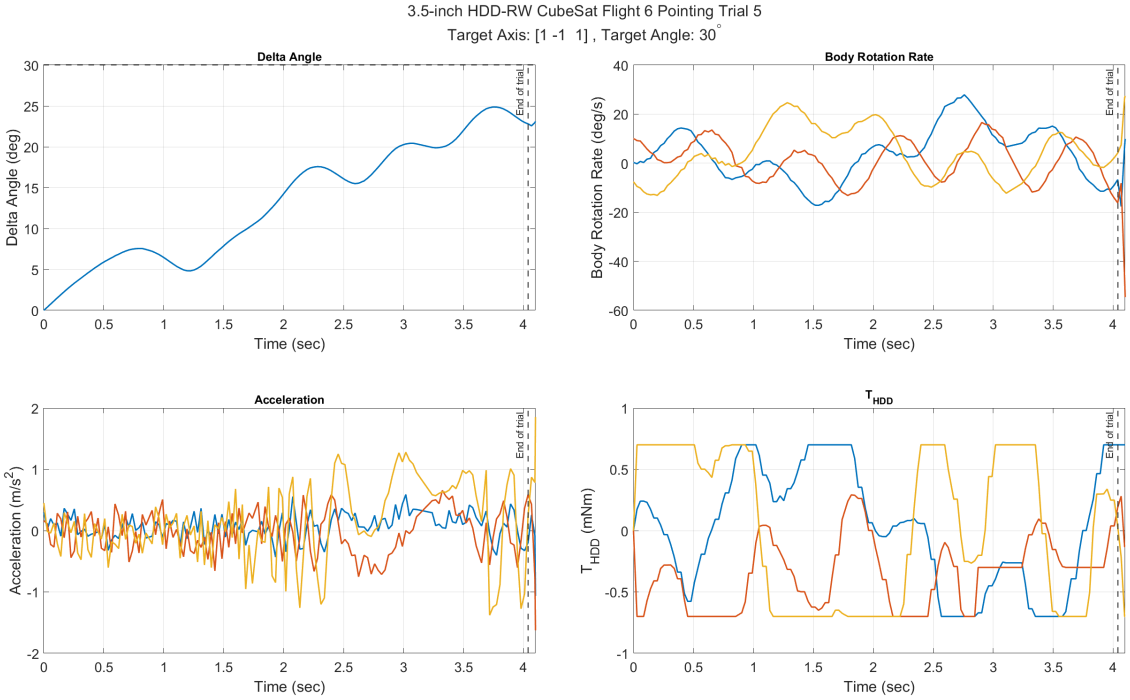

Figure 3.28: 3.5-inch HDD-RW CubeSat Flight 6 Pointing Trial 5

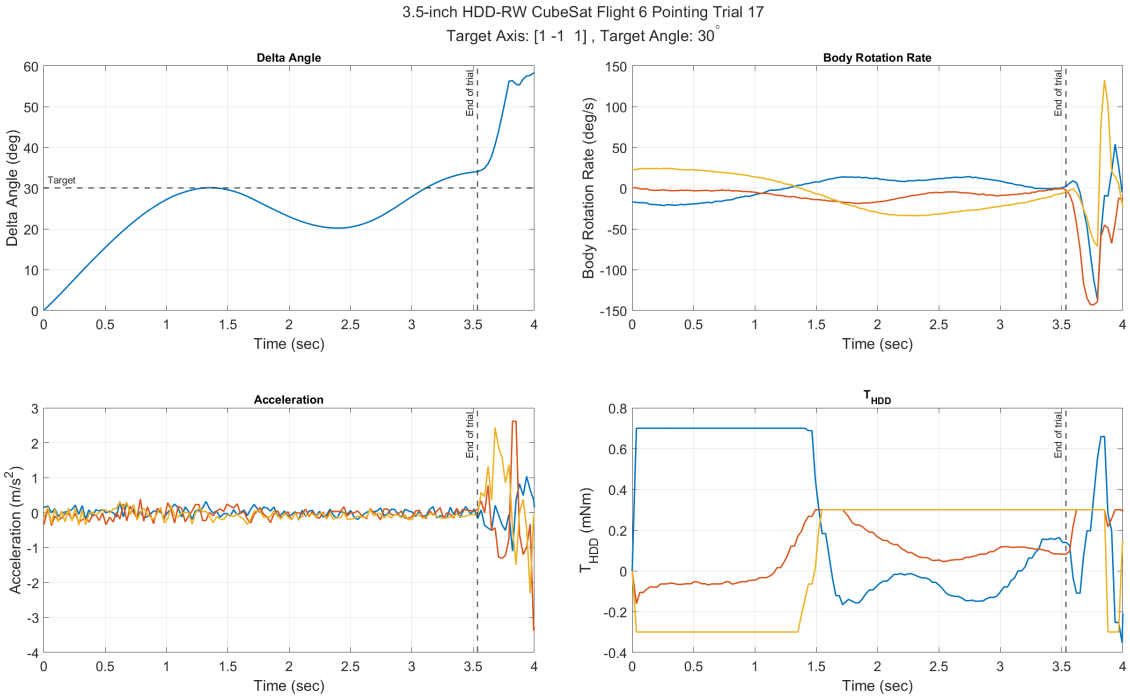

Figure 3.29: 3.5-inch HDD-RW CubeSat Flight 6 Pointing Trial 17

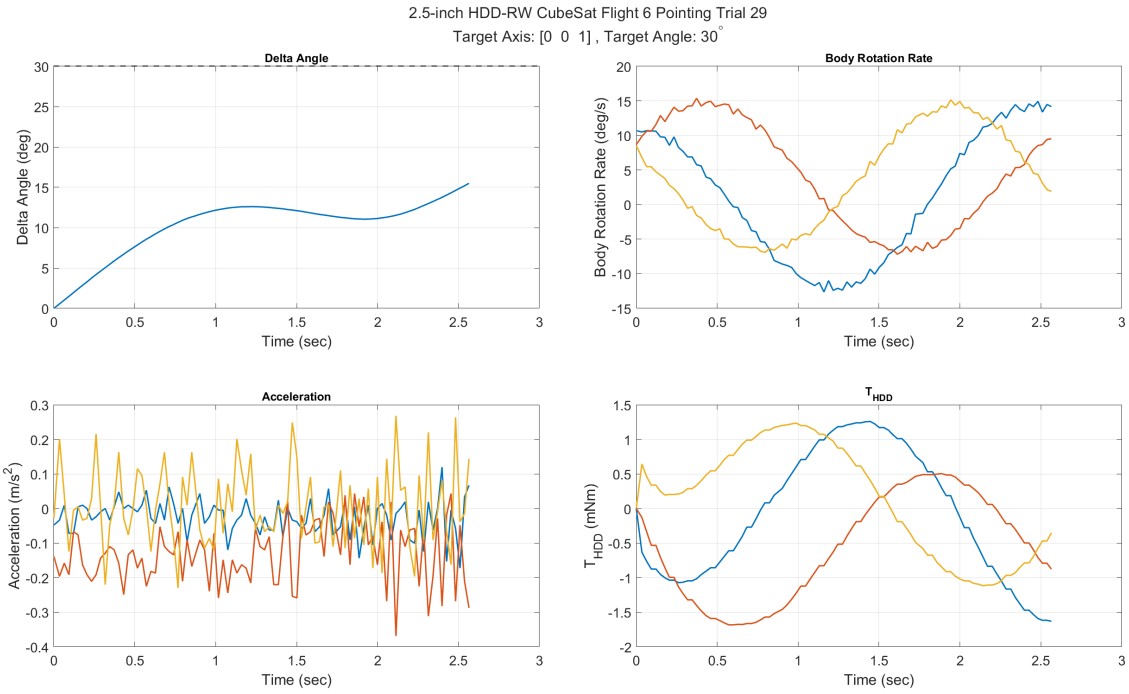

Figure 3.30: 2.5-inch HDD-RW CubeSat Flight 6 Pointing Trial 29

Overall, the pointing controller of the 2.5-inch HDD-RW CubeSat performed better than that of the 3.5-inch HDD-RW CubeSat. Figure 3.31 shows an example of pointing with the 2.5-inch HDD-RWs where the CubeSat testbed had a target angle of 15 degrees about axis [+1, -1, +1]. An overshoot of +2.29 degrees was observed, which was expected since the pointing controller was required to be aggressive due to the short floating duration per trial. The CubeSat testbed reached a final angle error of 0.86 degrees before the CubeSat testbed was caught by a researcher, as indicated by the spike in gyroscope and accelerometer data.

Figure 3.32 shows another example pointing trial with the 2.5-inch HDD-RWs, where the target angle is 30 degrees about axis [+1, -1, +1]. Oscillations about the 30 degree target were observed where the final oscillation peak had an angle error of 4.2 degrees. As expected from the controller, the oscillations were observed to decay over time. The target angle is expected to have been reached within tens of seconds given longer microgravity duration.

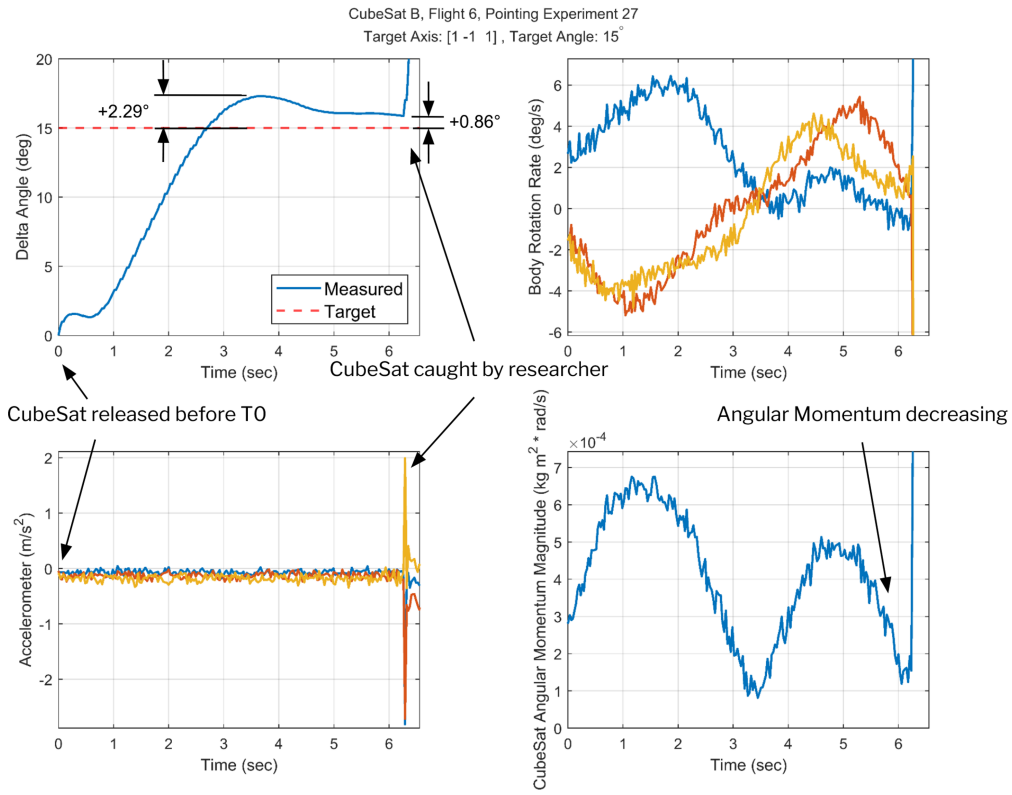

Figure 3.31: Flight 6 15° Pointing Trial

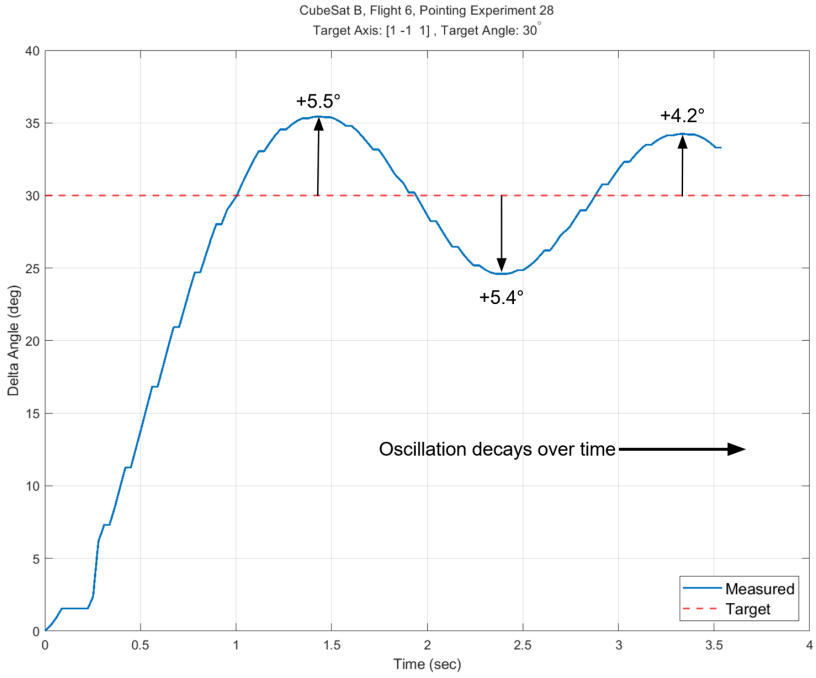

Figure 3.32: Flight 6 30° Pointing Trial

3.4.3 Summary of Results

Parabolic flight testing of the HDD-RWs have demonstrated that they can be used as CubeSat reaction wheels. In stabilization and pointing demonstrations, the HDD-RWs successfully stabilized and reoriented the CubeSat testbed. The 2.5-inch HDD-RW and 3.5-inch HDD-RW demonstrated momentum storage of 7.4 mNms and 45.0 mNms - values that are comparable to commercial reaction wheels. The 2.5-inch HDD-RW demonstrated pointing with an angular error less than 1°. The constraint of 3 - 7 seconds of free-floating time per trial proved to be challenging and required an over-aggressive controller. Although the stabilization and pointing tests were not able to bring the CubeSat rotation rates and angular error to zero due to the short duration of microgravity period in flight, the tests demonstrate promising capability. When designing the controller for space, where CubeSats typically have on the order of minutes to perform attitude maneuvers, it is recommended to reduce the gain values from what is used in this project.

3.5 Simulation

3.5.1 Simulation Based System Identification

Data from parabolic flight testing was used to develop a model and simulation of the HDD-RWs, controller, and CubeSat dynamics. The simulation model was used to: 1) perform system identification of the HDD-RWs and CubeSat system, and 2) simulate results for different controller parameters. 18 system parameters, listed in Table 3.2, were estimated using gradient descent optimization.

The optimization cost function was defined as the mean absolute error of the body rotation rate between the model and the flight data, as shown in Equation 3.20. Training data from flight testing had a sampling rate of approximately 30 Hz. The simulation time rate was set to 200 Hz. For calculation of the cost function, the simulated body rotation rate was resampled at the timestep of the training data by linearly interpolating the training data.

$$J(\theta) = \frac{1}{n}\sum_{i=1}^{n}\left|\omega_i^{sim} - \omega_i^{data}\right| \tag{3.20}$$

$$\frac{\partial}{\partial \theta^j} J(\theta) = \frac{J(\theta_1, ...\theta_j + d\theta_j, ...\theta_m) - J(\theta_1, ...\theta_j, ...\theta_m)}{d\theta_j} \tag{3.21}$$

$$\theta_{i+1}^j = \theta_i^j - \alpha^j \frac{\partial}{\partial \theta_i^j} J(\theta) \tag{3.22}$$

The gradient at each iteration was numerically found by individually perturbing each parameter by a small fraction and re-evaluating the cost function with the perturbed parameter - the equation for gradient was then found using Equation 3.21. The update step is shown in equation 3.22, where θ is the parameter, j is the parameter index, i is the iteration index, and α is the step size. The initial guesses for the HDD time constants were found from the HDD-RW step response test described in Section 3.3.1.1. The initial guess for the system time delay was based on an estimate based on typical values. The initial guesses for the CubeSat inertia matrix and the HDD-RW moment of inertia were based on CAD models. The initial guesses for the ESC command to RPM mapping were found from the HDD-RW step response test. The step size for each parameter was manually tuned; parameters that the cost function was found to be more sensitive to were given a smaller step size.

Table 3.2: 2.5-inch HDD-RW system identification optimization parameters

Parameter	**Initial Value**	**Optimization-Based Value**	**Percent Change**
CCW Time Constant (sec)	1.3	1.28	-1.85%
CW Time Constant (sec)	1.3	1.24	-4.95%
CCW Braking Time Constant (sec)	1.2	2.89	140.60%
CW Braking Time Constant (sec)	1.2	3.16	163.60%
Controller Time Delay (sec)	0.01	0.045	357.09%

MOI HDD-RW (g cm^2)	4.91E+01	4.71E+01	-3.98%
MOI CubeSat X (g cm^2)	4.56E+04	4.62E+04	1.32%
MOI CubeSat Y (g cm^2)	4.72E+04	4.80E+04	1.76%
MOI CubeSat Z (g cm^2)	4.98E+04	4.43E+04	-11.02%
MOI CubeSat XY (g cm^2)	3.91E+01	-1.81E+03	-4729.71%
MOI CubeSat XZ (g cm^2)	-7.66E+01	-1.54E+03	1909.53%
MOI CubeSat YZ (g cm^2)	-2.48E+01	-6.18E+02	2395.25%
CW Coeff. c2	-0.03706	-0.04784	29.10%
CW Coeff. c1	76.3503	75.3043	-1.37%
CW Coeff. c0	-3.0762	-2730.77	88671.00%
CCW Coeff. c2	-0.03039	-0.02742	-9.77%
CCW Coeff. c1	70.1948	65.2811	-7.00%
CCW Coeff. c0	-1.2619	680.53	-54029.20%
Mean Absolute Error (deg/s)	**0.1452**	**0.029**	**-80.03%**

The flight data was randomly split into two sets: a training set and a test set. Optimization of the system parameters was performed on the training data while the test set was reserved for cross-validation to ensure that the optimal values were not over-fitting to the training data. The parameter values found from the optimization are shown in Table 3.2. The cost function values for the initial guess were 0.1452 deg/s and 0.1148 deg/s for the training and test data sets, respectively. Optimization of the parameters reduced the cost

function value to 0.0290 deg/s and 0.0320 deg/s for the training and test data sets, respectively. The optimized parameters reduced the cost function value by 80.0% and 72.13% for the training and test data sets, respectively. For the optimized parameters, the cost function for the test data set was 10.34% greater than that of the trained data, indicating that there was not significant overfitting in the optimization, thus validating the optimization results.

The parameters that had the most significant difference between the optimization-based estimated values and initial estimated values were the braking time constants, controller time delay, MOI off-diagonal terms, and ESC to RPM mapping $c0$ coefficients. The optimization-based braking time constant estimates were found to be approximately 50% higher than the accelerating time constants - this significant difference indicates that the HDD-RW actuator model should differentiate between when the disk is accelerating or braking. The time delay was underestimated by a factor of approximately 4.5x or 0.035 seconds. Although the percent difference between the initial estimate and optimization-based estimate is significant, this time delay likely did not have a significant effect as the controller loop cycle time is 0.1 seconds which is an order of magnitude higher than the controller time delay.

The CubeSat MOI off-diagonal terms were each found to be approximately an order of magnitude higher than estimated from the CAD - this is likely due to the wire harnessing that was previously considered negligible in the CubeSat CAD. The underestimated significance of the MOI off-diagonal terms likely led to non-ideal performance in the controller. The ESC to RPM mapping $c0$ coefficients represent the bias value of the RPM mapping. Since the RPM value is on the order of 10^3 to 10^4 and the RPM mapping is more sensitive to the $c2$ and $c1$ coefficient values, the large percent deviation between the initial estimates and the optimization-based estimates are considered to be reasonable.

Figures 3.33, 3.34, and 3.35 show the simulated CubeSat body rotation rates and time derivatives of CubeSat body rotation of three sample trials from the trained data set. Figures 3.36, 3.37, and 3.38 show the simulated CubeSat body rotation rates and time derivatives of CubeSat body rotation of three sample trials from the test data set.

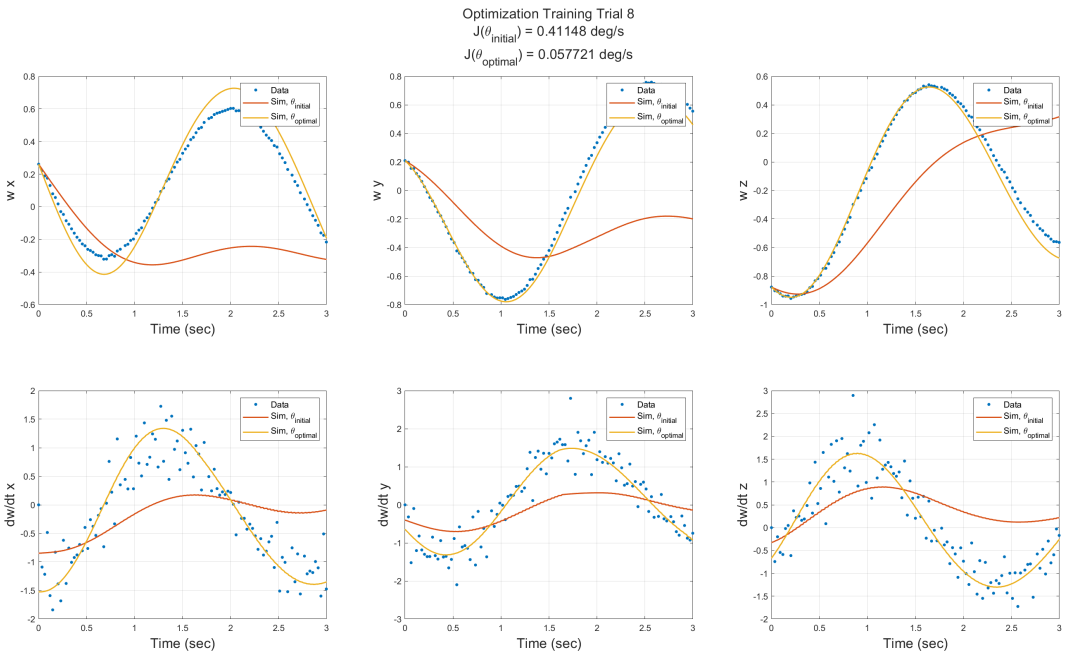

Figure 3.33: 2.5-inch HDD-RW CubeSat Model Comparison Trial 8

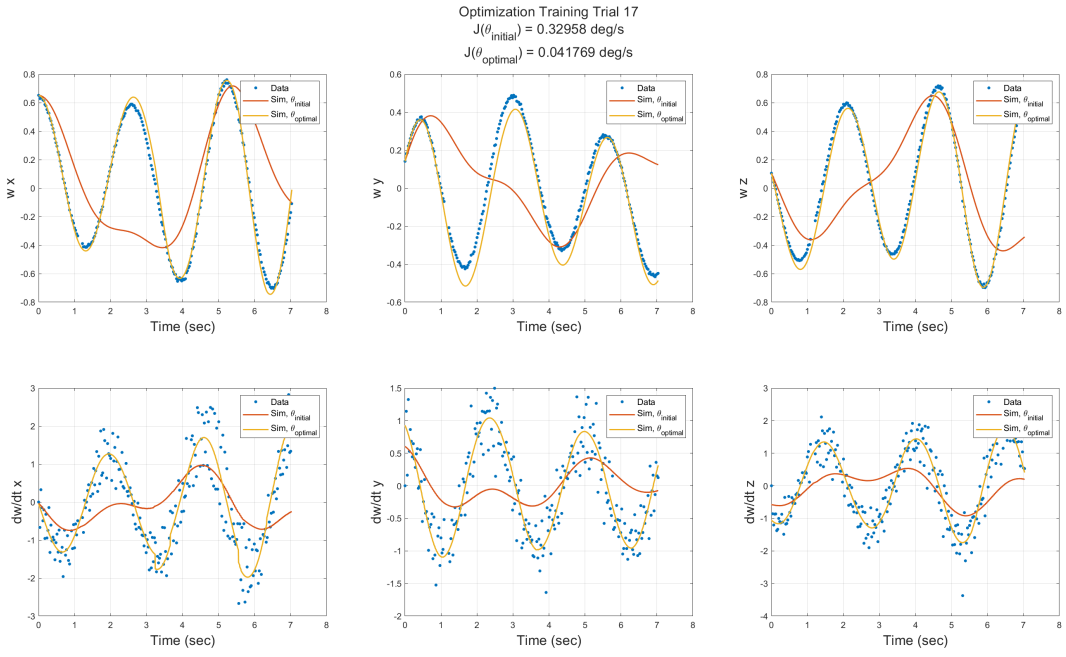

Figure 3.34: 2.5-inch HDD-RW CubeSat Model Comparison Trial 17

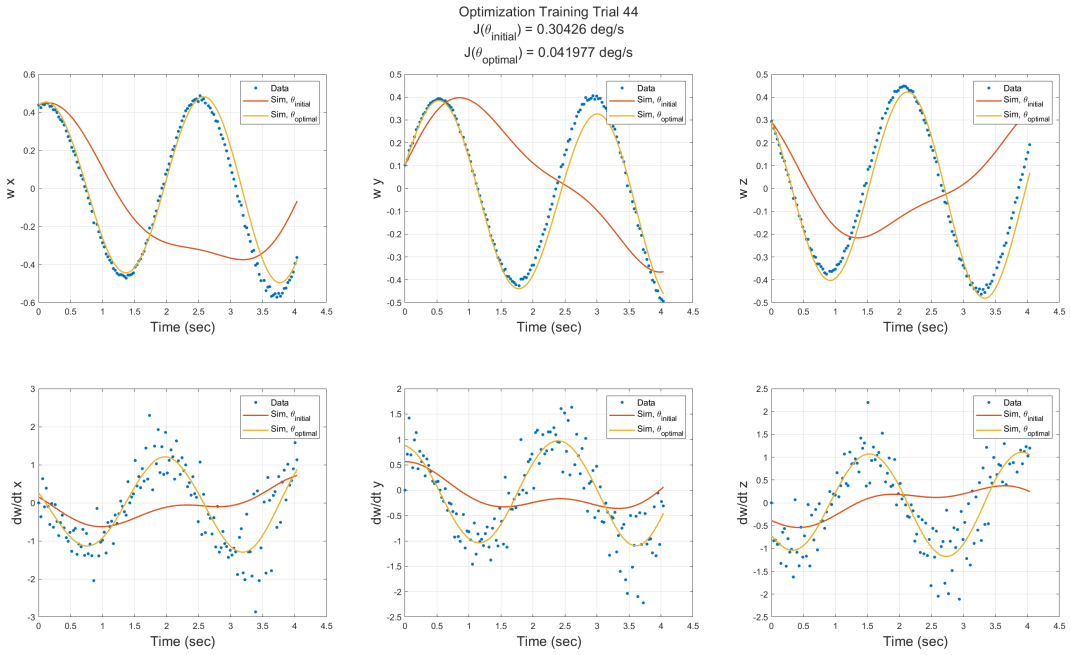

Figure 3.35: 2.5-inch HDD-RW CubeSat Model Comparison Trial 44

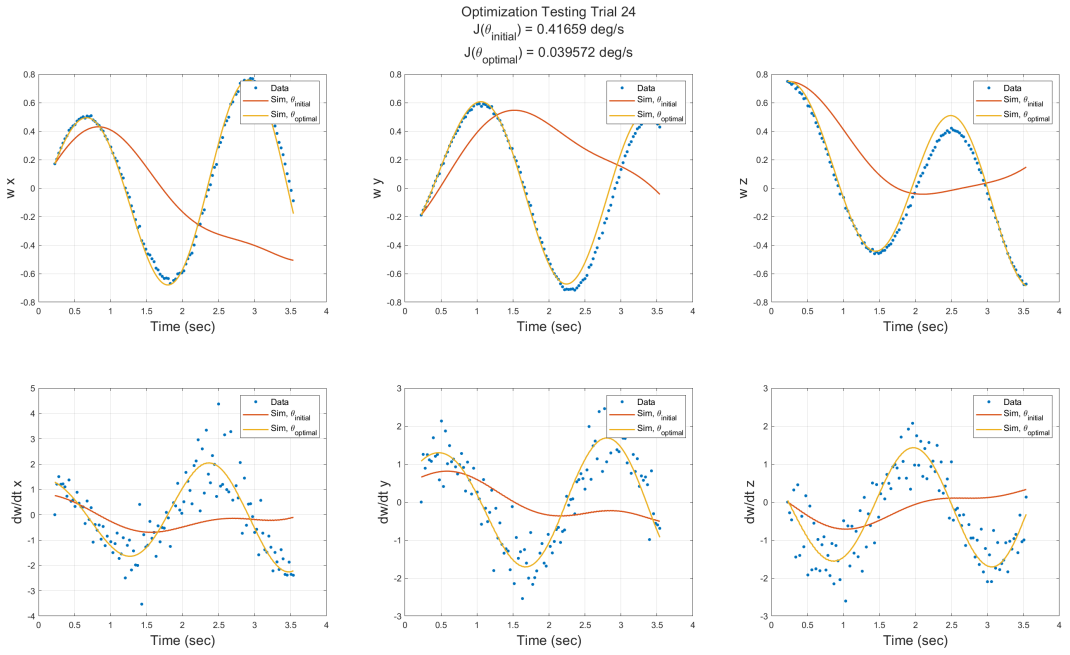

Figure 3.36: 2.5-inch HDD-RW CubeSat Model Comparison Trial 24

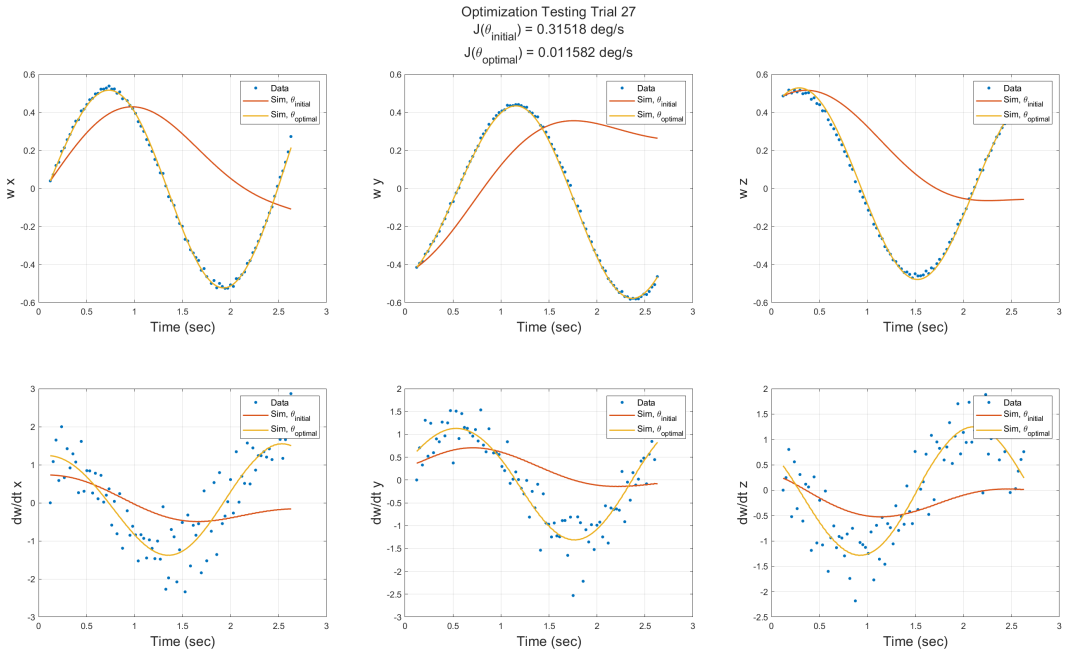

Figure 3.37: 2.5-inch HDD-RW CubeSat Model Comparison Trial 27

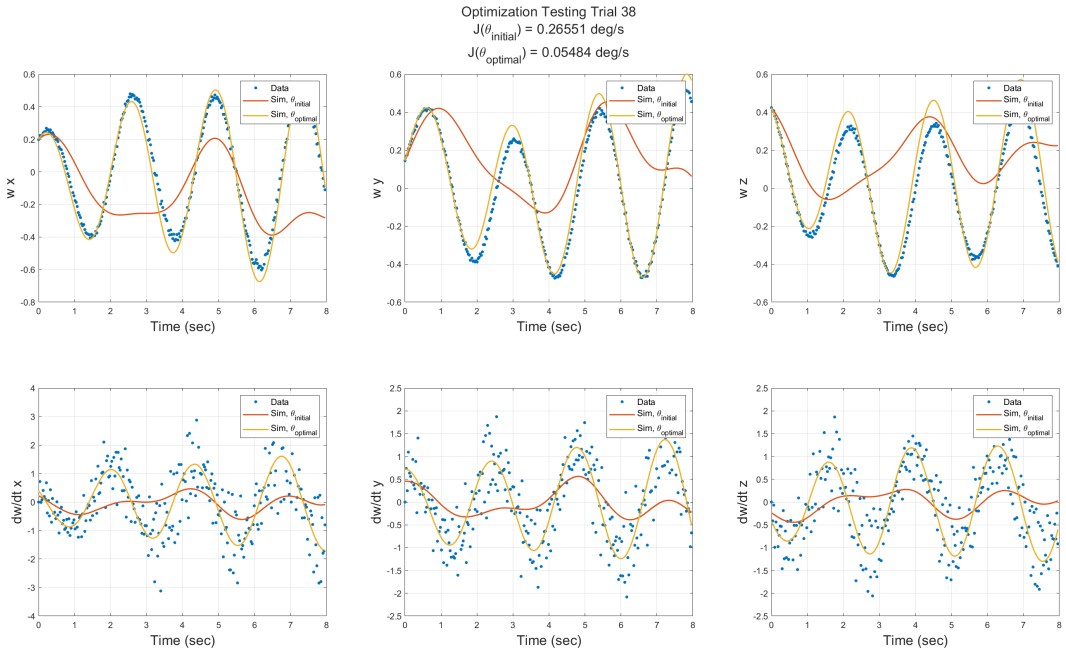

Figure 3.38: 2.5-inch HDD-RW CubeSat Model Comparison Trial 38

3.5.2 Re-tuned Controller Simulation

The model of the HDD-RW and CubeSat system found from system identification was used to simulate the CubeSat's behavior with re-tuned controller parameters. The modeled system included speed saturation of the HDD-RWs as well as time delay. In the flight software simulator, only the controller gains were changed. Each of the 2.5-inch HDD-RW trials previously shown in Section 3.5.1 were simulated with updated controller gains in Figures 3.39, 3.40, 3.41, 3.42, 3.43, and 3.44. The simulated CubeSat's initial angular velocity and target attitude values were identical to those from flight data. For each of the trials, the simulated CubeSat stabilized within 1 deg/s per axis and pointed within 0.5 degrees of its target. In Trials 8, 44, 17, 27, and 28, the CubeSat stabilized at its target attitude within 1.5 to 2 minutes and in trial 24, the CubeSat stabilized at its target attitude in 10 minutes due to a high initial angular velocity of 42.9 deg/s about the z-axis.

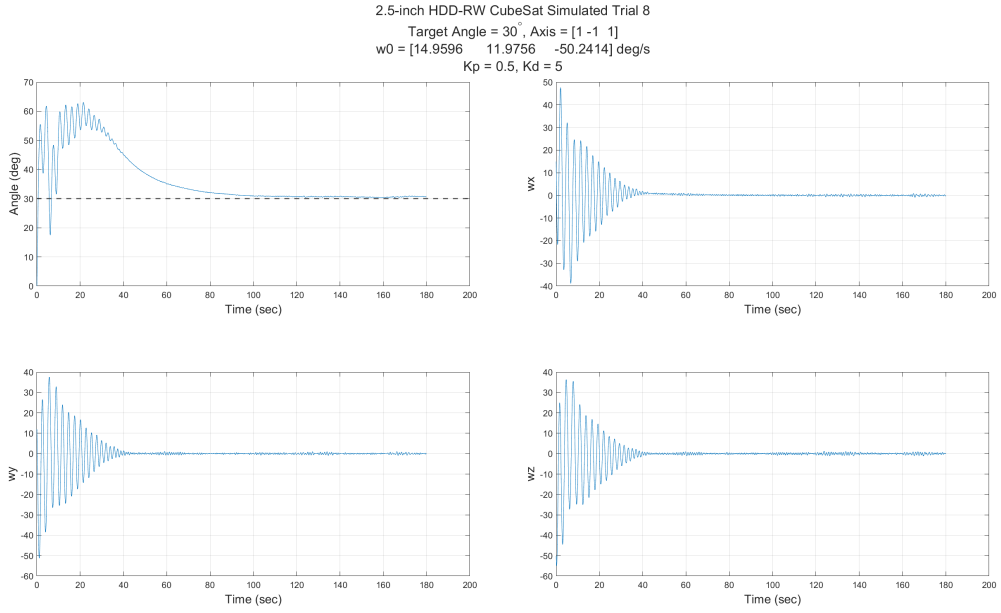

Figure 3.39: 2.5-inch HDD-RW CubeSat Simulation Trial 8

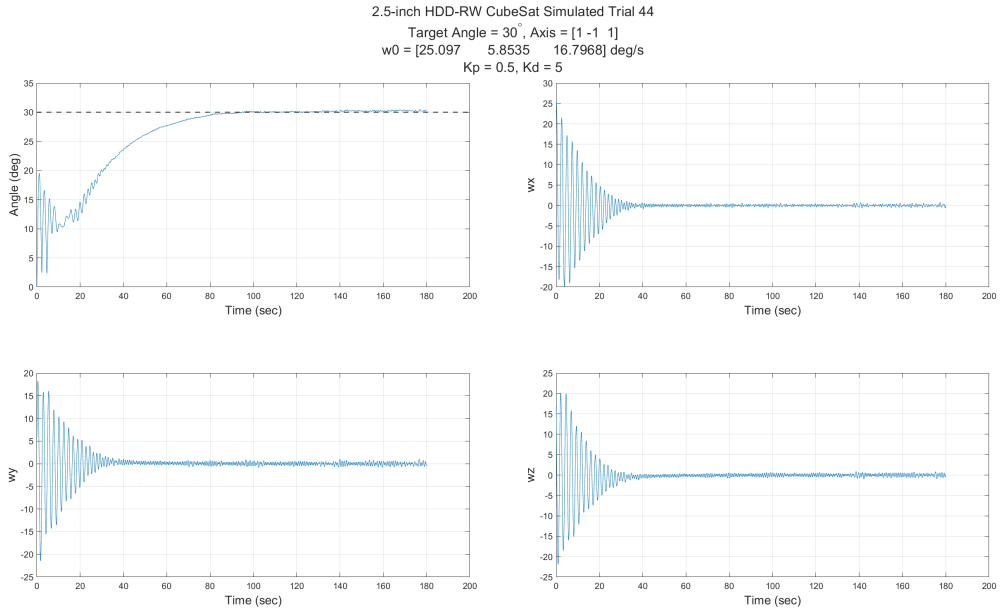

Figure 3.40: 2.5-inch HDD-RW CubeSat Simulation Trial 44

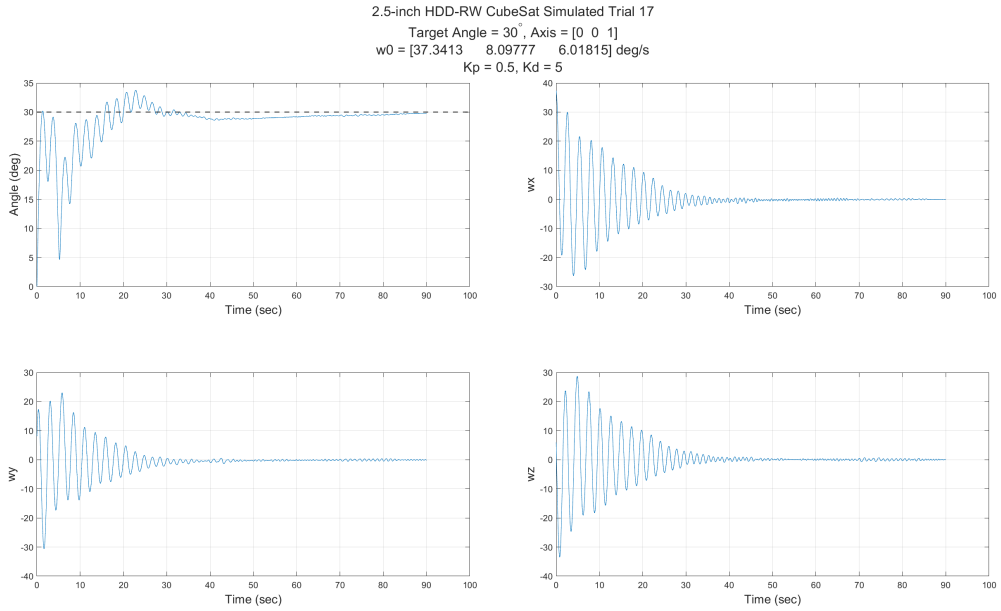

Figure 3.41: 2.5-inch HDD-RW CubeSat Simulation Trial 17

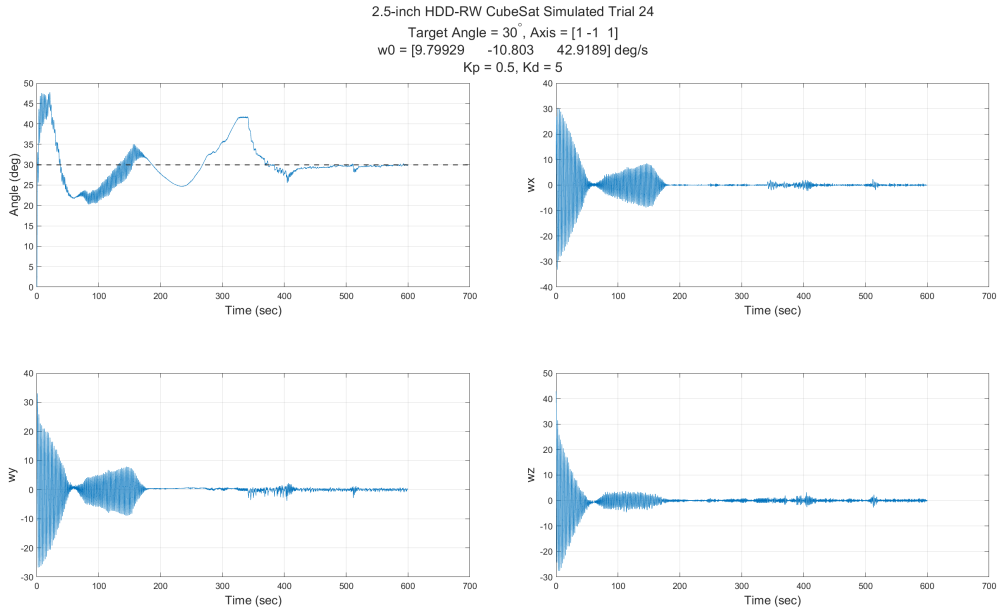

Figure 3.42: 2.5-inch HDD-RW CubeSat Simulation Trial 24

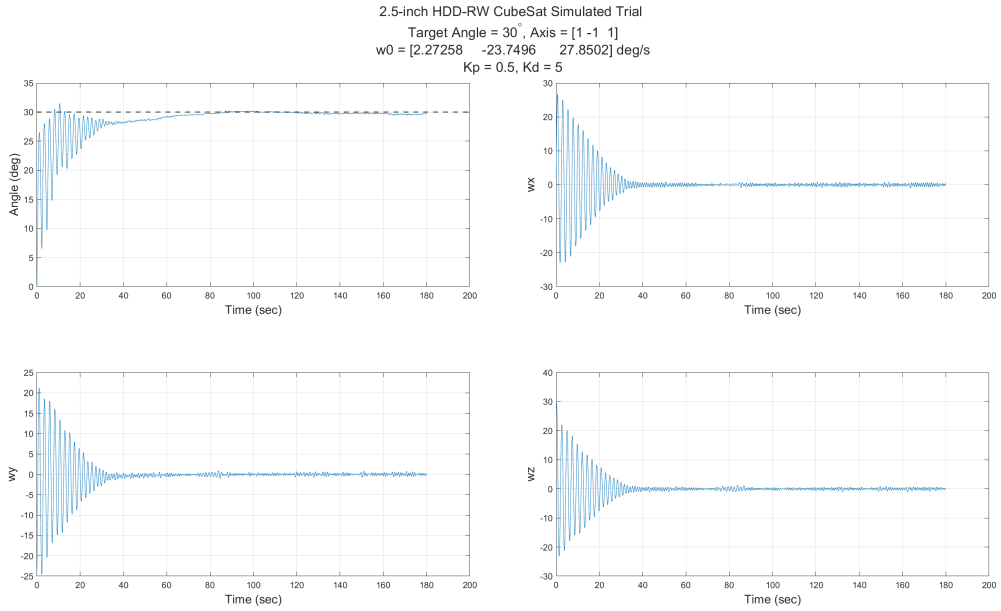

Figure 3.43: 2.5-inch HDD-RW CubeSat Simulation Trial 27

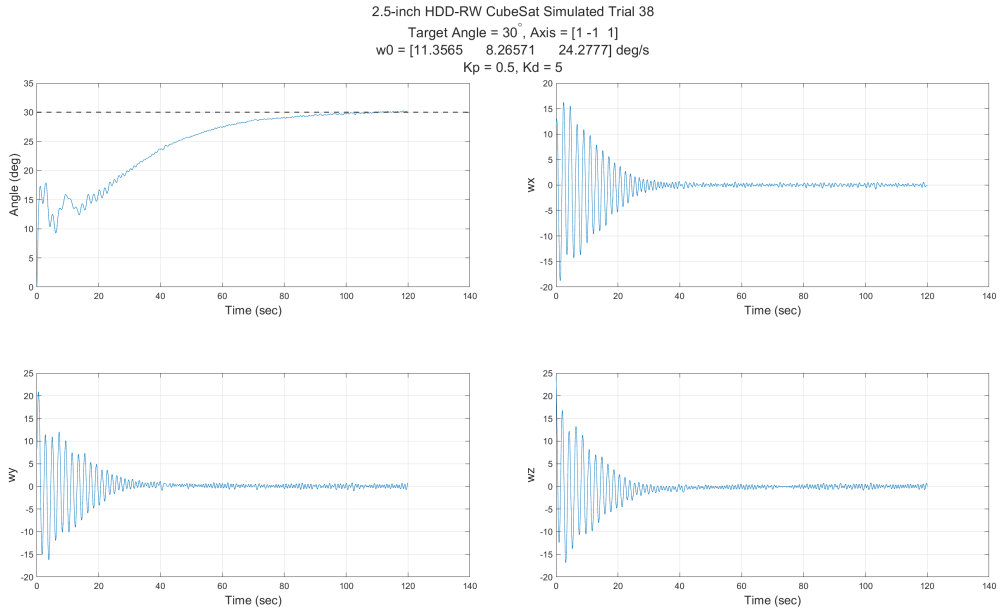

Figure 3.44: 2.5-inch HDD-RW CubeSat Simulation Trial 38

Each of the simulated flight trials had a target angle of 30° along an arbitrary axis. To test a wider range of cases, the controller was also verified for varying target angles and initial velocities. The CubeSat was simulated for target angles of 5°, 45°, 90°, and 180°, as shown in Figures 3.45, 3.46, 3.47, and 3.48. The initial rotation rates were set to a random value between -20 and +20 deg/s and the target axis was a random 3D vector. For each of the cases, the simulated CubeSat stabilized within 0.5 deg/s and pointed within 0.5 degrees of its target within 3 minutes.

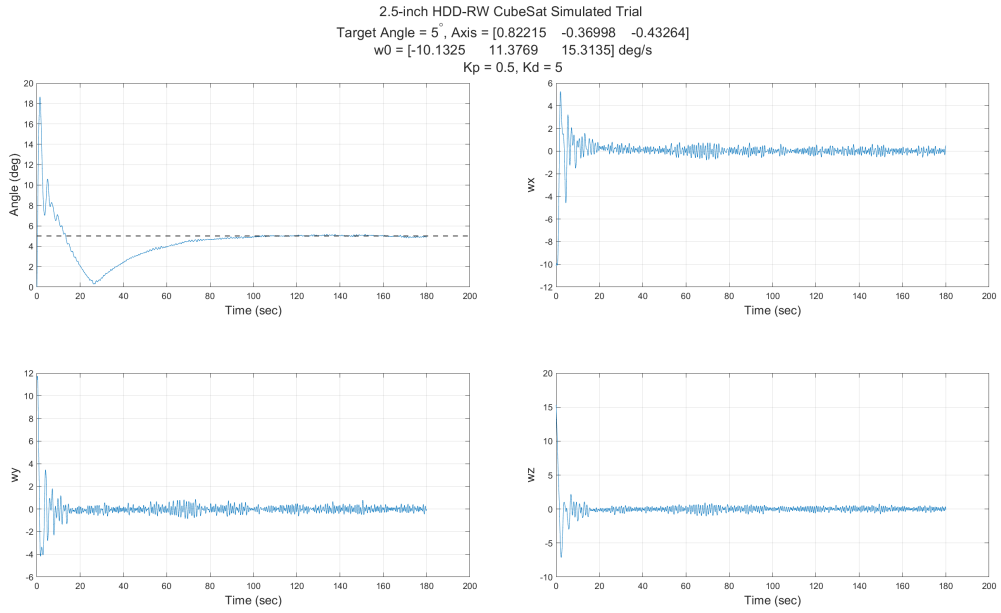

Figure 3.45: 2.5-inch HDD-RW CubeSat Simulation - 5°

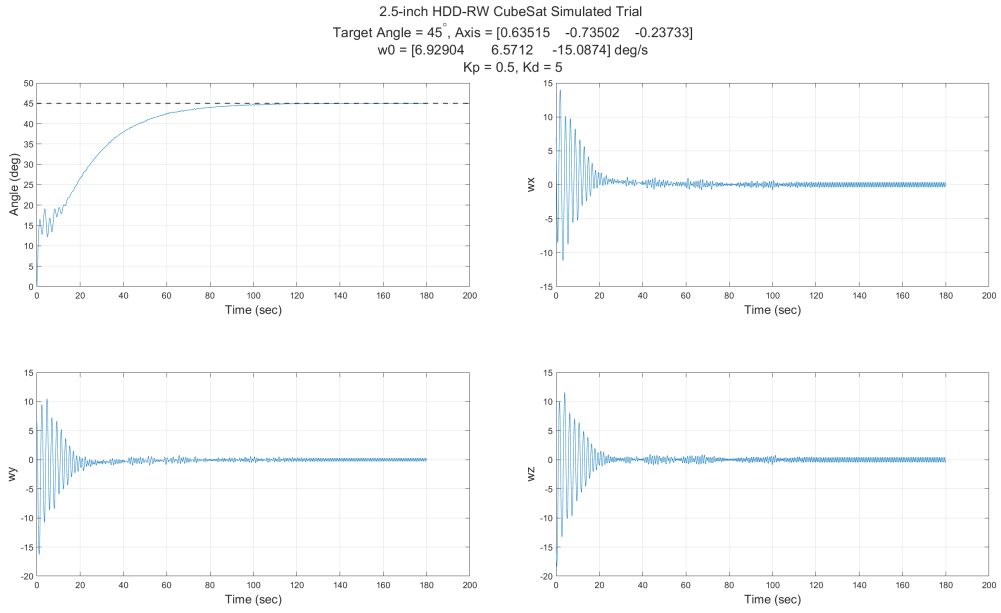

Figure 3.46: 2.5-inch HDD-RW CubeSat Simulation - 45°

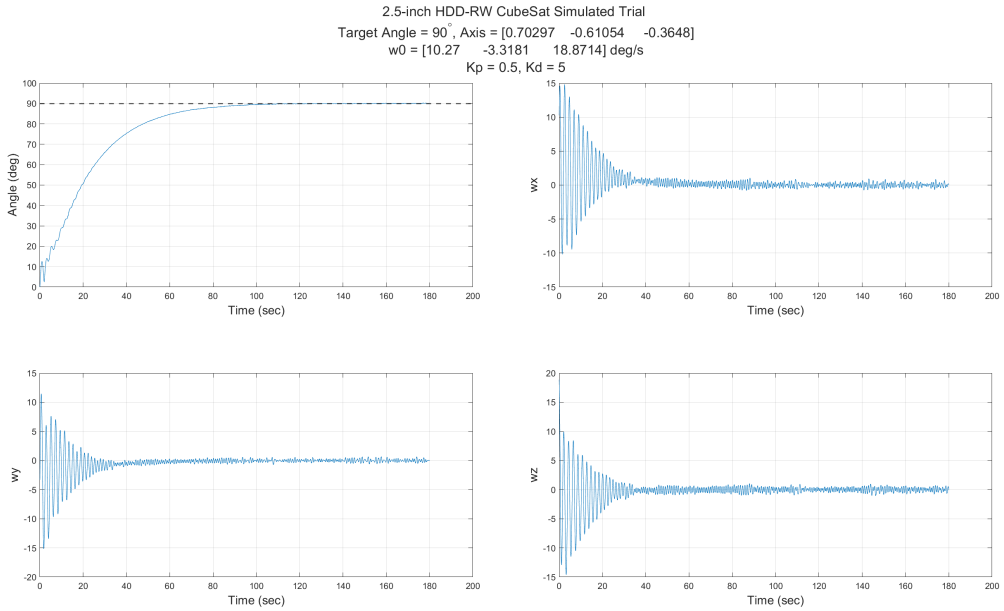

Figure 3.47: 2.5-inch HDD-RW CubeSat Simulation - 90°

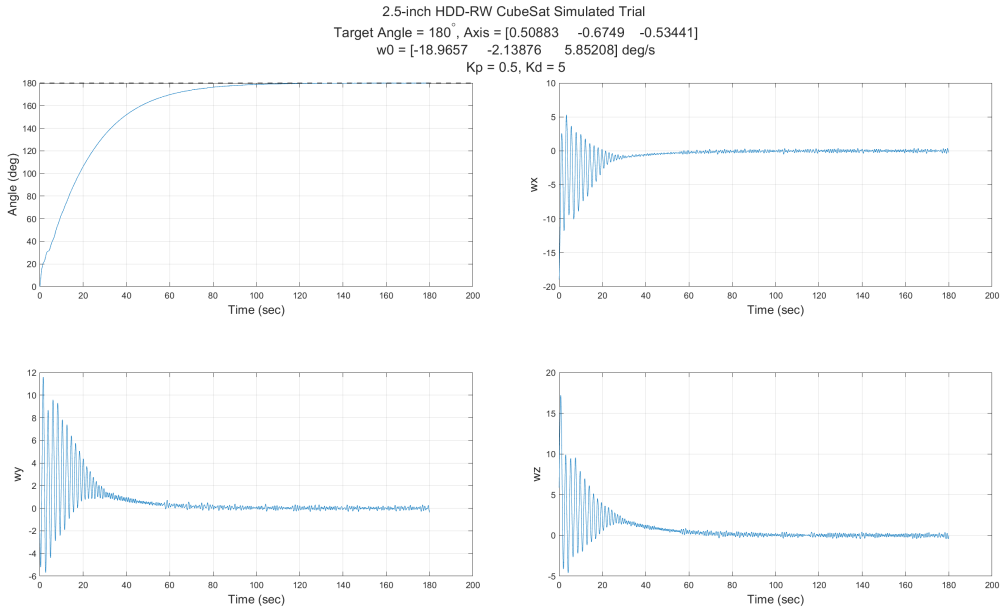

Figure 3.48: 2.5-inch HDD-RW CubeSat Simulation - 180°

3.6 Summary

Through ground testing, an actuator model and controller has been developed for the HDD-RWs. The HDD-RWs and controllers were demonstrated in microgravity parabolic flight testing. The 3.5-inch HDD-RWs demonstrated CubeSat stabilization and the 2.5-inch HDD-RWs demonstrated CubeSat pointing. Although the CubeSat had not stabilized at its target within the very brief microgravity period, the HDD-RWs mitigated the majority of the CubeSat's angular momentum and flight results indicate that the CubeSat would reach its target state within minutes, which is an appropriate time-frame for orbital flight.

The parabolic flight data was used to measure the momentum storage and torque of the 2.5-inch and and 3.5-inch HDD-RWs, which demonstrated to be comparable to commercial CubeSat reaction wheels. The flight data was also used to perform system identification and fine-tune the 2.5-inch HDD-RW actuator model. The system model was verified with flight data in a cross-validation study. Simulation results based on system identification also indicate that the 2.5-inch HDD-RWs and a re-tuned PD controller can point a CubeSat for various target attitudes and initial rotation rates.

A summary table of the HDD-RW performance specifications is shown in Table 3.3.

Table 3.3: HDD-RW performance specifications

Specification	2.5-inch HDD-RW	3.4-inch HDD-RW
HDD Model	HGST Travelstar Z7K500-500	Samsung Spinpoint HD161HJ
Mass	45.5 g	89.3 g
Volume	99.0mm x 69.8mm x 5.8mm	95.0mm x 95.0mm x 17.5mm
Disk + Spindle MOI	2.8E-6 kg mˆ2	1.9E-5 kg mˆ2
Max RPM CCW	25350 RPM	12975 RPM
Max RPM CW	25000 RPM	12750 RPM
Max Momentum CCW	7.5 mNms	45.0 mNms
Max Momentum CW	7.4 mNms	45.0 mNms
Max Torque CCW	1.6 mNm	6.0 mNm
Max Torque CW	1.3 mNm	6.0 mNm

Chapter 4

Guide for Using Hard Disk Drive Reaction Wheels

4.1 Converting a Hard Disk Drive to a Hard Disk Drive Reaction Wheel

The process of converting a HDD into a HDD-RW can be completed within a few hours. The conversion process does not require costly equipment and is similar for all HDD models with minor variations. The mechanical and electrical modifications are described in the following sections.

4.1.1 Mechanical Modifications

The mechanical modifications required for the HDD-RWs can be summarized as removing the HDD PCB, opening the HDD, removing the read and write arm, and closing the HDD. For the 3.5-inch HDD form factor, the motor may also be removed from its casing, as shown in Figures 4.1 and 4.2. These modifications can be completed with a standard computer repair tool kit. It is recommended to safely stow screws through the opening process as some of them will be required for the closing process. It is also recommended to take photographs after each step of the modification process for documentation purposes.

Figure 4.1: 3.5-inch HDD with casing

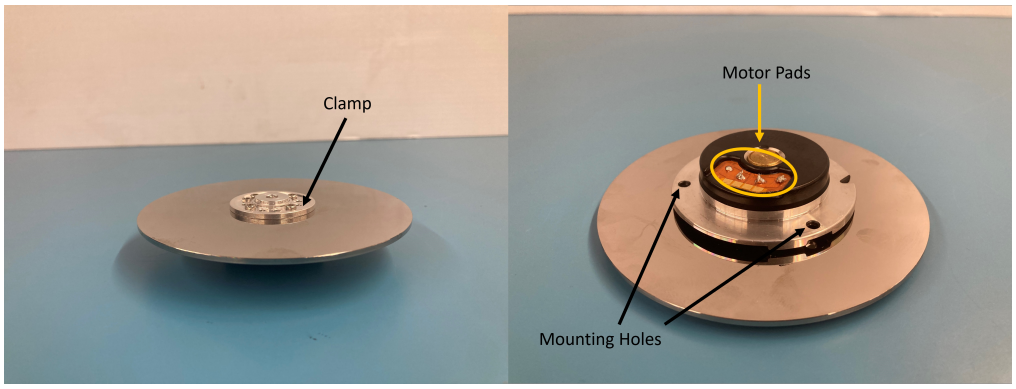

Figure 4.2: 3.5-inch HDD out of casing

Removing the read and write arm requires opening the casing of the HDD, which breaks its seal. Although the flight HDD-RWs tested in parabolic flight were not opened and handled in a clean environment, it is recommended that spaceflight units of HDD-RWs are handled with gloves and in a cleanroom-like environment to avoid foreign object debris (FOD). For the 1.8-inch and 2.5-inch HDD form factors, once the read and write arm is removed, the HDD casing may be reattached. For the 3.5-inch HDD form factor, the HDD-RW may be used in its casing; however, due to the high mass and volume of the metallic casing it is favorable to remove the HDD motor from its casing.

To remove the 3.5-inch HDD motor, the clamp must first be unscrewed. In order to prevent the disk from spinning while removing the screws fastening the top cap, the spindle may be carefully held along its circumference. Holding the disk by its face while removing the clamp is not recommended as doing so may apply too much pressure on the disk.

After taking the clamp off, the disk can be carefully removed. This will reveal the 3.5-inch HDD motor which is mounted by three screws equally spaced around its circumference. These three screws may be removed to extract the HDD motor from its casing. This is a good point to measure the individual masses of each of the components, if desired.

HDDs are designed to be mounted within laptops and computers using threaded holes within their casings. Conveniently, the same threaded holes can be used to mount the HDD-RWs. The standard screw sizes for the 1.8-inch, 2.5-inch, and 3.5-inch HDDs are M1.4, M3, and # 6-32 UNC, respectively. If the 3.5-inch HDD is used without its casing, the 3.5-inch HDD-RW can be mounted by using the three circumferential through holes around the motor. For integration purposes, it is important to note that the motor must be mounted without the disk and once the motor is mounted, the disk may be attached with the spindle hub. Additionally, it is important to note that the disk will not be inside a protective casing.

4.1.2 Electrical Speed Controller

4.1.2.1 COTS ESC

The rising popularity of unmanned aerial vehicles (UAVs) and remote control (RC) boats has led to an increasing number of available COTS ESCs on the market. The COTS ESCs that run the BLDC motors propelling UAVs and RC boats can be repurposed to run the BLDC motors of HDDs. This section will describe the types of COTS ESCs successfully used and recommendations.

When selecting a COTS ESC for HDD-RWs, it is important to select a bidirectional ESC to allow control of the HDD's rotation in both directions. Many UAV ESCs are designed for single direction as most UAVs only require their propellers to provide upwards thrust. COTS bidirectional ESCs are widely available and low-cost. Additionally, it is important to select an ESC with a "throttle" feature for the HDD-RWs as some ESCs, such as those for HDDs or computer fans, are limited to driving BLDC motors to discrete speeds. COTS ESCs are most often commanded using a pulse width modulation (PWM) signal. To command the HDD-RWs, the CubeSat flight computer must be capable of outputting a PWM signal for each HDD-RW.

Some UAV ESCs are also designed in a "4-in-1" form factor which consolidates 4 individual ESCs into a single board, as shown in Figure 4.3. This design significantly reduces the

ESC mass and volume. 4-in-1 ESCs also provide the benefit of easy mechanical integration as most have 4 mounting holes.

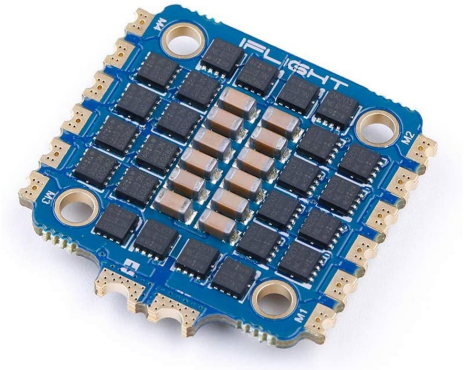

Figure 4.3: iFlight SucceX-E F4 V2 4-in-1 ESC [34]

It is also important to select an ESC that can supply sufficient power to the HDD-RWs. Based on lab testing, the recommended voltages for the 1.8-inch and 2.5-inch HDD-RWs is 12V while the recommended voltage for the 3.5-inch HDD-RW is 15V. The maximum (peak) current drawn from the 1.8-inch, 2.5-inch, and 3.5-inch HDD-RWs is 0.6 A, 0.6 A, and 1.0 A, respectively. COTS ESCs are often rated to 4S, meaning they support bus voltages of 4 standard lithium cells (4.2V max each) in series (16.8V max total). The current ratings for COTS ESCs are often on the order of 30A and higher than required for the HDD-RWs. It is also important to consider the current limits of the cells and any other components between the cells and HDD-RWs, such as battery management systems and voltage converters.

Reaction wheels are often one of the most high-power components within a CubeSat. Resistive heating occurs not only in the HDD-RW, but also in the ESC. Thus, it is important to take thermal effects into consideration for the ESC. If a 4-in-1 form factor ESC is used, it is also important to consider the effects of the heat loading being localized in a small area.

Lastly, COTS ESCs often have a capacitor in parallel to the input voltage to mitigate effects of input voltage fluctuations. Most often, this capacitor is an electrolytic type capacitor - it is important to replace this type of capacitor with one that has space heritage as electrolytic type capacitors have been observed to fail in space environment.

4.1.2.2 Custom ESC

While COTS ESCs provide the benefit of a ready-made solution, the custom ESC provides the benefits of design flexibility and custom tuning. CubeSats often need to consolidate various electrical subsystems on just a few PCBs. The custom ESC consists of a in-house designed PCB with a commercial motor driver IC chip - this can be consolidated with other electrical subsystems of the CubeSat for a more compact design.

The Texas Instruments (TI) DRV10983 BLDC motor driver was identified as a motor driver with appropriate specifications to drive the 2.5-inch and 3.5-inch HDD-RWs. Sahar et al. [21] used a similar motor driver, the DRV10975, to drive a 3.5-inch HDD-RW. The DRV10983 was successfully tuned to start up the 2.5-inch HDD-RW, but requires further tuning to transition from startup to ESC closed loop control. TI has provided a helpful tuning guide to identify tuning parameters for the DRV10983 with any given BLDC motor.

4.1.3 Electrical Connections

For all HDD form factors, most HDDs utilize a wye-connected motor and have four pads on the bottom of the HDD motor that connect to the original HDD ESC via four spring finger contacts on the PCB. For a wye-connected motor, of the four leads, three of the leads are motor leads while the fourth is the neutral point, as shown in Figure 4.4. To identify the neutral point, measure the resistances between each pair combination. The motor neutral-phase resistance will be approximately half of the phase-phase resistance. To run the HDD with the custom or COTS ESC, the three ESC phase leads must be connected to the three HDD phase leads.

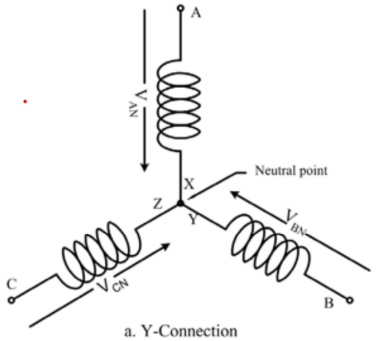

Figure 4.4: BLDC Motor Wye Connection [27]

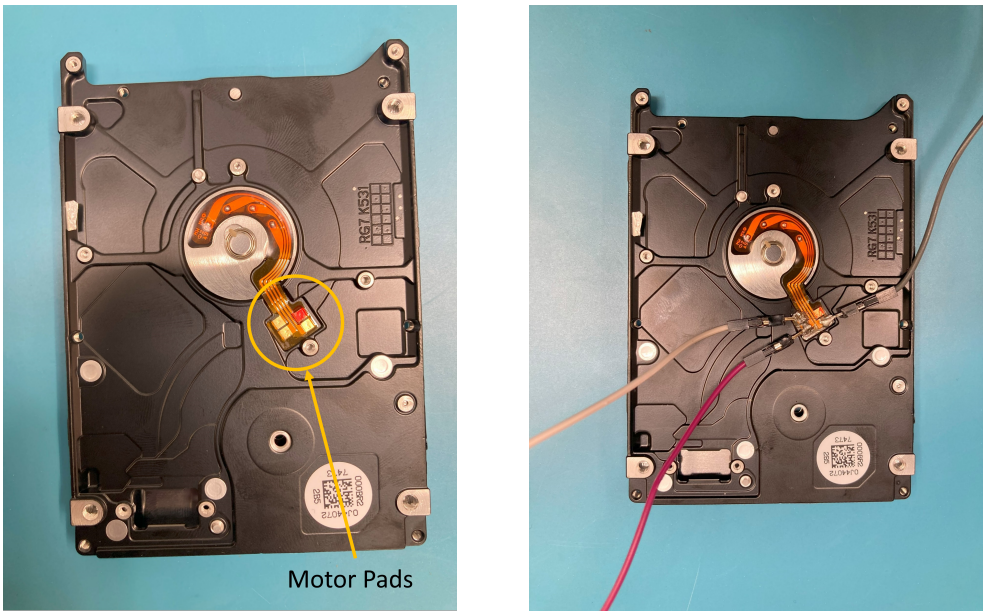

(a) 2.5-inch HDD Motor Pads

(b) 2.5-inch HDD Motor Pads with soldered wires

Figure 4.5: 2.5-inch HDD Motor Pads before and after soldering wires

For test units of HDD-RWs, the ESC can be connected to the HDD by soldering wires to the pads on the motor which are connected to the ESC via direct soldering or a breadboard. When soldering wires to the HDD pads, the soldering iron should not stay in contact with the pad for over 15 seconds as excessive heat may cause degradation of adhesive between the pad and casing. For this reason, resoldering of the wires to the pads should be avoided, if possible. Due to the proximity of the pads, it is recommended to ensure the pads are not shorted. This can be done by checking that the resistance between the leads does not significantly decrease from the original resistance values before soldering.

For flight units of HDD-RWs, solder joints are not recommended as they may fail under launch vibration and shock loading. An interfacing PCB may be designed to mechanically attach to the HDD-RW and make electrical contact with the HDD-RW motor. The contact can be made via spring finger contacts, shown in Figure 4.7, or via spring loaded pogo pins, shown in Figure 4.8, on the interfacing PCB. If a custom ESC is used, the interfacing PCB can be consolidated with the custom ESC PCB. If a COTS ESC is used, its leads can be connected to the interfacing PCB or directly mounted to the interfacing PCB, as shown in Figure 4.6

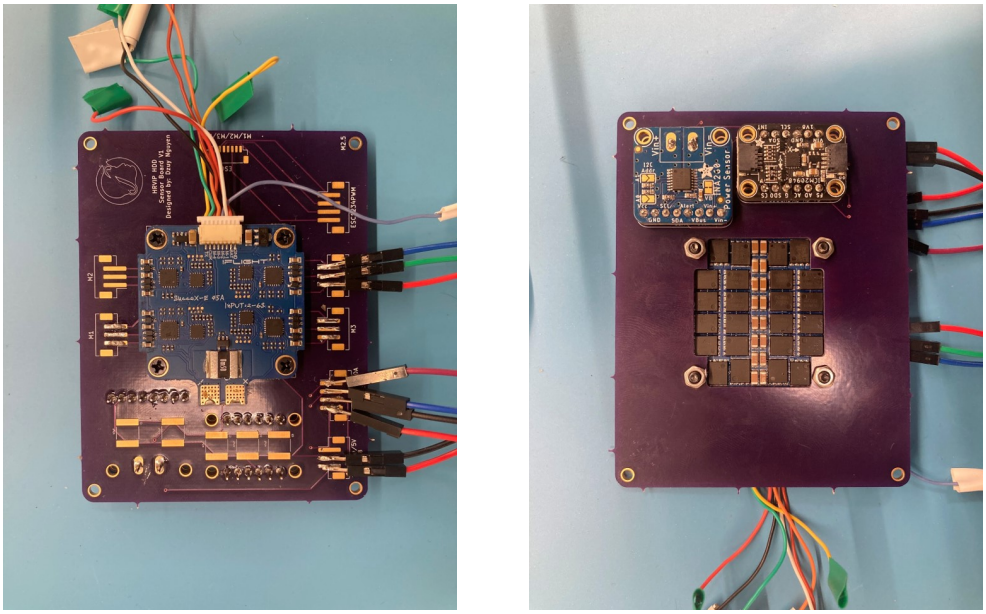

(a) ESC Board Top View **(b)** ESC Board Bottom View

Figure 4.6: ESC directly mounted on PCB

Figure 4.7: Spring Finger Contact [45]

Figure 4.8: Spring Loaded Pogo Pin [46]

4.2 Motor Control of HDD-RW

The process of developing control of a HDD-RW is summarized in the following steps:

1. Select configuration.
2. Find reliable startup sequences.
3. Perform input-response test to develop HDD-RW actuator model.
4. Determine keep-out-zone.
5. Design and test reliable direction switching algorithm.
6. Design, test, and tune HDD-RW attitude controller.

This process is not specific to the HDD motor and can be applied to develop bidirectional motor control of any BLDC motor.

Motor control requires tuning of several parameters. In general, the recommended practice is to begin with the most favorable parameters and then tune the parameters to fit the design constraints rather than constraining the testing parameters to fit within the design constraints. For example, it is recommended to begin HDD-RW motor control development with a COTS ESC, even if the final implementation will use a custom ESC, as they require less tuning and have proven reliability. Experience of testing the HDD-RW motor control with a COTS ESC provides valuable information for control with a custom ESC. Similarly, it is also recommended to begin motor control development at higher supply voltages and current limits, even if they are not within the design constraints, as the higher power allows the HDD-RW to more easily overcome static friction.

ESC selection is discussed in Section 4.1.2. It is recommended to begin testing with the iFlight SucceX-E ESC or a similar 4-in-1 ESC. It is also recommended to power the ESC with a DC power supply unit to test various input voltages and eliminate current supply limitations as a potential issue.

Once an ESC is selected, a reliable start-up sequence should be found. A reliable start-up sequence will consistently begin spinning the HDD-RW motor and transition from below 100 RPM to above 1000 RPM. A start-up sequence that consistently spins the HDD-RW after up to two failed start-up attempts may be considered reliable if the start-up is relatively quick. As discussed in Section 3.3.3.3, BLDC motors are not well-suited for spinning at low speeds, making motor start-up a challenge. A reliable start-up sequence can be found by testing various step input sequences, such as the sequences shown in 3.4. The step size and step duration should be varied. A step size that is too small or a step duration that is too long will not allow command sufficient torque to overcome static friction. A step size that is too large or a step duration that is too short will result in the ESC becoming out of phase with the motor. Most COTS ESCs have a fail-safe feature that will stop providing current to the motor if it detects that the ESC is out of phase with the motor. A step size of approximately 2% to 10% of the ESC throttle range in one direction and a step duration of approximately 1 to 10 second is suggested as a starting point. Once a reliable start-up sequence is found for a given configuration (input voltage and current limit), the configuration and start-up sequence can be iterated until a reliable start-up sequence is found for the desired configuration.

If a multimeter or oscilloscope is used to probe the HDD motor leads, it is important to be mindful of the device's impedance as it may interfere with the back-EMF which the ESC uses as feedback to perform motor commutation. Additionally, it is important to be aware of any current limitations from power supplies or voltage regulators, especially since insufficient current would prevent the motor from overcoming static friction.

Once a reliable start-up sequence is found for the desired configuration, an input-response test should be conducted to develop an actuator model of the HDD-RW. One such input-response test may be the step response test described in Section 3.2. If a set of different start-up sequences are identified, each one of the sequences can be tested. For the step response test, a longer step duration is preferable as it allows sufficient time for the HDD-RW to reach steady state speeds. Larger step sizes will allow for better estimation of the HDD-RW time constants, while smaller step sizes will for allow higher resolution mapping of the ESC command to HDD-RW RPM. Other input sequences can be used for actuator modeling, such as variable frequency input, as described in [41]. The HDD-RW actuator model can be verified by measuring the HDD-RW RPM to the modeled RPM values for a given ESC command sequence. Note that several system identification software tools such as System Identification Toolbox [42] by MATLAB and Comprehensive Identification from FrEquency Responses (CIFER) [43] exist which can be used for modeling of the HDD-RW, identification of parameters, and estimation of parameter uncertainties.

Once an actuator model is developed for the HDD-RW, the keep-out-zone should be found to allow for reliable direction switching. The KOZ can be found by spinning the HDD-RW to a steady rotation rate and incrementally reducing the ESC command until the HDD-RW rotation becomes unstable and/or stops. The KOZ should be found for both the CW and CCW directions. Once the KOZ is determined, an algorithm should be designed to reliably pass through the KOZ for bidirectional control. One such algorithm is presented in 1 and discussed in Section 3.3.3.3. The implemented KOZ algorithm should be tested to tune the KOZ bounds and algorithm behavior.

Finally, the attitude controller using the HDD-RWs should be designed and tested. This can be done using a fishing line setup, as described in Section 3.3.4. Alternatively, an air-bearing testbed may also be used for ground testing. It is recommended to develop

attitude control in the following order: single-axis stabilization, single-axis pointing, three-axis stabilization, three-axis pointing. A PD controller such as the one described in Section 3.3 may be implemented. Advanced control techniques, such as model predictive control (MPC) are recommended for the final implementation; however, it is recommended to begin development with a simple PD controller to establish baseline performance before utilizing more advanced control techniques.

It is recommended to develop a system model of the testbed used in ground testing in order to isolate the performance of the HDD-RW and controller. For example, for fishing line testing, a model of the fishing line may be developed that includes torsional stiffness, pendulum motion, and spring motion. For air-bearing testing, a model of the bearing friction as a function of pressure, position, orientation, velocity, and angular velocity may be developed. The level of fidelity of such models should ideally be able to capture external torques that are at least above or at the same order of magnitude as the torque of the HDD-RW.

System identification of the HDD-RW and CubeSat system may be performed using the optimization-based system identification technique described in Section 3.5.1. This method can also be used to perform system identification of the testbed. It is also recommended to utilize existing system identification software tools, as previously mentioned.

Once a system and testbed model has been developed and validated, simulation may be utilized to design and tune a controller for space application. Such simulations may include effects such as external torques due to atmospheric drag and solar radiation. A Monte Carlo simulation approach may be applied to quantify the performance of the HDD-RWs and the controller for varying scenarios.

Chapter 5

Conclusions

5.1 Summary

The research work presented herein has matured the HDD-RW technology from a lab prototype to a working reaction wheel. The mechanical and electrical modifications to convert HDDs into HDD-RWs have been defined and documented. Commercial-off-the-shelf (COTS) electronic speed controller (ESC) models and input voltage values which provide stable driving of the HDD-RW have been identified. A methodology of developing an actuator model of a HDD-RW is described. A technical guide to produce HDD-RWs and develop attitude control capabilities with them has been documented. A methodology to create an actuator model and controller for the HDD-RWs has been established.

Attitude control using the HDD-RWs has been demonstrated through microgravity parabolic flight testing. The HDD-RWs are shown to be capable of performing three-axis attitude stabilization and pointing of a CubeSat testbed in microgravity environment. Performance metrics of the HDD-RWs have been measured. A methodology for system identification, which allows future users to develop and tune HDD-RW controllers, has been verified via results from parabolic flight testing. Simulation of the CubeSat system model has shown that the HDD-RWs and controller are robust to various initial rotation rates and target attitudes. In summary, the process to engineer a HDD-RW has been defined and improved through a combination of lab testing and parabolic flight testing. And by demonstrating reaction wheel functions in microgravity environment, the technology readiness level of the HDD-RWs has been raised from TRL 4 to TRL 6.

5.2 Recommendations

When beginning to use a HDD-RW, it is recommended to drive the motor using a COTS ESC, even if a custom ESC design is the intended final design. The initial parameters of a custom ESC may not be able to start up the HDD motor and provide little feedback on tuning of the parameters; whereas a COTS ESC will likely begin working with little tuning and provide a stable platform to understand effects of each parameter on performance. This knowledge and experience can later be used during tuning of a custom ESC. When starting the motor, it is important to be mindful of current limits of the power supply and any components between the power supply and the HDD motor such as voltage regulators. Without sufficient current, the motor can not overcome static friction. Probing of the HDD motor leads with an oscilloscope may interfere with the back-EMF signal used by the ESC, which may lead to degraded performance. It is recommended to first test the ESC without an oscilloscope to evaluate its performance and to be mindful of the impedance of the oscilloscope when using one. When purchasing HDDs, it is recommended to purchase them in batches such that there are sufficient units of the same model available for flight, and ground-testing. Additionally, it is recommended to track and log usage of each unit such that its history can be referenced to resolve potential performance discrepancies between different units. Incorporating speed sensing capability, either through the ESC, a back-EMF sensor or an encoder, is recommended to be able to directly determine the motor speed rather than relying on ESC to RPM mapping or back-calculation from CubeSat rotation rates.

When developing an actuator model of the HDD-RWs, the presented model and method may be used as a baseline. It is recommended to also utilize existing system identification software tools such as System Identification Toolbox by MATLAB [42] and Comprehensive Identification from FrEquency Responses (CIFER) [43]. Such system identification software tools are also recommended when modeling the CubeSat system. It is recommended to develop a model relating HDD-RW speed to power consumption - such a model would be incredibly useful for health-monitoring of the HDD-RWs. Additionally, it is recommended to develop different models for the HDD-RW for when its disk is accelerating and decelerating, in both clockwise and counter-clockwise directions - as the motor dynamics depends on the direction of velocity and acceleration. A more sophisticated model may also be developed

where the motor dynamics also takes motor speed and temperature into account. When designing a controller for the HDD-RWs, it is recommended to begin with a PD controller to establish baseline performance and then later develop and utilize more advanced techniques such as model predictive control (MPC). When performing ground-testing of the HDD-RWs, either with fishing line testing or air-bearing testing, it is recommended to model and develop a simulation of the dynamics of the fishing line or air bearing. This allows the dynamics of the testbed to be taken into account in order to isolate the performance of the HDD-RWs and the controller.

5.3 Lessons Learned

In a complex engineering project, it is important to define and re-evaluate priorities - this facilitates making sound decisions when evaluating trade-offs and risks. Initially, this project had aimed to perform parabolic flight demonstration of the HDD-RWs with a custom ESC - this was because our team saw a custom ESC as an important element of the final implementation of HDD-RWs in CubeSats. However, while developing a custom ESC, our team realized that it would take a significant amount of time to develop a working solution. Upon re-evaluating the technology being demonstrated, we determined that the HDD-RW was the priority and that although the custom ESC solution was preferable, its development timeline would detract from development of the HDD-RW and the flight experiment. We re-scoped the flight project to demonstrate the HDD-RWs with a COTS ESC. In retrospect, had we continued pursuing the custom ESC, we would have incurred significant timeline and technical risk to the project.

A step-wise approach of incrementally developing capabilities lends itself towards successfully navigating the inherent unknowns of technology development. This philosophy was embodied through this project in several ways. Firstly, the milestone of driving the HDD-RWs with a custom ESC, a more advanced capability, was placed after driving the HDD-RWs with a COTS ESC. Beginning with the easier problem allowed us to reach a working solution earlier. Furthermore, it provided more experience with the HDD-RW which was very informative when tuning parameters of the custom ESC and reduced overall development time. Generally, this approach of beginning with a simple working solution or solving a simplified

problem, gaining experience and knowledge of the system, and then developing more complex solutions or solving more complex problems worked well for our team. Secondly, developing incremental capabilities for each set of parabolic flights - control of HDD-RWs, stabilization with HDD-RWs, and pointing with HDD-RWs - provided feasible scope and allowed for integration of knowledge and experience from past set of flights to the next set of flights. The first parabolic flight campaign was designed to have a single contained experiment. Experience from this flight campaign informed our team of the need for longer floating duration and the ability to push the envelope of our experiment with the inclusion of an external experiment. Lastly, performing parabolic flight demonstration provided a wealth of testing data that greatly informs the controller design for orbital flight demonstration. Without parabolic flight demonstration, an orbital flight demonstration of the HDD-RWs may have not been designed to resolve challenges such as spinning at low speeds or, alternatively, may have been designed to meet overly-conservative requirements.

5.4 Future Work

Microgravity parabolic flight testing has served as a key stepping stone for the HDD-RWs between lab testing and demonstration in space. The next steps for the HDD-RWs are environmental testing and demonstration in space environment. Other future work for the HDD-RWs also includes degradation testing and development of a custom ESC.

The UC Davis Center for Spaceflight Research (CSFR) is currently aiming to perform environmental testing of the HDD-RWs. The UC Davis CSFR is also developing a single-axis HDD-RW demonstration mission in partnership with NASA Johnson Space Center (JSC). A single 2.5-inch HDD-RW will fly on-board a NASA JSC 6U CubeSat as a secondary payload aiming to demonstrate the HDD-RW technology performing attitude change in space environment. Initial hardware and software integration tests were performed with the HDD-RW and the NASA JSC CubeSat in May 2022, and the hardware was officially sent to NASA JSC for final testing and integration in July 2023. The mission will provide valuable data on the performance of the HDD-RWs in space environment. A successful demonstration will raise the TRL of the HDD-RW technology to TRL 8.

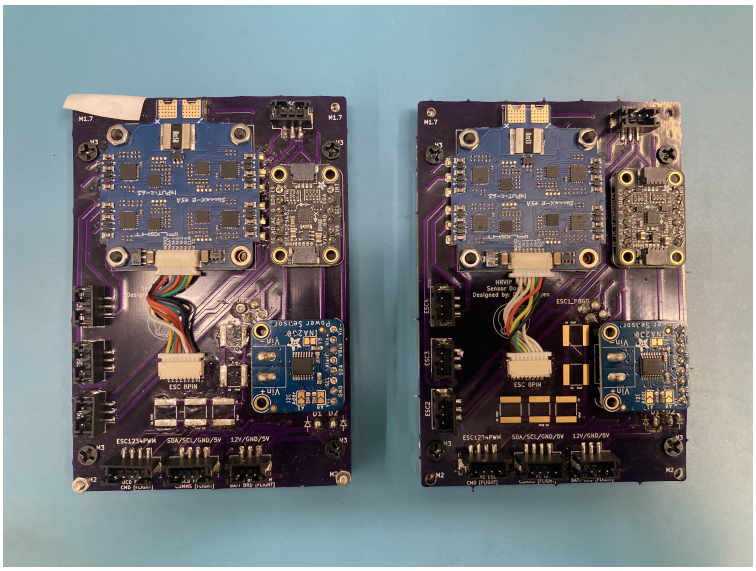

Figure 5.1: UC Davis / NASA JSC CubeSat HDD-RW PCB attached to back of HDD - Flight Unit and Engineering Unit

Degradation testing of the HDD-RWs will provide valuable insight into their expected performance and lifetime in space. It is recommended for degradation testing to be incorporated in future environmental testing and in-space demonstration/operation of the HDD-RWs. Development of a degradation model can be used for active health-monitoring of HDD-RWs used in CubeSats.

Development of a custom ESC will enable future HDD-RW users to more easily integrate the ESC with other PCBs within the CubeSat, which are most often also designed in-house. The design flexibility of the custom ESC also allows for more efficient thermal management of heat generated by the HDD-RW motor. It is recommended that custom ESC designs developed in the future are made open-source such that other HDD-RWs users may adapt the design for their use-cases.

Following the single-axis HDD-RW demonstration mission, the next step for the HDD-RW technology is to perform three-axis CubeSat attitude control in space. Successful demonstration would provide valuable in-space performance data and raise the technology readiness level of the HDD-RW technology to TRL 9. The significant cost-reductions enabled by the HDD-RW technology will lower the barriers to entry, allowing resource-constrained organizations and many students to develop low-cost, rapid, and reliable CubeSat missions.

Bibliography

[1] K. R. Cooper, "Computer vision system design for attitude validation of free-floating cubesat testbed in parabolic flights," Master's thesis, University of California, Davis, 2023.

[2] K. Woellert, P. Ehrenfreund, A. J. Ricco, and H. Hertzfeld, "Cubesats: Cost-effective science and technology platforms for emerging and developing nations," *Advances in Space Research*, vol. 47, no. 4, pp. 663–684, 2011.

[3] A. Poghosyan and A. Golkar, "Cubesat evolution: Analyzing cubesat capabilities for conducting science missions," *Progress in Aerospace Sciences*, vol. 88, pp. 59–83, 2017.

[4] W. Pang, B. Bo, X. Meng, X. Yu, J. Guo, and J. Zhou, "Boom of the cubesat: A statistic survey of cubsats launch in 2003-2015," 09 2016.

[5] The CubeSat Program, Cal Poly SLO, "Cubesat design specification." https://www.cubesat.org/s/CDS-REV14_1-2022-02-09.pdf, 2022. Accessed: 2023-09-10.

[6] S. Jayaram and M. Swartwout, *A Review of the Role of Student-Built Spacecraft in Workforce Training and Innovation: Ten Years of Significant Change*.

[7] J. R. Wertz, D. F. Everett, and J. J. Puschell, *Space mission engineering: The new smad*. Microcosm Press, 2018.

[8] P. W. Fortescue, J. Stark, and G. Swinerd, *Spacecraft Systems Engineering*. John Wiley & Sons, 2011.

[9] X. Xia, G. Sun, K. Zhang, S. Wu, T. Wang, L. Xia, and S. Liu, "NanoSats/CubeSats ADCS survey," in *2017 29th Chinese Control And Decision Conference (CCDC)*, (Chongqing, China), pp. 5151–5158, IEEE, May 2017.

[10] N. J. B. Jr, "Master of Science in Mechanical Engineering,"

[11] T. A. Joseph, G. Benari, H. Podmore, and R. S. K. Lee, "Assessing Reaction Wheel Sizing for CubeSat Attitude Control,"

[12] A. M. Lee, D. Leon, C. P. Casillas, and R. McCarver, "3-Axis Reaction Wheel System for CubeSats,"

[13] G. Capovilla, "Development of a ultrathin reaction wheel for modular nanosatellites," Master's thesis, 2019.

[14] E. H. Dekens, G. F. Brouwer, J. Bouwmeester, and J. M. Kuiper, "Development of a Nano-Satellite Reaction Wheel System with Commercial Off-The-Shelf Motors," 2010.

[15] J. Bhagatji, S. Asundi, M. G, N. S, and V. K. Agrawal, "Design, Simulation and Testing of a Reaction Wheel System for Pico/Nano-Class CubeSat Systems," in *2018 AIAA SPACE and Astronautics Forum and Exposition*, (Orlando, FL), American Institute of Aeronautics and Astronautics, Sept. 2018.

[16] J. A. Louke, E. S. Schmidt, and C. J. Young, "An Open-Source Reaction Wheel System for Oregon's First Satellite," in *AIAA SPACE 2016*, (Long Beach, California), American Institute of Aeronautics and Astronautics, Sept. 2016.

[17] E. Deems, "Risk Management of Student-Run Small Satellite Programs," in *57th International Astronautical Congress*, (Valencia, Spain), American Institute of Aeronautics and Astronautics, Oct. 2006.

[18] J. K. Wayer, J.-F. Castet, and J. H. Saleh, "Spacecraft attitude control subsystem: Reliability, multi-state analyses, and comparative failure behavior in LEO and GEO," *Acta Astronautica*, vol. 85, pp. 83–92, Apr. 2013.

[19] M. Tafazoli, "A study of on-orbit spacecraft failures," *Acta Astronautica*, vol. 64, pp. 195–205, Jan. 2009.

[20] R. Sperber, "Better with age and experience - Observed satellite in-orbit anomaly rates," in *15th International Communicatons Satellite Systems Conference and Exhibit*, (San Diego,CA,U.S.A.), American Institute of Aeronautics and Astronautics, Feb. 1994.

[21] L. Sahar, E. Edlerman, H. Agalarian, V. Balabanov, and P. Gurfil, "Hard Disk Drive Based Reaction Wheels for CubeSat Attitude Control," *Journal of Spacecraft and Rockets*, vol. 55, pp. 236–241, Jan. 2018.

[22] M. Driedger, J. Chornick, E. Olaniyanu, K. Dick, R. Sahani, and F. P., "Using hard drive based reaction wheels for attitude control on the tsat-5 cubesat," in *70th International Astronautical Congress (IAC)*, (Washington D.C., United States), Oct. 2019.

[23] "Nasa flight opportunities." https://www.nasa.gov/stmd-flight-opportunities/.

[24] "Nasa flight opportunities selection 2020." https://www.nasa.gov/humans-in-space/commercial-space/nasa-selects-31-promising-space-technologies-for-commercial-flight-tests/.

[25] T. Ustrzycki, R. Lee, and H. Chesser, "Spherical air bearing attitude control simulator for nanosatellites," in *AIAA Modeling and Simulation Technologies Conference*, p. 6272, 2011.

[26] "Zero-g research programs." https://www.gozerog.com/zero-g-research-programs/.

[27] A. Al Mamun, C. Bi, and G. Guo, *Hard Disk Drive: Mechatronics and Control*. CRC Press, 2007.

[28] "Digital storage and memory projections for 2023, part 1." https://www.forbes.com/sites/tomcoughlin/2022/12/18/digital-storage-projections-for-2023-part-1/.

[29] "Nanosats database." https://www.nanosats.eu/.

[30] H. Shimizu, M. Tokuyama, S. Imai, S. Nakamura, and K. Sakai, "Study of aerodynamic characteristics in hard disk drives by numerical simulation," *IEEE Transactions on Magnetics*, vol. 37, no. 2, pp. 831–836, 2001.

[31] W. C. Blount, "Fluid Dynamic Bearing Spindle Motors," 2007.

[32] "Hard disk head crash." https://en.wikipedia.org/wiki/Head_crash.

[33] "Amazon - bidirectional 20a brushless esc 2-4s 2a 5v ubec electric speed controller for rc car boat underwater propeller." https://www.amazon.com/Readytosky-Bidirectional-Brushless-Pneumatic-Underwater/dp/B086QK6B4Z.

[34] "Succex-e 45a 2-6s blheli˙s dshot600 4-in-1 esc." https://www.fatboyfpv.com/index.php?route=product/product&product_id=69.

[35] "Amazon - dc-dc buck, drok power supply module lm2596 dc buck converter 5v-36v to 1.25-32v step down voltage regulator stabilizer 3a 5a cc volt transformer reducer." https://www.amazon.com/DROK-Converter-Adjustable-Stabilizer-Transformer/dp/B07LCHTVCM/.

[36] C. Mellor, "Nidec takes seagate out for a patent spin." https://blocksandfiles.com/2021/01/20/nidec-sues-seagate-patents/.

[37] D. Nguyen, S. Guertin, and J. Patterson, "The Effect of Total Ionizing Dose Degradation on Laptop Hard Disks," in *2005 8th European Conference on Radiation and Its Effects on Components and Systems*, (Cap d'Agde, France), pp. PW9–1–PW9–4, IEEE, Sept. 2005. ISSN: 0379-6566.

[38] K. K. Allums, P. M. ONeill, B. D. Reddell, C. R. Bailey, and K. V. Nguyen, "Radiation Test Results on COTS and Non-COTS Electronic Devices for NASA Johnson Space Center Spaceflight Projects," in *2012 IEEE Radiation Effects Data Workshop*, (Miami, FL, USA), pp. 1–9, IEEE, July 2012.

[39] NASA, "General environmental verification standard (gevs) for gsfc flight programs and projects." https://standards.nasa.gov/standard/GSFC/GSFC-STD-7000, 2021. Accessed: 2023-09-10.

[40] *NASA Systems Engineering Handbook: NASA/SP-2016 -6105 REV2˙2017*. NASA, 2017.

[41] C. Xiang, X. Wang, Y. Ma, and B. Xu, "Practical Modeling and Comprehensive System Identification of a BLDC Motor," *Mathematical Problems in Engineering*, vol. 2015, pp. 1–11, 2015.

[42] "Matlab system identification toolbox." https://www.mathworks.com/products/sysid.html.

[43] "Comprehensive identification from frequency responses (cifer)." https://www.sjsu.edu/researchfoundation/resources/flight-control/cifer.php.

[44] B. Wie and P. M. Barba, "Quaternion feedback for spacecraft large angle maneuvers," *Journal of Guidance, Control, and Dynamics*, vol. 8, pp. 360–365, May 1985.

[45] "Digikey ips-4039t-01y901 spring finger contact." https://www.digikey.com/en/products/detail/iriso-usa-inc/IPS-4039T-01Y901/14291317.

[46] "Mouser 855-p70-2000045r spring loaded pogo pin." https://www.mouser.com/ProductDetail/Harwin/P70-2000045R?qs=k41KVqW3ymqv0Hl6W6r7MQ%3D%3D.